Wearable Flexible Biopotential Measurement Systems

Shibam Debbarma

Department of Electrical and Computer Engineering
Faculty of Engineering, McGill University
Montreal, Canada

September 2023

A thesis submitted to McGill University in partial fulfilment of the requirements for the degree of Doctor of Philosophy.

Acknowledgements

The research life of a Ph.D. scholar is like a roller-coaster ride with interesting twists and turns. The only constant component during the unpredictable journey towards achieving a Ph.D. degree is having a supportive environment from the supervisor, family, colleagues, and friends.

First, I acknowledge my immense gratitude to my thesis supervisor Prof. Sharmistha Bhadra for giving me this amazing opportunity to be part of the prestigious McGill community and contribute to its research. Her constant guidance, patience, encouragements, advices, and support indeed helped me through the thick and thin of my Ph.D. research and my Ph.D. thesis to become a reality. I would like to thank my committee, Prof. Milica Popović and Prof. Mourad N. El-Gamal, for their insights and guidance at different stages of research. I would also like to thank my Master's supervisor Prof. P. C. Pandey (IIT Bombay, India) as his knowledge and guidance helped me learn the art of Electronics and become a decent engineer.

I acknowledge my gratitude to the McGill University for providing me financial support through the McGill Engineering Doctoral Awards (MEDA) scholarship. It would have been impossible for me to pursue my Ph.D. degree without this support.

I would also like to thank my colleagues Amirhossein Shahshahani, Seyedfakhreddin Nabavi, and Kiran Kumar Sappati for their invaluable suggestions and discussions which helped me achieving my research milestones. I cannot thank enough all my friends and lab-mates Arun, Tasnim Sorwar, Mian Hamza, Jack Hu, Shahab Mahmoudi Sadaghiani, Hossein Anabestani, Ajaypal Singh, Jasmine Boparai, and Mahmoud Abdalla for their kindness and emotional support which helped me keeping my sanity and boost my morale throughout my Ph.D. research.

Finally, my deepest respect to family, my mother Mrs. Nibedita Sarkar Debbarma, my brother Mr. Manoj Debbarma, my sister-in-law Mrs. Fulkumari Debbarma, and my niece Miss. Nyrra Debbarma for their unconditional love and support that shaped me become a better human being. I would also like to express my love to my late father Mr. Nirabendra Debbarma for all his love and support during his lifetime and beyond.

Abstract

Recent advances in smart wearables have brought clinical standard health monitoring services at our home and now smart wearables are used in our day-to-day life. One such application of wearables is smart headband/eye-masks based biopotential monitoring system capable of measuring electroencephalogram (or EEG) and electrooculogram (or EOG) signals. These are useful in sleep study and treating sleep disorders like obstructive sleep apnea. However, most of the state-of-the-art biopotential wearables are heavy and uncomfortable to wear, use rigid electrodes and rigid printed-circuit boards (or PCBs), suffer from motion artifacts due to movements of the wearers, and are not suitable for long term study.

In this research, we propose a wearable for EOG measurement which is implemented on flexible Polyimide PCB with integrated printed gold contact electrodes and the biopotential acquisition system. The wearable can be easily integrated with headbands/eye-masks. The system metrics such as gain (> 68.5 dB), bandwidth (1.6 Hz–40 Hz), and common-mode rejection ratio (or CMRR, > 70 dB) are also evaluated, which meets biopotential measurement standards set by the "International Federation of Clinical Neurophysiology (or IFCN)". The system performance has also been validated using a MATLAB based algorithm for the detection of different eye activities such as eye blinks, eye winks, and horizontal eye movements with an accuracy of 77.08 %. But this prototype requires electrode gel for better EOG detection and is sensitive to random motion artifacts. Therefore, the EOG wearable design is redesigned with parallel non-contact (or capacitive) electrode pairs, which have better sensitivity and do not require gel for EOG detection. The parallel electrode pairs are configured differentially for motion artifacts sensing and reduction during EOG measurement. The system metrics such as gain (> 37 dB), bandwidth (1 Hz–40 Hz), and CMRR (> 74 dB) are also evaluated for the new EOG prototype, which meets the IFCN standards. The proposed wearable is then validated for acquiring EOG signals in the presence/absence of motion artifacts. However, forehead/eye-masks based wearables are still uncomfortable to wear and prone to displacements due to movements during sleep.

In recent studies, EEG signals are successfully acquired intra-orally from the palate region, which can be easily accessed using comfortable oral appliances such as mandibular advancement devices or MADs. Here, we propose a smart MAD which integrates flexible printed electrodes and measurement system for intra-oral EEG acquisition. The measurement system also utilizes an accelerometer to track intra-oral motions such as tongue movements, teeth grinding, and gulping. A MATLAB based algorithm is implemented to decompose the intra-oral EEG signals using empirical mode decomposition (EMD) followed by independent component analysis (ICA). Then the accelerometer signals are used to identify and remove motion corrupted segments from the decomposed independent components containing the motion activities. A clean intra-oral EEG is reconstructed from the modified independent components. The effectiveness of the proposed algorithm is validated both qualitatively and quantitatively. The EEG system metrics such as gain (> 57 dB), bandwidth (0.16 Hz–40 Hz), and CMRR (>74 dB) are also evaluated, which again meets the IFCN standards. This smart MAD has been successfully validated for acquiring intra-oral EEG signals and extracting features for ‘eye open’ and ‘eye close’ activities from the intra-oral EEG spectrums, both in the presence and absence of intra-oral motions. This smart MAD system for intra-oral EEG can be a potential alternative solution to headband/eye-masks based wearables.

The biopotential measuring wearable devices proposed here are flexible, lightweight, comfortable to the wearer, and have potential to be used in sleep related studies and treatments.

Résumé

Les récents progrès dans les technologies prêt-à-porter ont permis d'offrir des services de surveillance de la santé à domicile standardisés, qui sont maintenant utilisés dans nos vies quotidiennes. Une telle application des technologies prêt-à-porter est un masque/bandeau intelligent de surveillance des biopotentiels, capable de mesurer les signaux électroencéphalographiques (ou EEG) et électrooculographiques (ou EOG). Un tel dispositif serait utile dans l'étude (du sommeil) et le traitement des troubles du sommeil tels que le syndrome d'apnées obstructives du sommeil. Cependant, ce type de dispositif est lourd et inconfortable, utilise des électrodes et des circuits imprimés (PCB) rigides et souffre d'artéfacts de mouvement, le rendant inapproprié pour l'étude à long terme.

Dans cette recherche, nous proposons un dispositif prêt-à-porter d'électrooculographie implémenté sur un circuit imprimé flexible en polyimide, incluant des électrodes imprimées en or et un système d'acquisition des signaux biopotentiels. Le dispositif peut être facilement intégré à un bandeau/masque pour les yeux. Les paramètres du système tels que le gain (> 68.5 dB), la bande passante (1.6 Hz–40 Hz) et le taux de rejet en mode commun (ou CMRR, >70 dB) sont également évalué(e)s, ce qui répond aux normes de mesure des signaux biopotentiels établies par la "International Federation of Clinical Neurophysiology (ou IFCN)". La performance du système a également été validée à l'aide d'un algorithme MATLAB de détection des différentes activités oculaires telles que les clignements et les mouvements latéraux avec une précision de 77.08 %. Mais ce prototype nécessite un gel électrode pour une meilleure détection de l'EOG et est sensible aux artefacts de mouvement aléatoires. Par conséquent, la conception du dispositif portable EOG est redéfinie avec des paires d'électrodes parallèles sans contact (ou capacitifs), qui ont une meilleure sensibilité et ne nécessitent pas de gel pour la détection de l'EOG. Les paires d'électrodes parallèles sont configurées de manière différentielle pour la détection et la réduction des artefacts de mouvement pendant la mesure de l'EOG. Les métriques du système telles que le gain (> 37 dB), la bande passante (1 Hz–40 Hz) et le CMRR (> 74 dB) sont également évaluées pour le nouveau prototype EOG, qui répond aux normes de l'IFCN. Le dispositif portable proposé est ensuite validé

pour l'acquisition de signaux EOG en présence/absence d'artefacts de mouvement. Cependant, les dispositifs portables basés sur les bandeaux/masques pour les yeux sont encore inconfortables à porter et sujets aux déplacements dus aux mouvements pendant le sommeil.

Dans des études récentes, des signaux EEG sont acquis avec succès intra-oralement à partir de la région du palais, qui peut être facilement accédée en utilisant des appareils oraux confortables tels que des dispositifs d'avancement mandibulaire ou MAD. Nous proposons ici un MAD intelligent qui intègre des électrodes imprimées flexibles et un système de mesure pour l'acquisition EEG intra-orale. Le système de mesure utilise également un accéléromètre pour suivre les mouvements intra-oraux tels que les mouvements de la langue, le grincement des dents et la déglutition. Un algorithme basé sur MATLAB est mis en œuvre pour décomposer les signaux EEG intra-oraux en utilisant la décomposition en mode empirique (EMD), suivie de l'analyse en composantes indépendantes (ICA). Ensuite, les signaux de l'accéléromètre sont utilisés pour identifier et supprimer les segments corrompus par le mouvement des composantes indépendantes décomposées contenant les activités de mouvement. Un EEG intra-oral propre est reconstruit à partir des composantes indépendantes modifiées. L'efficacité de l'algorithme proposé est validée à la fois qualitativement et quantitativement. Les métriques du système EEG telles que le gain (> 57 dB), la bande passante (0.16 Hz–40 Hz) et le CMRR (> 74 dB) sont également évaluées, répondant encore une fois aux normes de l'IFCN. Ce MAD intelligent a été validé avec succès pour l'acquisition de signaux EEG intra-oraux et l'extraction de caractéristiques pour les activités "yeux ouverts" et "yeux fermés" à partir des spectres EEG intra-oraux, à la fois en présence et en absence de mouvements intra-oraux. Ce système MAD intelligent pour l'EEG intra-oral peut être une solution alternative potentielle aux dispositifs portables basés sur des bandeaux de tête/masques pour les yeux.

Les dispositifs portables de mesure de biopotentiels proposés ici sont flexibles, légers, confortables pour le porteur et ont le potentiel d'être utilisés dans des études et des traitements liés au sommeil.

Contribution of Authors

This thesis is comprised of three journal articles. Two journal articles are published and one of them is under review after first submission. All articles are multi-authored. Shibam Debbarma is the first author of all journals. Contributions of authors for each article is given below.

Chapter 2: S. Debbarma and S. Bhadra. "A Lightweight Flexible Wireless Electrooculogram Monitoring System with Printed Gold Electrodes." IEEE Sensors Journal 21.18 (2021): 20931 – 20942. For this article, S. Bhadra and S. Debbarma have planned the steps of designing a flexible, wearable instrument with printed electrodes for biopotential measurements. S. Debbarma has done the required research on wearable devices for Electroencephalogram (or EEG) and Electrooculogram (or EOG) applications reported in recent scholarly articles. Then he has designed a wireless, wearable EOG measurement system, implemented it on a flexible Polyimide substrate, carried out the system characterization, and acquired real-time EOG signals from forehead using the wearable prototype. He has also implemented a MATLAB based algorithm to detect different EOG features from the measured signals. The work has been performed under the sole supervision of S. Bhadra. S. Debbarma has prepared the manuscript and S. Bhadra has edited it.

Chapter 3: S. Debbarma and S. Bhadra. "A Flexible Wearable Electrooculogram System with Motion Artifacts Sensing and Reduction." IEEE Transactions on Biomedical Circuits and Systems 16.2 (2022): 324 – 335. For this article, S. Bhadra and S. Debbarma have planned to improve the shortcomings of the previous wearable EOG measurement prototype. S. Debbarma has done further literature reviews to resolve the shortcomings of the previous design and proposed an improved design for EOG measurement. In this design, he has implemented a parallel electrode based system to mitigate the impact of motion artifacts during EOG measurements. S. Debbarma has designed and implemented the improved EOG wearable on a flexible Polyimide substrate, characterized it thoroughly, and used it to acquire real-time EOG

signals in the presence of motion artifacts. The work has been performed under the sole supervision of S. Bhadra. S. Debbarma has prepared the manuscript and S. Bhadra has edited it.

Chapter 4: S. Debbarma and S. Bhadra. "A Sensor-Fusion Method for Motion Artifacts Reduction in Intra-oral EEG Signals." in IEEE Sensors Journal (Early Access), August 2023, doi: 10.1109/JSEN.2023.3306311. For this article, S. Bhadra and S. Debbarma have planned to acquire Electroencephalogram (or EEG) signals intra-orally using mandibular advancement devices (or MADs). S. Debbarma has done the required research on scalp and intra-oral based EEG applications reported in recent scholarly articles. In this design, he has implemented a sensor-fusion of EEG electrodes and accelerometer, and fabricated a flexible Polyimide substrate based circuitry following the design steps of the previous EOG systems. The sensors and the system has then been integrated with a customized MAD for intra-oral measurements. The smart prototype houses a single EEG channel and an accelerometer to sense intra-oral EEG signal and intra-oral motions simultaneously. A MATLAB based algorithm has also been implemented by S. Debbarma to identity and denoise the motion corrupted intra-oral EEG segments. The algorithm first utilizes empirical mode decomposition (EMD) followed by independent component analysis (ICA) to decompose the single channel EEG data into ICA components. Then the ICA components containing the intra-oral motion artifacts are mapped with the accelerometer sensor based motion data to identify the motion corrupted data segments and nullify those segments present in the ICA components. A motion artifacts reduced intra-oral EEG signal is then reconstructed using inverse ICA-EMD method. The efficacy of the proposed algorithm is validated both qualitatively and quantitatively. The smart MAD system and the proposed algorithm has also been applied to acquire motion artifacts reduced intra-oral EEG signals in the presence of intra-oral motions. The smart MAD system has been developed under the sole supervision of S. Bhadra. S. Debbarma has prepared the manuscript and S. Bhadra has edited it.

Contents

List of Figures

List of Tables

List of Copyrighted Materials for which Permissions were Obtained

- N. Kosmyna, C. Morris, U. Sarawgi, T. Nguyen, and P. Maes, "AttentivU: A wearable pair of EEG and EOG glasses for real-time physiological processing," *2019 IEEE 16th Int. Conf. on Wearable and Implantable Body Sens. Netw. (BSN)*, 2019, pp. 1–4. Figure 1.4 in chapter 1 of this thesis contains a reconstructed version of figure 1 from this paper.
- A. Dabbaghian *et al.*, "A 9.2-g fully-flexible wireless ambulatory EEG monitoring and diagnostics headband with analog motion artifact detection and compensation," *IEEE Trans. Biomed. Circuits & Syst.*, vol. 13, no. 6, pp. 1141–1151, Dec. 2019. Figure 1.4 in chapter 1 and figure 5.1 in chapter 5 of this thesis contains a reconstructed version of figures 5 and 8 from this paper.
- J. Xu *et al*., "A wearable 8-channel active-electrode EEG/ETI acquisition system for body area networks," *IEEE J. Solid-State Circuits*, vol. 49, no. 9, pp. 2005–2016, Sept. 2014. Figure 1.4 in chapter 1 of this thesis contains a reconstructed version of figure 20 from this paper.
- J. Arnin *et al.*, "Wireless-based portable EEG-EOG monitoring for real time drowsiness detection," *2013 IEEE 35th Annu. Int. Conf. Engg. Medicine and Biol.*, 2013, pp. 4977-4980. Figure 1.4 in chapter 1 of this thesis contains a reconstructed version of figure 7 from this paper.

- S. -F. Liang et al., "Development of an EOG-based automatic sleep-monitoring eye mask," *IEEE Trans. Instrum. Meas.*, vol. 64, no. 11, pp. 2977–2985, 2015. Figure 1.4 in chapter 1 of this thesis contains a reconstructed version of figure 2 from this paper.
- S. -W. Kim *et al*., "Wearable Multi-Biosignal Analysis Integrated Interface With Direct Sleep-Stage Classification," *IEEE Access*, vol. 8, pp. 46131-46140, 2020. Figure 1.4 in chapter 1 of this thesis contains a reconstructed version of figure 27 from this paper.
- S. Rostaminia *et al.*, "PhyMask: Robust Sensing of Brain Activity and Physiological Signals During Sleep with an All-textile Eye Mask," *ACM Trans. Comput. Healthcare*, vol. 3, no. 3, pp. 1–35, Jul. 2022. Figure 1.4 in chapter 1 of this thesis contains a reconstructed version of figure 2 from this paper.
- S. Debbarma and S. Bhadra, "A Lightweight Flexible Wireless Electrooculogram Monitoring System With Printed Gold Electrodes," *IEEE Sens. J.*, vol. 21, no. 18, pp. 20931-20942, September 2021. Chapter 2 of this thesis contains the entire materials from this paper.
- S. Debbarma and S. Bhadra, "A Flexible Wearable Electrooculogram System with Motion Artifacts Sensing and Reduction," *IEEE Trans. Biomed. Circuits Syst.*, vol. 16, no. 2, pp. 324-335, April 2022. Chapter 3 of this thesis contains the entire materials from this paper. Figure 5.1 in chapter 5 of this thesis contains a reconstructed version of figure 2 from this paper.
- S. Debbarma, and S. Bhadra, "A Sensor-Fusion Method for Motion Artifacts Reduction in Intra-oral EEG Signals," *IEEE Sens. J.*, (Early Access), August 2023, doi: 10.1109/JSEN.2023.3306311. Chapter 4 of this thesis contains the entire materials from this paper. Figure 5.1 in chapter 5 of this thesis contains a reconstructed version of figure 4 from this paper.
- J. Golparvar and M. K. Yapici, "Electrooculography by wearable graphene textiles," *IEEE Sens. J.*, vol. 18, no. 21, pp. 8971–8978, 2018. Figure 5.1 in chapter 5 of this thesis contains a reconstructed version of figure 1 from this paper.

- T. Vehkaoja *et al*., "Wireless head cap for EOG and facial EMG measurements," *2005 IEEE 27th Annu. Conf. Engg. Medicine and Biol.*, 2006, pp. 5865–5868. Figure 5.1 in chapter 5 of this thesis contains a reconstructed version of figure 2 from this paper.
- C. -T. Lin *et al.*, "Forehead EEG in Support of Future Feasible Personal Healthcare Solutions: Sleep Management, Headache Prevention, and Depression Treatment," *IEEE Access*, vol. 5, pp. 10612-10621, 2017. Figure 5.1 in chapter 5 of this thesis contains a reconstructed version of figure 1 from this paper.

Nomenclature

ADC	Analog to Digital Converter
AFE	Analog Front-end
BCI	Brain-Computer Interface
BLE	Bluetooth Low Energy
CCA	Canonical Correlation Analysis
CMR	Common Mode Rejection
CMRR	Common Mode Rejection Ratio
CMOS	Complementary Metal-Oxide Semiconductor
CPAP	Continuous Positive Airway Pressure
CrossCorr	Cross Correlation
DC	Direct Current
DRL	Driven Right-Leg
DWT	Discrete Wavelet Transform
ECG	Electrocardiogram
EEG	Electroencephalogram
EMD	Empirical Mode Decomposition
EEMD	Ensemble Empirical Mode Decomposition
EMG	Electromyogram
EOG	Electrooculogram
ETI	Electrode-Tissue Impedance
f_c	Cut-off Frequency

$f_{c,LPF}$	Cut-off Frequency of Low-pass Filter
$f_{c,HPF}$	Cut-off Frequency of High-pass Filter
f_N	Cut-off Frequency of Notch Filter
HCI	Human-Computer Interface
HPF	High-pass Filter
IA	Instrumentation Amplifier
IC	Integrated Circuits
ICA	Independent Component Analysis
IFCN	International Federation of Clinical Neurophysiology
IMU	Intertial Measurements Unit
LED	Light Emitting Diode
LCR	Inductance (L), Capacitance(C), and Resistance (R)
LPF	Low-pass Filter
MA	Motion Artifacts
MAD	Mandibular Advancement Device
MAR	Motion Artifacts Removal
MATLAB	Matrix Laboratory
OpAmp	Operational Amplifier
OSA	Obstructive Sleep Apnea
PCA	Principal Component Analysis
PCB	Printed Circuit Board
PPG	Photoplethysmogram
PSG	Polysomnogram
REM	Repetitive Eye Movement
SpO_2	Saturation of Peripheral Oxygen
SSA	Singular Spectrum Analysis

Chapter 1

Introduction and Literature Review

Wearable devices and technologies have made profound advancements in many healthcare related applications. Thanks to the innovations in science and engineering which made it possible to have smart, miniaturized, wearable devices capable of providing standard healthcare facilities in hospitals, clinical setups, and even at home monitoring environments. Several physiological parameters and mental states, such as heart rate, blood pressure, blood oxygen saturation (or SpO_2), breath, calories, sleep, stress, hypertension, and many more now have the possibility of being monitored using modern gadgets we may use in our day-to-day activities such as smart phones, smart wristwatches, smart headbands, smart eye-masks, smart therapeutic devices, smart mandibular advancement devices (or MADs) etc [1]−[8].

Wearables generally use smart sensors for non-invasive monitoring of physiological indices and can be easily integrated with accessories, clothing, and therapeutic gadgets. However, designing a wearable device has several inherent challenges such as sensor fabrication, battery-life, miniaturized form factor, meeting medical standard specifications, comfortability, and most importantly the scope of its use and application before making it commercially available. One such potential application of smart wearables is studying sleep, which can be useful for treating sleep disorders such as obstructive sleep apnea (or OSA) [9], [10]. Sleep study (also known as polysomnography or PSG) is a clinically standard procedure performed in sleep labs which involves overnight monitoring of physiological parameters such as heart rate, SpO_2, breath, and

assessing various sleep stages by studying biopotentials like Electrooculography (or EOG) and/or Electroencephalography (or EEG) [9], [11], [12]. Sleep study in sleep labs is generally performed under the supervision lab technicians. The patient under test is mounted with several medical grade sensors interfaced with bulky medical grade instruments using long wires during sleep monitoring [9], [11], [12]. Such arrangements are uncomfortable for the patient, limit patient's movements, and definitely impact patient's sleep quality which is being studied. The number of sleep labs across North America is also limited and patients need to wait a long time (around a year or more) for their sleep test after specialist's consultation [12]. A smart, wearable system capable of recording all these physiological parameters and sending the data wirelessly to a nearby computer/smart phone can be a potential solution which may help patients monitor their sleep at home and reduce dependency on sleep labs with long wait times.

1.1 Obstructive Sleep Apnea (or OSA) and Sleep Study Parameters

Obstructive sleep apnea (or OSA) is a health condition where a person suffers from breathing difficulties, loud snoring, and sometimes cessation leading to awakening during sleep [9]–[13]. The usual symptoms of OSA are fatigue, daytime sleepiness, insomnia, morning headaches etc., thus impacting our day-to-day life. If left undiagnosed or untreated, OSA can become an underlying cause of several health issues such as high blood pressure, cardiovascular diseases, obesity, and even degenerative disease like Alzheimer's [13]. The standard method of treating OSA is continuous positive airway pressure (CPAP) devices which are mounted around the nostrils and oral cavity of a patients to help them breath properly during sleep [9], [10]. However, CPAP devices are big, bulky, and uncomfortable to wear for a long time. Moreover, CPAP devices just help in breathing as the patients sleep and do not monitor any physiological parameters during sleep. Another alternative of CPAP devices is the use of oral appliances such as mandibular advancement devices (or MADs) [10]. MADs are special type of rigid oral appliances used for treating OSA patients. MADs are smaller in size and easier to wear in comparison to the conventional CPAP devices. MAD-based treatments are an aid to help in breathing for people suffering from OSA [10]. However, to understand the effectiveness of MAD based treatment for

OSA patients, sleep study during the MAD treatment is recommended by physicians. Therefore, a smart MAD can be a potential solution which not only helps in treating OSA patients but also monitors physiological parameters (intra-orally or some other way) using smart sensors for sleep study. However, the challenges still remain to combine the smart sensors, their read-out circuitry with the MAD and/or any other wearable platform for such sleep study based applications.

1.1.1 Cardiorespiratory Parameters Monitoring during Sleep Study

The cardiorespiratory parameters such as heart-rate, blood oxygen saturation (or SpO_2), breathing can be acquired easily using a photoplethysmography (or PPG) sensor [14], [15]. Several commercial smart watches (e.g. Fitbit, Samsung Smart Watch, Apple Smart Watch etc.) are already using PPG sensors and smart algorithms to measure cardiorespiratory parameters during sleep. In hospitals and clinical setups, these parameters are acquired using both PPG sensors and Electrocardiogram (or ECG) sensors interfaced with sophisticated medical grade measurement systems. Carescape One Monitor by GE Healthcare [16], Intellivue X2 by Phillips [17], Cardiocap 5 by Daytex Ohmeda [18], BeneVision N1 by Mindray [19], SOMNOmedics [20] etc. are some examples of many commercially available cardiorespiratory parameter monitoring devices.

1.1.2 Biopotential Measurements during Sleep Study

Among different biopotentials, Electroencephalogram (or EEG) signals and Electrooculogram (or EOG) signals are standard methods used extensively in many clinical neurocognitive related research such as sleep study, psychiatry, depression, cognitive behaviors, gaze estimations, and in human-computer interface (HCI) based commercial applications [21]–[32]. A brief background of both EEG and EOG methods are presented in the following subsections.

1.1.2.1 Electroencephalography (EEG) Basics: Conventional EEG monitoring involves study of small electrical impulses, ranging from 0.5 μVolts to 100 μVolts of amplitudes, elicited during various brain activities [33], [34]. EEG signals can be measured non-invasively by placing two or more electrodes around the scalp/forehead and interfacing them with the EEG measurement system using long wires. Depending on their frequency responses, EEG signals are classified into

five categories: delta band ranging from 0.1 Hz to 4 Hz, theta band ranging from 4 Hz to 8 Hz, alpha band ranging from 8 Hz to 13 Hz, beta band ranging from 13 Hz to 30 Hz, and gamma band ranging from 30 Hz and above [33], [34]. The spectrum energies of these EEG bands show different behaviours during various brain activities and can be analyzed for sleep stage classifications, e.g. awake stage, light sleep (or N1) stage, deep sleep (or N2) stage, deepest sleep (or N3 stage), and repetitive eye movement (or REM) stage indicating a person in dream [35]. The N1, N2, and N3 stages are also called non-REM stage collectively.

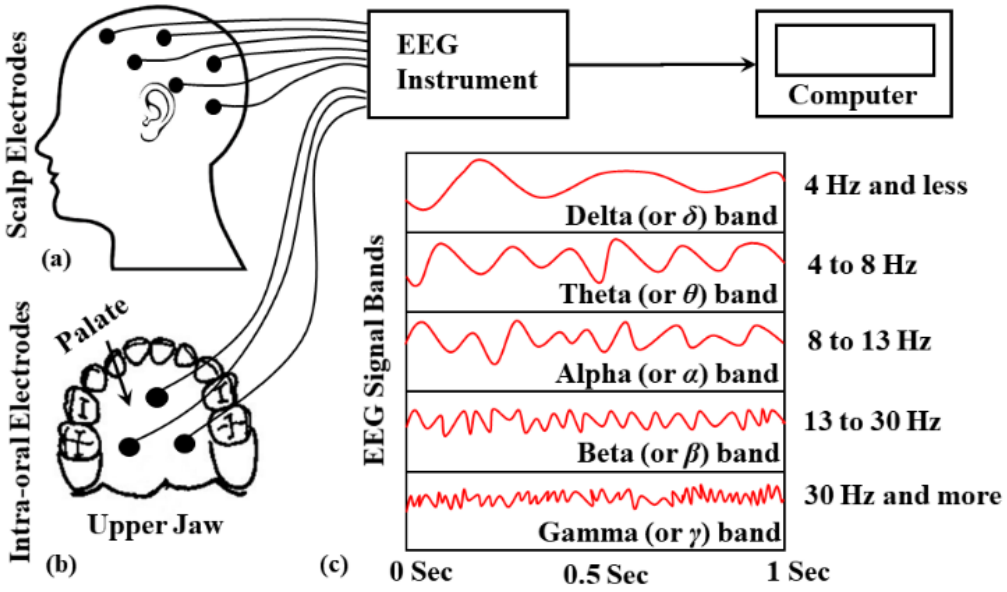

Fig. 1.1. EEG measurement setup: (a) scalp EEG electrodes, (b) intra-oral EEG electrodes, and (c) EEG bands classification.

Scholarly research also reported acquiring EEG signals intra-orally from the palate region [36], [37]. The palate region inside the oral cavity is the closest accessible surface (which does not require incision) to the hypothalamus section of the brain which is responsible for controlling our sleep [38]. One possible way to access the palate for EEG measurements is using some customized oral appliances like MADs with measurement electrodes mounted on them. However, very limited research has been done so far on the possibility of intra-oral EEG measurements and its challenges. *Cohen* reported an oral appliance prototype with EEG electrodes mounted on it and acquired basic

EEG signals involving ‘eye open’ and ‘eye close’ activities [36]. His preliminary intra-oral EEG study showed distinguishable change in intra-oral EEG spectrums during ‘eye open’ and ‘eye close’ activities. In another work by *Radmand*, an oral appliance was reported with different EEG electrode configurations for intra-oral EEG monitoring [37]. However, his work did not report any convincing EEG data acquired intra-orally. Since both the studies involve basic study of intra-oral EEG measurements, their prototypes use long wires coming out of the patient’s mouth to interface the intra-oral EEG electrodes with the EEG measurement systems. Such measurement setups are uncomfortable to wear for long term monitoring and not at all recommended for overnight sleep study. A basic EEG measurement setup showing a simplified schematic of scalp and intra-oral EEG measurements is presented in Fig. 1.1.

1.1.2.2 Electrooculography (EOG) Basics: EOG is another non-invasive technique of acquiring biopotentials developed around the eye during different eye activities such as eye blink, eye wink, and eyeball movements [39], [40]. The eyeball acts like a dipole and generates a potential between the cornea and the retina of an eye [40]. The EOG potential ranges from 0.05 mV to 3.5 mV and has a useful bandwidth of 1 Hz to 40 Hz [29], [40]. The EOG potential changes during horizontal/vertical eye movements and eye blinking and is directly proportional to the displacement of the eyeball from its initial position. The EOG potential can be measured by placing two or more electrodes around the eye. EOG signals are relatively larger in amplitude in comparison to EEG signals and have distinguishable features in the time domain for different eye activities. Therefore, unlike EEG, EOG signals are analyzed in time domain. EOG signals have also been reported to be used in sleep study. The eyeballs move differently during various non-REM (N1, N2, and N3) and REM sleep stages which can be recorded using EOG measurements to detect various sleep stages [26]. A conventional EOG system in clinical setups also uses long wires to interface the EOG electrodes with the measurement system which is uncomfortable to use for long term monitoring such as sleep study. A basic EOG measurement system schematic is presented in Fig. 1.2.

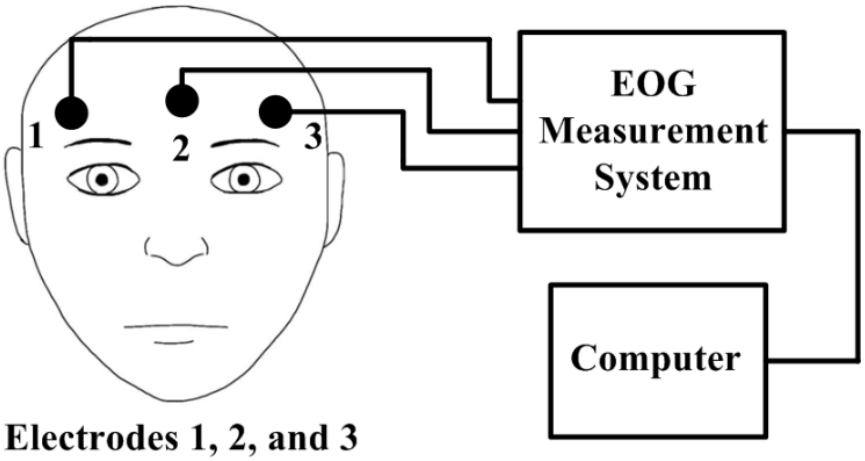

Fig. 1.2. EOG measurement setup with three electrode configuration: electrode 1 as active electrode 1, electrode 2 as reference electrode, and electrode 3 as active electrode 3.

1.1.3 Biopotential Measurement Methodology and Challenges

1.1.3.1 Measurement Electrode Configurations: Any kind of biopotential measurements (e.g. electroencephalogram, electrooculogram, electrocardiogram or ECG, electromyogram or EMG etc.) requires two or more electrodes to sense the biopotentials from the skin surface. The measurement electrodes can be configured in two ways during biopotential measurements: unipolar electrode configuration and bipolar electrode configuration. In unipolar electrode configuration, each measurement channel uses two electrodes, one as active electrode responsible for biopotential sensing with respect to the other electrode known as the ground (or reference) electrode [41]. Unipolar electrode configurations are generally implemented in multi-channel electrode setups with one ground (or reference) electrode for all the channels, which can be configured with either the analog ground of the circuit or the average common-mode signal of all active channels through a driven right leg (or DRL) circuit [42]. In case of bipolar electrode configuration, each measurement channel uses three electrodes with two of them as active electrodes connected in differential configuration at the input stages of the measuring instrument and the third one is known as the ground (or reference) electrode [41], [42]. For bipolar configuration, the ground (or reference) electrode is interfaced with either the analog ground of the measuring instrument or the common-mode node of the two active electrodes through a driven

right leg (or DRL) circuit. Since the active electrodes in bipolar electrode configuration are configured differentially, this configuration is capable of effectively minimizing the common-mode signals such as polarization voltages and DC drifts generated at the skin-electrode contact interface.

The driven right leg (or DRL) circuit is an OpAmp based unity gain buffer implemented to feed the common-mode signals of the active electrodes back to the subject's body through the ground (or reference) electrode. This configuration helps in improving the common-mode rejection response of the entire biopotnetial measurement system [42], [43]. The output of the DRL circuit can be interfaced with a current limiting resistor as a preventive measure before feeding it back to the subject's body, as suggested in biopotential measurements standards involving human subjects set by IFCN [43]. It should be noted that interfacing the ground electrode directly with the circuit ground for biopotential measurements always involves a risk of potential shock due to system failure. Figure 1.3 presents a basic concept of unipolar and bipolar electrode configurations with/without DRL circuit and instrumentation amplifiers.

1.1.3.2 Measurement Electrode Types: The biopotential measurement electrodes can be broadly classified into two types: contact electrodes and non-contact electrodes (or capacitive electrodes) [44]–[46]. Both types have their advantages and disadvantages. Contact electrodes are directly placed on the skin for biopotential measurements. These type electrodes may require the use of electrode gel and skin preparation to minimize the impedance at the skin electrode contact impedances prior to biopotential measurements [44]. Contact electrodes also suffer from polarization voltages at the skin-electrode contact interfaces and are generally coupled with capacitor-resistor based high pass network to lower the impact of polarization voltages during biopotential measurements [44], [46]. Contact electrodes are generally manufactured with biocompatible metals, however they can still cause irritations if the subject under test is allergic to metals [45]. Non-contact electrodes, on the other hand, use a dielectric layer in between the skin and the metal part of the electrode, thus forming a capacitor at the skin-electrode interface. Non-contact electrodes do not suffer from polarization voltages and also do not cause any allergic

reactions to the subject under test [46]. Interfacing non-contact electrodes with the measurement system is easy and requires just a resistor to form the resistor-capacitor based high-pass network at the input stages of the amplifier, which also determines the initial cut-off frequency of the entire system. But the effective capacitances of non-contact electrodes at the skin-electrode interfaces are very small and require very high load resistors (usually > 1 GΩ) at the input stage for the low-frequency biopotential measurement applications [46]. Moreover, given their capacitive nature, non-contact electrodes are extremely sensitive to motions and nearby environmental vibrations [46].

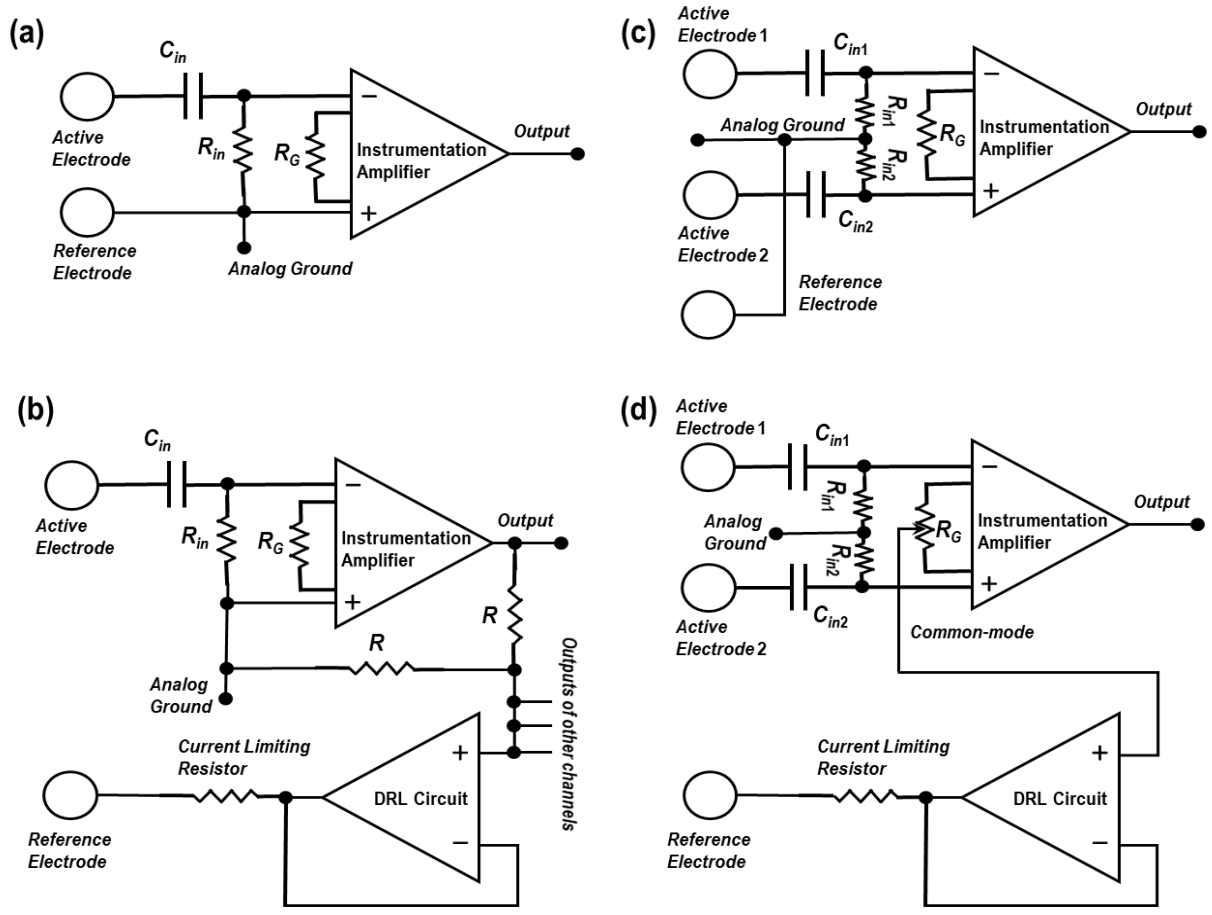

Fig. 1.3. Unipolar and bipolar electrode configurations using Instrumentation Amplifiers: (a) unipolar electrode configuration without DRL circuit, (b) unipolar electrode configuration with DRL circuit, (c) bipolar electrode configuration without DRL circuit, and (d) bipolar electrode configuration with DRL circuit.

It should be noted that IFCN standards recommend the implementation of DRL circuits for safety in the measurement systems involving contact electrodes as they make direct contact with the patient's skin. Biopotential systems with non-contact (or capacitive) electrodes do not require DRL circuit for signal measurements as they do not make direct contact with the patient's skin and do not suffer from polarization voltages.

1.1.3.3 Biopotential System Design Metrics Requirements: The EEG and EOG signals (or any other biopotential signals) have very small amplitudes in the range of 0.5 μVs to a few millivolts [29], [33], [34], [40]. Therefore, biopotential measurement amplifiers (or systems) should be designed to qualify certain circuit parameter standards (such as amplifier input impedance, input-referred noise, CMRR etc.) for a good quality biopotential signal sensing and amplification. Such system metrics are set by global scientific organizations such as International Federation of Clinical Neurophysiology (or IFCN, as mentioned before) [43]. The recommended values of the system metrics recommended by IFCN for EEG and EOG measurements are as follows: first stage amplifier input impedance should be100 MΩ or greater, input-referred noise should be 1.5 μV peak-to-peak over the signal bandwidth 0.5 Hz to100 Hz, and CMRR should be at least 70 dB or above [43].

1.1.3.4 Motion Artifacts in Biopotential Measurements: Biopotential measurements can get severely disrupted by random motions picked up from the patient's voluntary/involuntary movements and nearby vibrations [46]–[50]. The electrode placements and the long interfacing wires (if used) may get affected in the presence of motion, thereby abruptly changing the impedance properties along the measurement path during biopotential sensing. This sometimes results in output saturation of the biopotential measurement system. Motion artifacts are very random in nature and have large dynamic amplitude and frequency responses in comparison to the measured biopotentials (here EEG and EOG signals). Motion artifacts are most likely to appear within the useful bandwidth of the measured biopotential signals, thus making it difficult to remove them using conventional filtering technique [46]–[50]. Therefore, in clinical study, motion corrupted biopotentials are generally inspected visually and discarded from analysis, which is a

tiresome manual job while handling a large amount of data (for example sleep monitoring). Several researchers have already reported different strategies to reduce/eliminate the impact of motion artifacts. In one reported work, use of interdigitated electrodes are proposed for ambulatory EEG measurements to effectively reduce motion artifacts during the measurement [46]. In other reported technique, a combination of both hardware and signal processing, such as using sensor-fusion of biopotential electrodes and accelerometer is reported [51]. The accelerometer is used to capture a reference motion signal which is later used in adaptive filtering for removing motion artifacts from the measured biopotentials. In another report, electrode tissue impedance (or ETI) signals are measured along with the biopotential signal using the same measurement electrodes [49]. In this case, the ETI signal is used as the reference motion signal for adaptive filtering. Each of these methods of reducing the impact of motion artifacts have their own limitations and are exercised depending on the scope of the intended applications.

In conventional multichannel EEG measurements, sophisticated statistical approaches like Independent Component Analysis [51]–[53], Canonical Correlation Analysis (CCA) [52], [54], principal component analysis (PCA) [55] have already been employed successfully to reduce motion artifacts from EEG channels. For single channel EEG systems, decomposition methods like Discrete Wavelet Transform [56], Singular Spectrum Analysis (SSA) [57], Empirical Mode Decomposition (EMD) [58], and Ensemble EMD (EEMD) [59] have been used which generally convert a single channel EEG data into a data matrix. Then the data matrix is further processed through thresholding or multichannel methods like ICA/CCA to separate the motion artifacts from the underlying EEG signatures and remove them effectively [56], [59]. Such statistical methods are powerful enough to effectively remove motion artifacts while preserving the most EEG signal features, but they are computationally expensive [51]–[59]. In some studies, even machine learning algorithms have been implemented for reducing artifacts in EEG measurements, but the models did not perform optimally for effective removal of motion artifacts from motion contaminated EEG signals and require more training datasets for achieving better accuracy [60]–[62]. In this

thesis, we shall also investigate the challenges and possible solutions related to biopotential wearable design and motion artifacts.

1.1.3.5 Other Interferences in Biopotential Measurements: Apart from motion artifacts, any specific biopotential (say EEG) can suffer interferences from other biopotentials (e.g. EOG, EMG etc.) during measurement [51], [52], [59], [60]. These unwanted biopotential interferences can have similar bandwidth like the signal of interest [51], [52], [59], [60]. These interferences can be minimized by placing measurement electrodes to the right locations where the interested biopotential is stronger than the other biopotentials. For example, in EOG measurement, it is recommended to place the EOG electrodes as much close to the eyes as possible for better EOG signal detection with respect of the other nearby interferences such as EEG, EMG potentials. If required, statistical methods like ICA, wavelet decompositions can also be employed to further reduce the other unwanted biopotential interferences [51], [56], [59].

Biopotential measurements also suffer from power-line interferences because the long wires used to interface the measurement electrodes are capable of picking up electro-magnetic noises from any nearby power sources [51]. One way to minimize the power-line noise is to use shorter wires for electrode interfacing. Another way to minimize the power-line noise is implementing and using notch filters (with notch cut-off frequency centered around the power-line noise frequency) in the biopotential measurement systems [51].

1.1.3.6 Conventional Biopotential Measurement Setups and Their Issues: In hospital and clinical setups, biopotentials are generally monitored using bulky and sophisticated measurement systems under the supervision of a technician. NeuroCap^{TM} by *Brain Scientific* [63], EEGO^{TM} Mylab by *ANT Neuro* [64], Bittium NeurOne [65], EOG Pod by *ADInstruments* [66], EOG Amplifier by *Biopac Systems* [67], SOMNOmedics [20] etc. are some examples among several EEG/EOG based commercial systems used in hospitals, clinical setups, and in HCI applications. All these systems use long wires to interface the measurement electrodes during biopotential measurements, thus compromising with the comfort and limiting the mobility of the patient. As mentioned before, biopotential measurements are sensitive to motion and may result in output

saturation during measurements due to the patient's voluntary/involuntary movements. On the other hand, the commercially available electrodes (e.g. Silver, Silver-Silver Chloride, Gold electrodes etc. [44]) are rigid and may cause discomfort to the wearer during long term monitoring. Therefore, the clinical setups are not suitable enough for long term biopotential monitoring such as sleep study.

One potential replacement of rigid electrodes is the use of flexible electrodes and there are several flexible electrodes already reported in many research works [68]–[74]. However, designing flexible electrodes may incur extra cost in the system design. Flexible PCB based wearable devices with flexible electrodes as a part of the PCB, for biopotential measurements, can be a potential solution to the system design challenges mentioned above.

1.2 EEG/EOG Application based Wearable Devices

Several wearable devices involving EEG and EOG based applications have been prototyped and commercialized in the market [75]–[81]. Some of those devices, along with their usefulness and limitations, are reviewed here.

1.2.1 EEG/EOG Application based Commercial Devices

1.2.1.1 The MUSE Headset [75]: The MUSE headset is a popular commercial wearable device known for meditation guidance and sleep study. The headset houses EEG electrodes, PPG sensor, accelerometer, and gyroscope to monitor the important vitals (sleep stages, cardiovascular indices, head movements, and breathing patterns) during sleep. The device also comes with a smart app to provide audio guidance during meditation therapy. The system is compact, implemented on rigid PCBs, and housed inside a rigid platform before integrating the setup with the fabric of the headband. This may cause discomfort to the wearer during overnight monitoring.

1.2.1.2 Dreem EEG Headband [76]: The Dreem EEG headband is another commercial device used for sleep monitoring. This device includes EEG electrodes and PPG sensor for the detection of sleep stages and cardiovascular indices. Just like the MUSE headband, the sensors and the

measurement system are housed inside a rigid platform before integrating them with their special flexible headset to monitor sleep, which may cause discomfort to the wearer. This device also comes with a smart app based audio guidance for the sleep therapy.

1.2.1.3 Sleep Shepherd [77]: Sleep Shepherd is another EEG monitoring based commercial device for sleep monitoring. The device also includes EEG instruments for sleep study and earplugs to provide audio therapy during sleep. The measurement system is implemented on rigid PCBs and requires a rigid housing before integrating them with the fabric headband. Again, this may cause some discomfort to the wearer during overnight monitoring.

1.2.1.4 SmartSleep Headband by Phillips [78]: Deep Sleep is another wearable smart headband designed by Phillips. This smart headband utilises PPG sensor for monitoring cardiorespiratory indices just like other reported devices, and biopotential electrodes positioned behind the ear for EEG/EOG study and sleep stage classification. This device also comes with a smart app to monitor all these sleep indices and also provide special sound therapy to help induce sleep. The headband prototype uses soft fabric to cover up the rigid hardware of the measurement system to provide extra comfort to the wearer.

1.2.1.5 EMOTIV Headsets [79]: The EMOTIV headset is a EEG based headset used for brain-computer interface (or BCI) applications and monitor different mental states such as stress, engagement, interest, relaxation, focus and excitements. This headset is strictly designed for BCI applications and is not intended to be used for any diagnosis or treatment of diseases.

1.2.1.6 JINS MEME [80]: JINS MEME is an EOG based smart eyeglass which includes EOG electrodes and highly sensitive accelerometer/gyroscope sensors. The EOG measurement are used to determine a subject's mental state and concentration. Whereas, the accelerometer/ gyroscope sensor evaluates the body posture suitable for desk jobs. This smart eyeglass also comes with a smart app to monitor these said health metrics.

1.2.1.7 NapWell [81]: NapWell is an EOG based wearable eye mask which monitors sleep and detect sleep onset. The device monitor sleep duration and prepares the wearer to wake up by

lighting up LEDs gradually mimicking the sunrise event. This device prototype is already demonstrated in various science and technology events and is set to be commercialized in near future. The present prototype uses commercial ICs, LEDs, and microcontrollers with rigid PCBs integrated in a soft eye-mask.

1.2.2 EEG/EOG Application based Wearable Prototypes reported in Scholarly Articles:

There are many EEG/EOG based wearable prototype reported in several scholarly articles. The EEG/EOG measurements are employed in sleep related study, mental state analysis, and in assisted technologies [29], [50], [68]–[71], [82]–[85]. Many of these prototypes focused on designing flexible electrodes comfortable to wear [46], [68]–[71], [83], [85]. One prototype also reports EEG system implemented on flexible Polyimide substrate [46]. These wearable sensors are integrated with wearable headbands or eye masks to acquire EEG/EOG data from forehead, scalp, and ear. Some of these wearables are reviewed below.

1.2.2.1 J. Arnin *et al.*, "Wireless-based portable EEG-EOG monitoring for real time drowsiness detection." 35th IEEE EMBC Conference (2013): 4977 – 4980. [68]

In this study, a wearable headband prototype is developed which monitors EEG/EOG signals for drowsiness study. The device uses conductive fabric (92% silver-plated and 8% nylon) based dry electrodes for the measurement and a wireless EEG/EOG measurement device implemented on rigid PCB. The flexible fabric EEG electrodes and the EEG/EOG instrument are then integrated with the wearable headband. This wearable requires skin preparation for a good quality EEG/EOG measurement due to the usage of dry electrodes.

1.2.2.2 J. Xu *et al.*, "A Wearable 8-Channel Active-Electrode EEG/ETI Acquisition System for Body Area Networks." IEEE JSSC 10.9 (2014): 2005 – 2016. [50]

This study proposes a dry active electrode based, 8 channel EEG headset worn around the scalp. This headset is implemented on rigid platform which covers almost the entire scalp. Hence, this device is not suitable for sleep monitoring for sure. This system is more suitable for EEG study in research, clinical, and BCI applications.

1.2.2.3 S. –F. Liang *et al.*, "Development of an EOG-Based Automatic Sleep-Monitoring Eye Mask." IEEE TIM 64.11 (2015): 2977 – 2985. [71]

This study proposes an EOG measurement based eye mask for sleep monitoring. The wearable eye mask houses dry fabric sensor (20% high performance silver and 80 % Polyamide) as EOG electrodes. The wireless EOG acquisition is implemented on rigid board and integrated with the eye mask. Their report also proposes an automated sleep stage classification algorithm. The wearable device is relatively lightweight and comfortable to wear.

1.2.2.4 C. –T. Lin *et al.*, "Forehead EEG in Support of Future Feasible Personal Healthcare Solutions: Sleep Management, Headache Prevention, and Depression Treatment." IEEE Access 5 (2017): 10612 – 10621. [82]

This study proposes a forehead EEG measurement wearable for sleep, stress, depression study. The system uses dry flexible silicon based electrodes (silicon, $AgSiO_2$, gel, and thick-film pastes) for the EEG measurement, whereas the measurement systems are implemented on rigid PCB and housed in a plastic-made EEG headband. The EEG measurement system is relatively big and a bit heavy, which makes the housing of the instrument and the headband bigger in size and heavier. Moreover, the plastic-made headband is also not comfortable to wear for long term monitoring.

1.2.2.5 A. J. Golparvar and M. K. Yacipi, "Electrooculography by Wearable Graphene Textiles." IEEE Sensor Journal 18.21 (2018): 8971 – 8978. [70]

This study reports another EOG based headband integrated with graphene textile based flexible EOG electrodes and a rigid PCB based EOG acquisition system. Although the flexible EOG electrode is comfortable to wear, its conductivity is not good. Therefore, we need very big electrodes (~ 3 cm × 3 cm) for the EOG measurement which is not acceptable. Having big electrodes or acquisition system will force us to have a bigger wearable platform which is undesirable.

1.2.2.6 A. Dabbaghian *et al.*, "A 9.2-g Fully-Flexible Wireless Ambulatory EEG Monitoring and Diagnostics Headband With Analog Motion Artifact Detection and Compensation." IEEE TBCAS 13.6 (2019): 1141 – 1151. [46]

This study presents an 8 channel ambulatory EEG monitoring wearable implemented on a flexible Polyimide board. This is reportedly the first EEG wearable prototype implemented on flexible substrate. The measurement electrodes are printed as pad with the flexible PCB. The wearable system offers the feature for motion artifacts compensation during EEG measurement. It uses interdigitated electrode pairs to sense EEG as well as motion artifacts (if present) from the same location. One of the electrodes in an interdigitated electrode pair is considered to be the EEG sensing path, whereas the other electrode in the same interdigitated electrode pair is considered to be the motion sensing path. The motion signal sensed by the motion electrode is then used to control the variable gain of the EEG sensing path, thereby reducing the impact of motion artifacts. However, their study did not report any real-time measurement of EEG signals using the proposed system.

1.2.2.7 N. Kosmyna *et al.*, "AttentivU: A Wearable Pair of EEG and EOG Glasses for Real-Time Physiological Processing." 16th IEEE BSN Conference (2019): 1 – 4. [29]

This study presents a smart EOG based eyeglass for augment learning activities. The eyeglass frame is designed in a stylish way for social acceptance. The smart system uses commercial silver/silver chloride electrodes for the EOG measurement. The compact EOG instrument, electrodes, wiring, and the battery are integrated very within the eyeglass frame without compromising its stylish appearance. The smart wearable can be useful in studying drowsiness, stress, assisted technologies etc., except for sleep study.

1.2.2.8 C. Beach *et al.*, "A Graphene-Based Sleep Mask for Comfortable Wearable Eye Tracking." 41st IEEE EMBC Conference (2019): 6693 – 6696. [83]

This study proposes another EOG measurement based eye mask. The flexible EOG electrodes are made of graphene oxide based nylon textile. Here also, the wireless EOG acquisition is

implemented on rigid board and integrated with the eye mask. Just like other textile based electrodes, this flexible electrodes also have relatively low conductivity, which is undesirable for a good quality EOG detection.

1.2.2.9 S. –W. Kim *et al.*, "Wearable Multi-Biosignal Analysis Integrated Interface With Direct Sleep-Stage Classification." IEEE Access 8 (2020): 46131 – 46140. [84]

This study proposes a multichannel biopotential measurement system for measuring EEG, EOG, and EMG signals from forehead. All these measured biopotentials are later processed for sleep stage classification. They have also developed their own biopotential sensing IC to extract all these biopotential features from the measured signal. The wearable uses commercial rigid electrodes for the measurement and the complete wireless acquisition system is implemented on rigid PCB. The rigid electrodes and the rigid PCB board are later integrated with the wearable headband. The wearable headband is made of rubber and mesh materials. This study basically focuses on the performance validation of their own IC designed for biopotential measurement.

1.2.2.10 S. Rostaminia *et al.*, "PhyMask: Robust Sensing of Brain Activity and Physiological Signals During Sleep with an All-textile Eye Mask." ACM Transaction on Computing for Healthcare 3.3 (2022): 1 – 35. [85]

This study proposes a textile fabric based eye mask integrated with flexible EOG/EEG electrodes, flexible pressure sensors, and the wireless data acquisition implemented on rigid PCB. The flexible EOG/EEG electrodes are reusable, conductive thread-based, hydrogel electrodes. The flexible electrodes are reported to have similar sensitivity like commercial rigid electrodes. The system also uses fabric-based piezoionic pressure sensors for detecting ballistic signal from heartbeats, thus acquiring data for cardiovascular parameter monitoring. It should be noted that the flexible electrodes require gel for proper EOG/EEG detection using the wearable system.

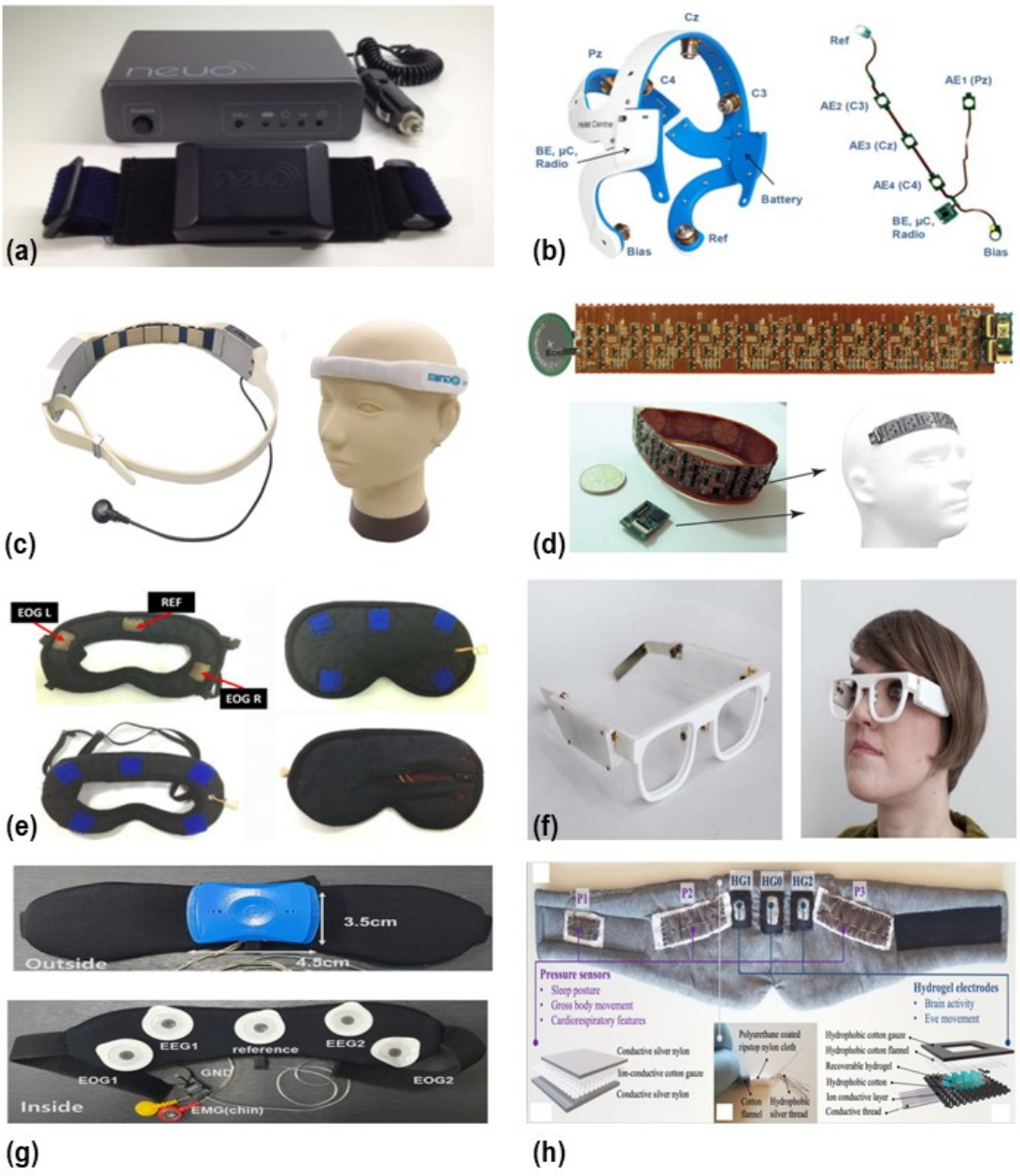

Fig. 1.4. Some of the reviewed non-commercial EEG/EOG wearables are reconstructed and presented here: (a) reprinted with permission from [68] © 2013 IEEE, (b) reprinted with permission from [50] © 2014 IEEE, (c) reprinted with permission from [83] © 2017 IEEE, (d) reprinted with permission from [46] © 2019 IEEE, (e) reprinted with permission from [71] © 2015 IEEE, (f) reprinted with permission from [29] © 2019 IEEE, (g) reprinted with permission from [84] © 2020 IEEE, and (h) reprinted with permission from [85] © 2022 ACM, respectively.

TABLE 1.1

COMPARISON OF THE STATE-OF-THE-ART COMMERCIAL/NON-COMMERCIAL WEARABLES FOR EEG/EOG BASED APPLICATIONS AND SLEEP MONITORING REPORTED IN THIS THESIS

The Work	EOG EEG	Heart-Rate (1), SpO_2 (2), Breath (3)	Any Other Indices	Electrodes	System PCB	Motion Artifacts Removal	Design	Wearable Type	Application
COMMERCIAL EEG/EOG AND NON-EEG/EOG WEARABLES									
MUSE [75]	Both	All	Head/Body Movements	Rigid	Rigid	NM	Wearable, Rigid Structure	Headband	Sleep Monitoring, Meditation
DREEM [76]	Both	3	Head/Body Movements	Rigid	Rigid	NM	Wearable, Rigid Structure	Headband	Sleep Monitoring
Sleep Shepherd [77]	Both	None	None	Rigid	Rigid	NM	Wearable, Semi Rigid Structure	Headband	Sleep Monitoring
Phillips Smart Sleep [78]	Both	All	None	Rigid	Rigid	NM	Wearable, Rigid Structure	Headband	Sleep Monitoring
EMOTIV [79]	EEG	None	None	Rigid	Rigid	NM	Wearable, Rigid Structure	Headset	Brain-Computer Interface
JINS MEME [80]	EOG	None	None	Rigid	Rigid	NM	Wearable, Rigid Structure	Eyeglasses	Brain-Computer Interface
NapWell [81]	EOG	None	None	**Flexible	Rigid	NM	Wearable, Semi Rigid Structure	Eye-mask	Sleep Monitoring
NON-COMMERCIAL EEG/EOG WEARABLES REPORTED IN SCHOLARLY ARTICLES									
J. Arnin *et. al.* [68]	Both	None	None	**Flexible	Rigid	No	Wearable, Semi Rigid Structure	Headband	Sleep Monitoring
J. Xu *et. al.* [50]	EEG	None	ETI	Rigid	Rigid	No	Wearable, Rigid Structure	Headset	Brain-Computer Interface

S. –F. Liang *et. al.* [71]	EOG	None	None	**Flexible	Rigid	No	Wearable, Semi Rigid Structure	Eye-mask	Sleep Monitoring
C. –T. Liu *et. al.* [82]	EEG	None	None	**Flexible	Rigid	No	Wearable, Semi Rigid Structure	Headband	Sleep Monitoring, Depression
A. J. Golparvar *et. al.* [70]	EOG	None	None	**Flexible	Rigid	No	Wearable, Semi Rigid Structure	Headband	Brain-Computer Interface, Sleep
A. Dabbaghian *et. al.* [46]	EEG	None	None	**Flexible	**Flexible	**YES	**Wearable, Flexible	Headband	Brain Signals, Epilepsy
N. Kosmyna *et. al.* [29]	EOG	None	None	Rigid	Rigid	No	Wearable, Rigid Structure	Eyeglasses	Stress, Drowsiness
C. Beach *et. al.* [83]	EOG	None	None	**Flexible	Rigid	No	Wearable, Semi Rigid Structure	Eye-mask	Sleep Monitoring
S. –W. Kim *et. al.* [84]	Both	None	EMG	Rigid	Rigid	No	Wearable, Semi Rigid Structure	Headband	Sleep Monitoring
S. Rostaminia *et. al.* [85]	Both	1	None	**Flexible	Rigid	No	Wearable, Semi Rigid Structure	Eye-mask	Sleep Monitoring

** refers to the advantageous features of the wearables.
NM : Not Mentioned.

1.2.3 A Comparative Study of all the EEG/EOG Wearables reported above:

In most of the reported wearables, the biopotential instrument is implemented on rigid PCB, except one in [46]. In some work, the focus was to design a comfortable flexible electrode for biopotential measurements, which added additional cost for a wearable design [68], [70], [71], [83], [85]. In other works, the wearable platform is designed carefully with flexible, stretchable materials to provide comfort to the wearer [46], [68], [70], [71], [82]–[85]. However, none of the wearables reported in the scholarly articles addressed the impact of motion artifacts during biopotential recording. Only one work is reported to have smart hardware arrangements for motion artifacts compensation [46]. But their study did not report any real-time biopotential measurements. In most of the commercial EEG/EOG headsets, the electrode and measurement system housing part of the wearable platform are relatively rigid thus limiting the skin conformability of the wearable device. Therefore, skin conformability, flexibility of the measurement electrodes and the measurement systems are important for smart wearables. Fig. 1.4 presents some of the non-commercial EEG/EOG wearable prototypes discussed here. Table 1.1 summarises the usefulness and of all the commercial and non-commercial biopotential wearables discussed here.

1.3 Intra-Oral based Wearable Devices

In recent healthcare technologies, intra-oral wearables (such as dental retainers, mouthguards, MADs etc.) are getting popular among researchers with potential of measuring physiological parameters and in assisted technologies [86]−[93]. In some studies, dental retainers are employed for integrating tongue movement-based sensor interface to use in BCI applications [90], [91]. In other studies, intra-oral locations are studied for potential location of acquiring physiological parameters such as cardiovascular parameters, breath, and even EEG signals [92], [93]. Oral cavity is less likely to experience disturbances due to users' body movements and can be an ideal location for smart sensor placements. Such intra-oral wearables are comfortable to wear, and several commercial oral appliances are already available for dental therapy and sleep disorder treatment applications such as teeth alignment, temporomandibular joint pain, teeth grinding (or bruxism),

snoring, OSA, and concussion detections [86]−[89]. Some of these intra-oral wearable devices, along with their usefulness and limitations, are reviewed here.

1.3.1 Commercial Oral Appliances and their Applications

1.3.1.1 Whole You [86]: Whole You is a popular organization known for providing custom-fitted mouthguard based oral treatments related to teeth alignment, temporomandibular joint pain, teeth grinding (or bruxism), and studying sleep. However, their oral appliances are not directly available to buy from the market and are provided only to their patients. Their MADs are just the usual oral appliances for treatment, and do not have any smart sensors integrated with the device.

1.3.1.2 SomnoMed [87]: SomnoMed is another organization known for providing custom-fitted mouthguard based oral treatments related to teeth grinding (or bruxism), snoring, and sleep apnea. The organization provides oral treatments and build customized MADs for their patients. Their oral appliances are available to buy from local distributers after consultations with sleep specialists. Just like Whole You, SomnoMed also provides the usual oral appliances for treatment, and do not have any smart sensors integrated with the device.

1.3.1.3 Sisu Sense [88]: Sisu Sense is a company which provides an accelerometer sensor and high-performance wireless processor based smart, flexible oral appliance. This device is designed specifically for athletes to monitor the event and impact of any head/neck injuries that may happen during sports. The product also comes with a smartphone app which records the details and impact of an injury, with a feature to notify the families of the user in case of serious head/neck trauma.

1.3.1.4 Prevent Biometrics [89]: Prevent Biometrics is another company which provides accelerometer sensor, wireless charging unit, and high-performance wireless processor based smart oral appliance. This device is also designed for athletes to prevent and monitor head impact data in real time and uses an app-based algorithm to calculate the force, location, direction and number of impacts during sports.

1.3.2 Intra-oral Wearable Prototypes reported in Scholarly Articles

The above study shows a fairly small fraction of the tremendous possibilities on intra-oral based wearable applications. There are other intra-oral wearable prototypes used in intra-oral assisted technologies, cardiorespiratory measurements, and sleep postures reported in scholarly articles and some of them are reviewed below.

1.3.2.1 H. Park *et. al*, "A Wireless Magnetoresistive Sensing System for an Intra-Oral Tongue-Computer Interface." IEEE ISSCC (2012): 124 – 126. [90]

In this study, a wireless, dental retainer (oral appliance) based wearable prototype is developed for intra-oral tongue computer interface (or ITCI). In this prototype, magnetoresistive sensors are used to track the tongue movements in different directions and send the sensor data wirelessly to the computer. The sensor data can be interpreted as commands and employed in ITCI based assisted applications for specially abled persons.

1.3.2.2 E. R. Lontis *et. al*, "Wheelchair Control With Inductive Intra-Oral Tongue Interface for Individuals With Tetraplegia." IEEE Sensors Journal 21.20 (2021): 22878 – 22890. [91]

This study presents another wireless intra-oral tongue computer (or ITCI) interface with inductive sensors used in assisted wheelchair. The inductive sensors, the read-out circuitry, and battery are encapsulated in a dental retainer. The sensor senses the tongue movements in different directions and sends command wirelessly to the control unit of the assisted wheelchair. This smart ITCI interface for assisted wheelchair control is developed for patients suffering from tetraplegia, a paralytic condition where patients are unable to voluntary move their upper and lower body parts.

1.3.2.3 S. Nabavi and S. Bhadra, "Oral Cavity Pressure Measurement-based Respiratory Monitoring System with Reduced Susceptibility to Motion Artifacts." 42nd IEEE EMBC Conference (2021): 5900 – 5904. [92]

In this study, a MAD based wearable integrated with pressure sensor for studying respiration. Pressure sensors are immune to motion artifacts or any other environmental parameters. The pressure sensor output in this study only depends upon the pressure created by airflow during

inhaling and exhaling. The wearable prototype is demonstrated for effective measurement of breathing activity and cessation, and may have potential application to monitor breathing patterns in OSA patients. However, the design requires the sensor to be placed in the middle of the oral cavity, which may create discomfort to the wearer. The prototype was developed by Dr. Seyedfakhreddin Nabavi in our lab.

1.3.2.4 S. Nabavi and S. Bhadra, "Smart Mandibular Advancement Device for Intraoral Monitoring of Cardiorespiratory Parameters and Sleeping Postures." IEEE TBCAS 15.2 (2021): 248 – 258. [93]

In this study, a smart MAD based wearable is prototyped for measuring cardiorespiratory parameters (e.g. heart-rate, SpO_2, and breathing) using PPG sensor and sleep postures using accelerometer sensor. The prototype was developed in our lab by my colleague Dr. Seyedfakhreddin Nabavi. And the initial study for acquiring cardiorespiratory signals using PPG sensors was done by me [85]. Later, Dr. Seyedfakhreddin Nabavi conducted the further research on acquiring better quality intra-oral PPG signals intra-orally, extracting the cardiorespiratory parameters from the acquired signal, and developed this prototype, which may have potential applications for treating OSA patients.

1.3.3 A Comparative Study of all the intra-oral Wearables reported above:

In most of the reported intra-oral wearables, only a handful uses smart sensors for physiological parameter measurements. Most of the commercially available intra-oral wearables reported above are used for usual oral treatments as reported above [86]−[89]. However, the reported non-commercial smart MAD prototypes already indicate immense potential in future healthcare applications. Table 1.2 summarises the usefulness of all the commercial and non-commercial intra-oral wearables discussed here.

TABLE 1.2

COMPARISON OF THE STATE-OF-THE-ART COMMERCIAL/NON-COMMERCIAL ORAL APPLIANCES (OR MOUTHGUARDS) REPORTED IN THIS THESIS

The Work	Smart Sensors	Cardiorespiratory Indices	Any Other Indices	Oral Appliance Type	Application
COMMERCIAL ORAL APPLIANCES					
Whole You [86]	—	—	—	Mouthguard, MAD	Teeth Grinding, Snoring, Temporomandibular Pain, Sleep Study
SomnoMed [87]	—	—	—	Mouthguard, MAD	Teeth Grinding, Snoring, Temporomandibular Pain, Sleep Study
Sisu Sense [88]	Accelerometer	—	Concussions	Mouthguard	Head Impact Monitoring in Sports
Prevent Biometrics [89]	Accelerometer	—	Concussions	Mouthguard	Head Impact Monitoring in Sports
NON-COMMERCIAL ORAL APPLIANCES REPORTED IN SCHOLARLY ARTICLES					
H. Park *et. al.* [90]	Magnetiresistive Sensor	—	—	Dental Retainer	Intra-oral Tongue Computer Interface for Assisted Technology
E. R. Lontis *et. al.* [91]	Inductive Sensor	—	—	Dental Retainer	Intra-oral Tongue Computer Interface for Assisted Technology
S. Nabavi *et. al.* [92]	Accelerometer, PPG Sensor, Temperature	Heart-rate, SpO_2, Breath	Temperature, Sleep Postures	MAD	OSA Treatment and Sleep Study
S. Nabavi *et. al.* [93]	Pressure Sensor	Only Breath	—	MAD	Breath Monitoring in Sleep and OSA Treatment

1.4 Motivation

In the context of the literature review done here, wearable biopotential measurement systems impose several issues in terms of design, usage, and performance. Most of the commercial EOG/EEG measurement devices use rigid electrodes and rigid PCB based measurement systems, which definitely makes the sensor and system integration challenging in wearable platforms (e.g. headset, headband, and eye-masks) [75]−[81]. Rigid electrodes and system PCBs require rigid housing in the wearable platform, causing discomfort to the wearers [75], [76], [78]−[80]. Sometimes soft materials are also padded around the sensor and system housing to provide extra comfort to the wearer, thus making the wearable platform bigger and heavier [77], [81]. Use of rigid electrodes and wearable platforms also raises the concern of skin conformability during usage. Some research works have recommended textile/fabric based flexible electrodes for EOG/EEG measurements. However, these flexible electrodes are reported to have relatively less sensitivity in comparison to the commercial rigid electrodes, designed in bigger size, and require electrode gel to sense a good quality biopotential [68]−[73]. They further increases the size, weight, and cost of the wearable platforms, thus making such designs less desirable for commercialization. Most of the EOG/EEG wearables reported here also suffer from motion artifacts, which is another limitation of biopotential systems [50], [68]−[71], [82]−[85].

In the first part of our research, we are motivated to resolve some of the limitations of the wearable biopotential systems mentioned above. Our primary focus is to propose a flexible and lightweight biopotential measurement system which is skin-conformable along the curvature of forehead, so that it can be worn by different people comfortably. The system can be integrated easily in fabric-based wearable such as headbands or eye-masks. Therefore, we shall also be looking into the possibility of designing flexible electrodes with improved biopotential sensing capability. Flexible PCB based electronics systems are lightweight, skin conformable, and can be a potential solution to our wearable design. We shall investigate the possibility of printing the measurement electrodes and implementing the measurement system on the same flexible substrate.

The system performance and limitations will be thoroughly tested for acquiring real-time biopotential signals, such as EOG.

In the next part of our research, we shall try to address the issues related to motion artifacts during EOG measurements, which were not investigated in our previous research. We shall try to propose smart circuit arrangements capable of mitigating motion artifacts during real-time EOG measurements. We shall also exercise the possibility of using non-contact (or capacitive) electrodes in our flexible system as they are superior in sensing biopotentials and do not require any electrode gel or skin preparations. This may help us further improving the overall performance of the forehead based, wearable EOG measurement system.

Even after niche design and engineering solutions to smart headband/eye-mask based wearables, users still find them somewhat uncomfortable to wear which compromises their sleep quality. Moreover, wearables like headbands or eye-masks are prone to displacements due to body/head movements during sleep which can change the smart system's placement integrated within the wearable and corrupt its recorded data. Another alternative approach to design sleep monitoring devices can be oral appliances (e.g. mouthguards, MADs etc.). Oral appliances are comfortable to wear and used in several dental and sleep therapy [10], [86]−[89]. On the other hand, EEG signals are also reported to have been acquired intra-orally from the palate region [36], [37]. This has motivated us to further research and investigate the possibility of designing a smart oral appliance (MAD in our application) integrated with EEG electrodes and the measurement system for acquiring intra-oral EEG signals. However, intra-oral motions (such as tongue movements, teeth grinding, and gulping) can still impose some limitations for intra-oral EEG measurements. Therefore, we shall study the possibility of implementing smart sensor-fusion based technique to address the issues related to intra-oral motions. If the proposed smart MAD is implemented successfully, it may have applications in intra-oral EEG based sleep studies and in treatment of OSA patients.

1.5 Contribution and Structure

1.5.1 Contribution

Major contributions of the research described in this thesis are listed below.

- **Design of flexible electrodes:** One of the key challenges in biopotential wearable systems is to design flexible, skin conformable electrodes which are comfortable to wear and has similar sensitivity to the commercial electrodes. For our EOG/EEG wearable prototypes, we have designed flexible gold electrodes printed on Polyimide substrate. The electrodes are designed both in contact and non-contact configurations. The contact gold electrodes showed similar sensitivity like commercial gold electrodes. Whereas, the non-contact (or capacitive) gold electrodes are found out to be at least 50 times (or more) sensitive in comparison to commercial contact gold electrodes. In our EOG based wearable prototypes, the flexible electrodes are printed as pads on the bottom layer of the wearable PCB board, thus easily integrating them with the measurement system directly. For our smart MAD based prototype, the flexible gold electrodes are mounted on the MAD itself with biocompatible adhesive. Given their flexibility and skin-conformability, the intra-oral EEG electrodes do not cause any discomfort to the wearer.
- **Flexible PCB based EOG wearables:** Our all EOG/EEG based prototypes are implemented on flexible Polyimide substrate. For the EOG prototypes, four-layer flexible PCBs are designed with the bottom layer containing printed contact/non-contact measurement electrodes and the top layer with the implemented biopotential acquisition unit. The second layer as the circuit ground plane and the third layer with active shielding between the discrete circuit components on the top layer and the measurement electrodes on the bottom layer. The EOG wearables are battery operated, suitable for long-term monitoring, and send data wirelessly using a Bluetooth 5.0 transceiver. The first EOG prototype uses contact electrodes and requires electrode gel for a good quality EOG detection. Whereas, the second EOG prototype uses non-contact electrodes which overcomes the sensitivity issue of the first prototype. In this prototype, the printed

flexible electrode pairs on the bottom layer are covered with a biocompatible kapton film, thus making them non-contact (or capacitive) electrodes Both the flexible substrate based EOG wearable prototypes are first of their kind ever reported in scholarly articles. Given their flexible substrates, both the prototypes are skin conformable and can be easily integrated with headbands/eye-masks.

- **Impact of motion artifacts on EOG measurements:** Motion artifacts are considered to be a major issue during biopotential measurements. Our first EOG prototype do not have any special circuit arrangements to be able to measure EOG in the presence of motion artifacts. However, in our second EOG prototype, this issue has been addressed. The second EOG prototype uses two parallel electrode pairs in differential configuration to reduce the impact of motions at the first input amplifier stage while picking up EOG potentials. This prototype is capable of capturing EOG potentials in the presence of slow to moderate level motion artifacts.
- **Study of intra-oral EEG signals:** This thesis also reports a detailed study of intra-oral EEG signals for the first time. Intra-oral EEG signals have been reported in a few scholarly articles in the past, but their detailed study and measurement challenges are never reported. In this study, various intra-oral locations are explored to acquire good quality intra-oral EEG signals. The intra-oral EEG signals are acquired using the flexible gold contact electrodes designed for our research. The study also reports the possible sources of intra-oral motion artifacts that can disrupt intra-oral EEG signals during measurements. Later, a smart mandibular advancement device (MAD) based wearable prototype is also developed to measure intra-oral EEG signals in the presence/absence of intra-oral motion artifacts using a single channel EEG acquisition. The smart MAD prototype uses EEG electrodes, accelerometer sensor, and the sensor read-out circuitry implemented on a flexible Polyimide substrate. The sensor read-out circuitry is battery operated and uses Bluetooth 5.0 transceiver for sending intra-oral EEG and motion signals wirelessly. The flexible substrate can be easily integrated along the curvature of the wearable MAD. The smart MAD based intra-oral EEG wearable prototype is also

first of its kind ever reported in scholarly articles which is capable of measuring intra-oral EEG and motion signals simultaneously. The smart wearable MAD is comfortable to wear and have potential in intra-oral EEG based applications, such as sleep study.

- **MATLAB based algorithm to reduce motion artifacts in intra-oral EEG signals:** Given the limited space inside oral cavity, the smart MAD prototype uses only a single channel EEG acquisition for intra-oral EEG measurements. Single channel EEG data generally requires sophisticated signal processing methods to reduce motion artifacts. In this work, we proposed a sensor-fusion based algorithm implemented in MATLAB for reducing motion artifacts in intra-oral EEG signals. The algorithm first uses the accelerometer data to detect the presence of any intra-oral motion activities and identify their time locations. If any motion events are detected, the then algorithm then decomposes the intra-oral EEG signal into independent components using empirical decomposition method (EMD) followed by independent component analysis (ICA). Then the decomposed independent components containing the motion signatures are mapped with the accelerometer data to locate motion corrupted data segments. Next the ICA components are denoised by nullifying the motion corrupted data segments. A motion artifacts reduced intra-oral EEG signal is then reconstructed using inverse ICA-EMD method. The effectiveness of the proposed algorithm is also validated in this study using qualitative and quantitative approaches. The smart MAD prototype, along with the proposed algorithm, is capable of measuring intra-oral EEG signals in the presence/absence of motion artifacts.

1.5.2 Structure

This thesis is primarily supported by the three journal articles published or submitted by the author. Chapter 1 presents a detailed introduction and literature review on wearable devices with the potential applications of sleep monitoring, commercially available wearable devices for sleep monitoring, wearable prototypes for sleep monitoring reported in recent scholarly articles, their design limitations with detailed reasoning, and the motivation behind the development of

biopotential measurement based wearable applications for sleep monitoring. Chapter 2 presents our first wearable, flexible prototype integrated with the EOG electrodes and the EOG measurement system. The system design approaches are described in detail and important system metrics such as gain, noise, common-mode rejection ratio (or CMRR) are quantified. The system performance is validated for the detection of various EOG eye activities. The system is also demonstrated for a potential sleep study application based on EOG measurements. Chapter 3 presents our second wearable, flexible prototype for EOG measurement capable of effectively suppressing motion artifacts while recording EOG signals. The system design approaches are described in detail and important system metrics such as gain, noise, CMRR are quantified. The system is also validated by recording EOG signals in the presence of motion artifacts and capable of capturing eye activities in the presence of motion artifacts. Chapter 4 presents smart MAD based prototype with sensor-fusion of EEG electrodes and accelerometer sensor. The smart MAD prototype is capable of measuring intra-oral EEG signals in the presence of intra-oral motions (e.g. tongue movements, teeth grinding, and gulping). The system design approaches are described in detail and important system metrics such as gain, CMRR are quantified. A MATLAB based algorithm is also developed to reduce intra-oral motion artifacts during intra-oral EEG measurements effectively. The smart MAD along with a MATLAB based algorithm, are validated both qualitatively and quantitatively by recording intra-oral EEG signals in the presence of intra-oral motions for ‘eye open’ and ‘eye close’ activities. Chapter 5 presents comprehensive scholarly discussion about the proposed biopotential measurement system prototypes, their design approaches, usefulness, and limitations. Finally, the thesis work is concluded in Chapter 6, with directions to future work.

1.6 List of Publications

The contents of this thesis are presented in three publications that include three journal articles, first two of them are published and the third one is submitted recently. Additionally, the author authored six additional conference publications related to the thesis and co-authored in three

additional conference publications, not related to this thesis. The following is a list of publications and contributions of the author.

1.6.1 Peer-reviewed Journal Articles:

- **Debbarma, Shibam,** and Sharmistha Bhadra. "*A Lightweight Flexible Wireless Electrooculogram Monitoring System With Printed Gold Electrodes."* IEEE Sensors Journal 21.18 (2021):20931–20942.
- **Debbarma, Shibam,** and Sharmistha Bhadra. *"A Flexible Wearable Electrooculogram System with Motion Artifacts Sensing and Reduction."* IEEE Transactions on Biomedical Circuits and Systems (TBCAS) 16.2 (2022): 324–335.
- **Debbarma, Shibam,** and Sharmistha Bhadra. *"A Sensor-Fusion Method for Measuring Motion Artifact Free Intra-oral EEG Signal."* Submitted in IEEE Sensors Journal (2023).

1.6.2 Peer-reviewed Conference Articles as a First Author:

- **Debbarma, Shibam,** and Sharmistha Bhadra. *"Intraoral Monitoring of Photoplethysmogram Signal to Estimate Cardiorespiratory Parameters."* 2020 2nd International EAI Healthwear Conference. Springer (2021).
- **Debbarma, Shibam,** Seyedfakhreddin Nabavi, and Sharmistha Bhadra. *"Multi-level Motion Artifacts Reduction in Photoplethysmography Signal using Singular Value Decomposition."* 2020 2nd International EAI Healthwear Conference. Springer (2021).
- **Debbarma, Shibam,** Seyedfakhreddin Nabavi, and Sharmistha Bhadra. *"A Wireless Flexible Electrooculogram Monitoring System With Printed Electrodes."* 2021 IEEE International Instrumentation and Measurement Technology Conference (I2MTC). IEEE, 2021.
- **Debbarma, Shibam,** and Sharmistha Bhadra. *"A Smart Mandibular Device for Intra-oral Electroencephalogram Monitoring."* 2021 IEEE Sensors Conference. IEEE, 2021.

- **Debbarma, Shibam,** and Sharmistha Bhadra. *"A Wearable Electrooculogram System with Parallel Motion Artifact Sensing and Reduction."* 2022 International Symposium on Circuits and Systems (ISCAS) Conference. IEEE, 2022.
- **Debbarma, Shibam,** and Sharmistha Bhadra. *"An Intra-oral EEG System with Accelerometer For Motion Artifact Free EEG Recording."* 2023 IEEE International Instrumentation and Measurement Technology Conference (I2MTC). IEEE, 2023. [Presented].

1.6.3 Peer-reviewed Conference Articles as a Co-Author:

- Seyedfakhreddin Nabavi, **Debbarma, Shibam,** and Sharmistha Bhadra. "*Measurement of Cardiac Parameters by Motion Artifacts Free Photoplethysmography Signals."* 2020 IEEE International Instrumentation and Measurement Technology Conference (I2MTC). IEEE, 2020.
- Seyedfakhreddin Nabavi, **Debbarma, Shibam,** and Sharmistha Bhadra. *"A Smart Mandibular Advancement Device for Intraoral Cardiorespiratory Monitoring."* 2020 42nd Annual International Conference of the IEEE Engineering in Medicine & Biology Society (EMBC). IEEE, 2020.
- Han Cat Nguyen, **Debbarma, Shibam,** and Sharmistha Bhadra, *"Flexible Fabric Electrodes Integrated with Mouthguard for Electroocoulogram Measurement."* 2023 IEEE International Conference on Flexible, Printable Sensors and Systems (FLEPS 203). IEEE, 2023. [accepted]

References

[1] S. M. Iqbal *et al.*, "Advances in healthcare wearable devices," *npj Flexible Electronics*, vol. 5, no. 1, pp. 1–14, 2021.

[2] A. Palumbo, P. Vizza, B. Calabrese, and N. Ielpo, "Biopotential signal monitoring systems in rehabilitation: A review," *Sensors*, vol. 21, no. 21, p. 7172, 2021.

[3] C. Ernsting *et al.*, "Using smartphones and health apps to change and manage health behaviors: A population-based survey," *J. Med. Internet Res.*, vol. 19, no. 4, p. e101, Apr. 2017.

[4] T.-C. Lu *et al.*, "Healthcare applications of smart watches," *Applied clinical informatics*, vol. 7, no. 03, pp. 850–869, 2016.

[5] G. Udovičić, A. Topić and M. Russo, "Wearable technologies for smart environments: A review with emphasis on BCI," *2016 24th Int. Conf. Softw. Telecommun. & Comput. Netw.* (SoftCOM), Split, Croatia, 2016, pp. 1-9.

[6] H. K. Chiang, M. Patel, D. J. Lesczyszyn, and G. G. Demerjian, "Dental Sleep Appliance Therapy for the Treatment of Obstructive Sleep Apnea," in *Dental Sleep Medicine: A Clinical Guide*, California, USA: Springer, 2022, pp. 233–266.

[7] S. Saganowski *et al.*, "Review of consumer wearables in emotion, stress, meditation, sleep, and activity detection and analysis," *arXiv preprint arXiv:2005.00093*, 2020.

[8] V. Hoffstein, "Review of oral appliances for treatment of sleep disordered breathing," *Sleep Breath.*, vol. 11, no. 1, pp. 1–22, 2007.

[9] N. M. Punjabi, "The epidemiology of adult obstructive sleep apnea," *Proc. Amer. Thoracic Soc.*, vol. 5, no. 2, pp. 136–143, 2008.

[10] D. J. Bratton, T. Gais, A. M. Wons, and M. Kohler, "CPAP vs mandibular advancement devices and blood pressure in patients with obstructive sleep apnea: a systematic review and meta-analysis," *J. Amer. Med. Assoc. (JAMA)*, vol. 314, no. 21, pp. 2280–2293, 2015.

[11] K. Sutherland *et al.*, "Oral appliance treatment for obstructive sleep apnea: an update," *J. Clin. Sleep Med.*, vol. 10, no. 2, pp. 215-27, Feb 2014.

[12] W. W. Flemons *et al.*, "Access to diagnosis and treatment of patients with suspected sleep apnea," *World J. Am. J. Respir. Crit. Care Med.*, vol. 169, pp. 668–672, Mar. 2004.

[13] R. A. Sharma *et al.*, "Obstructive sleep apnea severity affects amyloid burden in cognitively normal elderly: a longitudinal study," *World J. Am. J. Respir. Crit. Care Med*., vol. 197, no. 7, pp. 933-943, April 2017.

[14] J. G. Webster, *Design of Pulse Oximeters*, New York: Taylor & Francis, 1997.

[15] A. I. J. Brain, "Combined laryngeal mask and reflectance oximeter", US patent US005282464A, Feb. 1, 1994.

[16] "CARESCAPE ONE Monitor," gehealthcare.ca. https://www.gehealthcare.ca/en-ca/products/carescape-one (accessed Mar. 15, 2023).

[17] "Intellivue X2," philips.ca. https://www.philips.ca/healthcare/product/HC865039/intellivue-mms-x2-measurement-module-monitor (accessed Mar. 15, 2023).

[18] "Cardiocap 5," dremed.com https://www.dremed.com/datex-ohmeda-cardiocap-5/id/1691 (accessed Mar. 15, 2023).

[19] "BeneVision N1," mindray.com https://www.mindray.com/en/media-center/press/mindray-launches-benevision-n1-for-uninterrupted-monitoring-during-intra-and-out-of-hospital-patient-transport (accessed Mar. 15, 2023).

[20] "SOMNOmedics," somnomedics.ce. https://somnomedics.de/en/the-home-of-innovative-and-mobile-diagnostics/ (accessed Mar. 15, 2023).

[21] L. S. Debener, A. Beauducel, D. Nessler, B. Brocke, H. Heilemann, and J. Kayser, "Is resting anterior EEG alpha asymmetry a trait marker for depression?" *Neuropsychobiology*, vol. 41, no. 1, pp. 31–37, 2000.

[22] M. K. Islam, A. Rastegarnia and Z. Yang, "A Wavelet-Based Artifact Reduction From Scalp EEG for Epileptic Seizure Detection," *IEEE J. Biomed. & Health Inform.*, vol. 20, no. 5, pp. 1321–1332, Sept. 2016.

[23] B. Yang and H. Liu, "Automatic Identification of Insomnia Based on Single-Channel EEG Labelled With Sleep Stage Annotations," *IEEE Access*, vol. 8, pp. 104281–104291, 2020.

[24] Z. Li, S. Zhao, J. Duan, C. Su, C. Yang and X. Zhao, "Human Cooperative Wheelchair With Brain–Machine Interaction Based on Shared Control Strategy," *IEEE/ASME Trans. Mechatronics*, vol. 22, no. 1, pp. 185–195, Feb. 2017.

[25] A. Larson, J. Herrera, K. George, and A. Matthews, "Electrooculography based electronic communication device for individuals with ALS," *2017 IEEE Sens. Appl. Symp. (SAS)*, 2017, pp. 1–5.

[26] J. Virkkala, J. Hasan, A. Värri, S.-L. Himanen, and K. Müller, "Automatic sleep stage classification using two-channel electro-oculography," *J. Neurosci. Methods*, vol. 166, no. 1, pp. 109–115, 2007.

[27] E. Trull, J. Mize, A. Sadeghian, and M. Sadeghian, “Implementation and use of the electrooculogram in sleep monitoring,” *2015 IEEE Virtual Conf. Appl. Commercial Sens. (VCACS)*, Raleigh, NC, 2015, pp. 1-13.

[28] R. G. Lupu, R. G. Bozomitu, A. Păsărică, and C. Rotariu, “Eye tracking user interface for Internet access used in assistive technology, ” *2017 E-Health and Bioeng. Conf. (EHB)*, Sinaia, 2017, pp. 659-662.

[29] N. Kosmyna, C. Morris, U. Sarawgi, T. Nguyen, and P. Maes, “AttentivU: A wearable pair of EEG and EOG glasses for real-time physiological processing,” *2019 IEEE 16th Int. Conf. on Wearable and Implantable Body Sens. Netw. (BSN)*, 2019, pp. 1–4.

[30] M. A. D. Sucres, S. S. F. Pérez, I. V. G. Zavala, D. L. I. Ramírez, and N. R. Hernández, “EOG-based interface and speech recognition for wheelchair control,” *2019 IEEE Int. Conf. on Engg. Veracruz (ICEV)*, Boca del Rio, Mexico, 2019, pp. 1-4.

[31] W. Zheng, K. Gao, G. Li, W. Liu, C. Liu., J. Q. Liu, G. Wang, and B. L. Lu, “Vigilance Estimation Using a Wearable EOG Device in Real Driving Environment,” *IEEE Trans. Intell. Transp. Syst.*, vol. 21, no. 1, pp. 170-184, Jan. 2020.

[32] M. Lin and B. Li, “A wireless EOG-based human computer interface,” *2010 3rd Int. Conf. Biomed. Engg. and Inform.*, 2010, vol. 5, pp. 1794–1796.

[33] M. Teplan, “Fundamentals of EEG Measurement,” *Meas. Sci. Rev.*, vol. 2, no. 2, 2002.

[34] J. W. C. Medithe and U. R. Nelakuditi, "Study of normal and abnormal EEG," *2016 3rd Int. Conf. Adv. Comput. & Commun. Syst. (ICACCS)*, Coimbatore, India, 2016, pp. 1–4.

[35] M. Diykh, Y. Li, and P. Wen, “EEG Sleep Stages Classification Based on Time Domain Features and Structural Graph Similarity,” *IEEE Tran. Neural Syst. Rehabil. Eng.*, vol. 24, no. 11, pp. 1159-1168, Nov. 2016.

[36] M. S. Cohen, “EEG Data Collection Intrabuccal Method and Apparatus,” WO Patent 107446A1, 2014, Jul. 10, 2014.

[37] R. Radmand, “Intra-oral Electroencephalography Device and Method,” U.S. Patent 0 060 611 A1, 2020, Feb. 27, 2020.

[38] E. Mignot, S. Taheri, and S. Nishino, “Sleeping with the hypothalamus: emerging therapeutic targets for sleep disorders,” Nature Neurosci., vol. 5, pp. 1071–1075, Oct. 2002.

[39] A. Bulling, J. A. Ward, H. Gellersen, and G. Troster, “Eye movement analysis for activity recognition using electrooculography,” *IEEE Trans. Pattern Anal. Mach. Intell.*, vol. 33, no. 4, pp. 741–753, 2010.

[40] H. Manabe, M. Fukumoto, and T. Yagi, “Direct Gaze Estimation Based on Nonlinearity of EOG, ” *IEEE Trans. Biomed. Eng*., vol. 62, no. 6, pp. 1553-1562, June 2015.

[41] G. Deli *et al.*, “Comparison of the efficacy of unipolar and bipolar electrode configuration during subthalamic deep brain stimulation,” *Parkinsonism Related Disord.*, vol. 17, no. 1, pp. 50–54, Nov. 2011.

[42] M. Guermandi, E. F. Scarselli and R. Guerrieri, “A Driving Right Leg Circuit (DgRL) for Improved Common Mode Rejection in Bio-Potential Acquisition Systems,” *IEEE Trans. Biomed. Circuits and Syst.*, vol. 10, no. 2, pp. 507-517, April 2016.

[43] M. R. Nuwer et al., “IFCN standards for digital recording of clinical EEG,” *Electr. Clin. Neuroph.*, vol. 106, no. 3, pp. 259–261, Mar. 1998.

[44] Y. M. Chi, T. Jung, and G. Cauwenberghs, "Dry-contact and noncontact biopotential electrodes: methodological review," in IEEE Rev. Biomed. Eng., vol. 3, pp. 106–119, 2010.

[45] Y. Sun and X. B. Yu, "Capacitive Biopotential Measurement for Electrophysiological Signal Acquisition: A Review," *IEEE Sens. J.*, vol. 16, no. 9, pp. 2832-2853, May 1, 2016.

[46] A. Dabbaghian et al., "A 9.2-g fully-flexible wireless ambulatory EEG monitoring and diagnostics headband with analog motion artifact detection and compensation," IEEE Trans. Biomed. Circuits & Syst., vol. 13, no. 6, pp. 1141–1151, Dec. 2019.

[47] D. Svärd *et al.*, “Design and evaluation of a capacitively coupled sensor readout circuit, toward contact-less ECG and EEG,” *2010 Biomed. Circuits and Syst. Conf. (BioCAS)*, 2010, pp. 302–305.

[48] J. Ottenbacher *et al.*, "Reliable motion artifact detection for ECG monitoring systems with dry electrodes," *2008 30th Annu. Int. Conf. IEEE Eng. Medicine & Biol. Soc.*, 2008, pp. 1695–1698.

[49] N. Van Helleputte *et al.*, "A 160 μA biopotential acquisition IC with fully integrated IA and motion artifact suppression," *IEEE Trans. Biomed. Circuits & Syst.*, vol. 6, no. 6, pp. 552–561, Dec. 2012.

[50] J. Xu *et al*., "A wearable 8-channel active-electrode EEG/ETI acquisition system for body area networks," *IEEE J. Solid-State Circuits*, vol. 49, no. 9, pp. 2005–2016, Sept. 2014.

[51] I. Daly, M. Billinger, R. Scherer and G. Müller-Putz, "On the Automated Removal of Artifacts Related to Head Movement From the EEG," *IEEE Trans. Neural Syst. Rehabil. Eng.*, vol. 21, no. 3, pp. 427–434, May 2013.

[52] K. L. Snyder, J. E. Kline, H. J. Huang, and D. P. Ferris, “Independent component analysis of gait-related movement artifact recorded using EEG electrodes during treadmill walking,” *Frontiers Hum. Neurosci.*, vol. 9, pp. 1–13, 2015, Art. no. 639.

[53] S. Sadiya, T. Alhanai, and M. M. Ghassemi, "Artifact Detection and Correction in EEG data: A Review," *2021 10th Int. IEEE/EMBS Conf. Neural Eng. (NER)*, Italy, 2021, pp. 495–498.

[54] V. Roy *et. al.*, "Gaussian Elimination-Based Novel Canonical Correlation Analysis Method for EEG Motion Artifact Removal," *J. Healthc. Eng.*, vol. 2017, 2017, doi: 10.1155/2017/9674712.

[55] X. Jiang, G. B. Bian, and Z. Tian, "Removal of Artifacts from EEG Signals: A Review," *Sensors (Basel)*, vol. 19, no. 5, pp. 987, Feb. 2019, doi: 10.3390/s19050987.

[56] S. Shukla, V. Roy, and A. Prakash, "Wavelet based empirical approach to mitigate the effect of motion artifacts from EEG signal," *Proc. - 2020 IEEE 9th Int. Conf. Commun. Syst. Netw. Technol.(CSNT 2020)*, pp. 323–326, 2020.

[57] A. K. Maddirala and R. A. Shaik, "Motion artifact removal from single channel electroencephalogram signals using singular spectrum analysis," *Biomed. Signal Process. Control*, vol. 30, pp. 79–85, 2016.

[58] R. Ranjan, B. C. Sahana. and A. K. Bhandari, "Motion Artifacts Suppression From EEG Signals Using an Adaptive Signal Denoising Method," *IEEE Trans. Instrum. Meas.*, vol. 71, pp. 1-10, 2022.

[59] K. T. Sweeney, S. F. McLoone, and T. E. Ward, "The use of ensemble empirical mode decomposition with canonical correlation analysis as a novel artifact removal technique," IEEE Trans. Biomed. Eng., vol. 60, no. 1, pp.97–105, 2013.

[60] R. Akhter and F. R. Beyette, "Machine Learning Algorithms for Detection of Noisy/Artifact-Corrupted Epochs of Visual Oddball Paradigm ERP Data," 2022 7th Int. Conf. Data Sci. Mach. Learning Appl. (CDMA), Riyadh, Saudi Arabia, 2022, pp. 169–174.

[61] N. A. Chadwick, D. A. McMeekin, and T. Tan, "Classifying eye and head movement artifacts in EEG signals," *5th IEEE Int. Conf. Digit. Ecosyst. Technol. (IEEE DEST 2011)*, Daejeon, South Korea, 2011, pp. 285–291.

[62] H. Zhang *et. al.*, "Eegdenoisenet: A benchmark dataset for deep learning solutions of EEG denoising," *J. Neural Eng.*, vol. 18, no. 5, p. 056057, 2021.

[63] "NeuroCap™," brainscientific.com. https://brainscientific.com/products/ (accessed Mar. 17, 2023).

[64] "EEGO™ Mylab," ant-neuro.com. https://www.ant-neuro.com/products/eego-mylab (accessed Mar. 17, 2023).

[65] "Bittium NeuroOne," bittium.com. https://www.bittium.com/medical/bittium-neurone (accessed Mar. 17, 2023).

[66] "EOG Pod," adinstruments.com. https://www.adinstruments.com/products/eog-pod (accessed Mar. 17, 2023).

[67] "EOG Amplifier," biopac.com. https://www.biopac.com/product/electrooculogram-amplifier/ (accessed Mar. 17, 2023).

[68] J. Arnin *et al.*, "Wireless-based portable EEG-EOG monitoring for real time drowsiness detection," *2013 IEEE 35th Annu. Int. Conf. Engg. Medicine and Biol.*, 2013, pp. 4977-4980.

[69] A. T. Vehkaoja, J. A. Verho, M. M. Puurtinen, N. M. Nojd, J. O. Lekkala, and J. A. Hyttinen, "Wireless head cap for EOG and facial EMG measurements," *2005 IEEE 27th Annu. Conf. Engg. Medicine and Biol.*, 2006, pp. 5865–5868.

[70] A. J. Golparvar and M. K. Yapici, "Electrooculography by wearable graphene textiles," *IEEE Sens. J.*, vol. 18, no. 21, pp. 8971–8978, 2018.

[71] S. -F. Liang et al., "Development of an EOG-based automatic sleep-monitoring eye mask," *IEEE Trans. Instrum. Meas.*, vol. 64, no. 11, pp. 2977–2985, 2015.

[72] X. Guo, W. Pei, Y. Wang, Y. Chen, H. Zhang, X. Wu, X. Yang, H. Chen, Y. Liu, and R. Liu, "A human-machine interface based on single channel EOG and patchable sensor," *Biomed. Signal Process. and Control*, vol. 30, pp. 98–105, 2016.

[73] A. A. Chlaihawi, B. B. Narakathu, S. Emamian, B. J. Bazuin, and M. Z. Atashbar, "Development of printed and flexible dry ECG electrodes," *Sens. Bio-Sens. Res.*, vol. 20, pp. 9–15, Sep. 2018.

[74] C. Chen et al., "Novel Flexible Material-Based Unobtrusive and Wearable Body Sensor Networks for Vital Sign Monitoring," *IEEE Sens. J.*, vol. 19, no. 19, pp. 8502-8513, 1 Oct.1, 2019.

[75] "MUSE: The Brain Sensing Headset," choosemuse.com. https://choosemuse.com/ (accessed Mar. 18, 2023).

[76] "DREEM: Sleep Pioneers," dreem.com. https://dreem.com/ (accessed Mar. 18, 2023).

[77] "Sleep Shepherd: Sleep Optimizer and Tracker," sleepshepherd.com. https://sleepshepherd.com/ (accessed Mar. 18, 2023).

[78] "SmartSleep: Deep Sleep Headband," The Brain Sensing Headset" usa,Philips.com. https://www.usa.philips.com/c-e/smartsleep/deep-sleep-headband.html (accessed Mar. 18, 2023).

[79] "EMOTIVE EPOC+: 14-Channel Wireless EEG Headset," emotive.com. https://www.emotiv.com/product/emotiv-epoc-x-14-channel-mobile-brainwear/ (accessed Mar. 18, 2023).

[80] "JiNS MEME," jinsmeme.com. https://jinsmeme.com/en/ (accessed Mar. 18, 2023).

[81] Y. S. Pai *et al.*, "NapWell: An EOG-based Sleep Assistant Exploring the Effects of Virtual Reality on Sleep Onset," *Virtual Reality*, vol. 26, pp. 437–451 Sept. 2021, doi: /10.1007/s10055-021-00571-w.

[82] C. -T. Lin *et al.*, "Forehead EEG in Support of Future Feasible Personal Healthcare Solutions: Sleep Management, Headache Prevention, and Depression Treatment," *IEEE Access*, vol. 5, pp. 10612-10621, 2017.

[83] C. Beach, N. Karim and A. J. Casson, "A Graphene-Based Sleep Mask for Comfortable Wearable Eye Tracking," *2019 IEEE 41st Annu. Int. Conf. Eng. Med. Biol. Soc. (EMBC)*, Berlin, Germany, 2019, pp. 6693-6696.

[84] S. -W. Kim, K. Lee, J. Yeom, T. -H. Lee, D. -H. Kim and J. J. Kim, "Wearable Multi-Biosignal Analysis Integrated Interface With Direct Sleep-Stage Classification," *IEEE Access*, vol. 8, pp. 46131-46140, 2020.

[85] S. Rostaminia *et al.*, "PhyMask: Robust Sensing of Brain Activity and Physiological Signals During Sleep with an All-textile Eye Mask," *ACM Trans. Comput. Healthcare*, vol. 3, no. 3, pp. 1–35, Jul. 2022.

[86] "WholeYou: Live Out Loud Live Whole," wholeyou.com. https://www.wholeyou.com/ (accessed Mar. 20, 2023).

[87] "SomnoMed Patient: The Comfortable Alternative to CPAP," somnomed.com. https://somnomed.com/en/ (accessed Mar. 20, 2023).

[88] "Sisu Sense: Because Every Hit Matters," sisuguard.com. https://www.sisuguard.com/sisusense/ (accessed Mar. 20, 2023).

[89] "Prevent Biometrics: The Prevent Solution," preventbiometrics.com. https://preventbiometrics.com/our-story/ (accessed Mar. 20, 2023).

[90] H. Park *et al.*, "A wireless magnetoresistive sensing system for an intra-oral tongue-computer interface," *2012 IEEE Int. Solid-State Circuits Conf.*, San Francisco, CA, USA, 2012, pp. 1241–126.

[91] E. R. Lontis *et al.*, "Wheelchair Control With Inductive Intra-Oral Tongue Interface for Individuals With Tetraplegia," *IEEE Sens. J.*, vol. 21, no. 20, pp. 228781–22890, 15 Oct.15, 2021.

[92] S. Nabavi and S. Bhadra, "Oral Cavity Pressure Measurement-based Respiratory Monitoring System with Reduced Susceptibility to Motion Artifacts," *2020 42nd IEEE Annu. Int. Conf. Eng. Med. Biol. Soc. (EMBC)*, Montreal, QC, Canada, 2020, pp. 59001–5904.

[93] S. Nabavi and S. Bhadra, "Smart Mandibular Advancement Device for Intraoral Monitoring of Cardiorespiratory Parameters and Sleeping Postures," *IEEE Trans. Biomed. Circuits Syst.*, vol. 15, no. 2, pp. 248–258, April 2021.

[94] S. Debbarma and S. Bhadra, "Intraoral Monitoring of Photoplethysmogram Signal to Estimate Cardiorespiratory Parameters," *2nd Int. EAI Healthwear Conf.*, Cyberspace, 2020, pp. 23–33.

Chapter 2

A Lightweight Flexible Wireless Electrooculogram Monitoring System With Printed Gold Electrodes

2.1 Abstract

Electroocugraphy (EOG) is a simple and noninvasive method in which biopotentials developed across the eyes are measured during various eye activities such as eye blinking, winking, and horizontal/vertical eyeball movements. The measured biopotential is called the electroculogram (EOG) signal. This paper presents a single channel EOG measurement system which is implemented on a four layer flexible polymide substrate. The EOG measurement system with its signal conditioning stages is implemented on the top layer of the flexible board whereas, the EOG measurement electrodes are printed on the bottom layer of the flexible board using gold. This eliminates the requirement of external long wires during EOG monitoring. The middle two layers of the flexible substrate are used for implementing the circuit ground plane and active shielding. The entire circuit is powered by a rechargeable Li-ion coin battery. It also uses a Bluetooth 5.0 transceiver module to send the EOG data wirelessly. The system is designed for an effective EOG signal bandwidth of 1.6 Hz to 47 Hz with an effective signal gain above 68.5 dB over the signal bandwidth. The system also has an excellent common-mode rejection ratio (CMRR) response above 70 dB. The system is validated with eight healthy subjects for the detection of different eye activities with an accuracy of 77.08 %. The mass of the entire flexible board along with its battery

is only 7.7 g. Such light mass, flexible substrate, and integrated printed electrodes make this EOG monitoring prototype an ideal unit for long term monitoring of biopotentials, without causing any discomfort to the wearer.

Index Terms— Electrooculography, eye activities, biopotentials, printed electrodes, analog front-end, flexible, wearable, wireless.

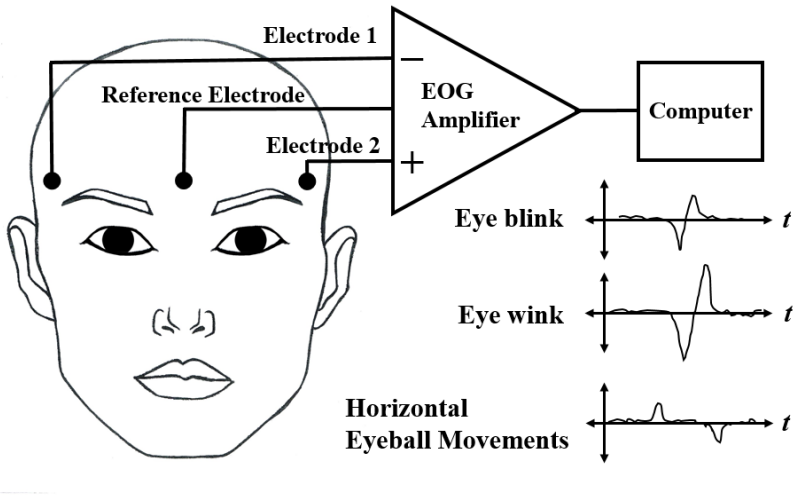

Fig. 2.1 The basic EOG measurement setup with three electrode configuration.

2.2 Introduction

In recent decades, Electrooculography (EOG) has been proven to be a very popular and well-established method used in studies related to neuroscience, cognition analysis, psychological behavior, assistive technology, and also in sleep studies. The EOG is a very simple, non-invasive technique where biopotentials are measured from around the eye of a human subject [1]. A potential field exists between the cornea and the retina of an eye, which changes during horizontal/vertical eyeball movements, eye reflex, and eye blinking activities. This change in potential is called Electrooculogram or EOG signal and can easily be picked up by placing two or more electrodes arrangement around the eyes, as shown in Fig. 2.1. The amount of change in the

EOG potential can be directly associated with the displacements of the eyeball from an initial position during eyeball movement activities and/or the amount of force that may have been used by the eye-muscles during eye reflex and eye blinking activities [2]. This simple concept of acquiring potential changes around the eyes has garnered the attention of researchers and opened up immense opportunities in research areas mentioned above [3]–[8]. This technique also played a key role in achieving tremendous advancements in several smart human-computer interface (HCI) applications and in assistive technologies for elderly people [6], [8]–[13].

The amplitude of EOG signals is small and normally ranges from 0.05 to 3.5 mV [10]. Although, the frequency of EOG signals can range from DC to 100 Hz [13], the useful EOG signal bandwidth can be limited from 0.1 Hz to 40 Hz [10]. The EOG signals get easily contaminated by other biopotentials like electroencephalogram (EEG) and electromyogram (EMG) signals which also lie within the same signal bandwidth [1], [13]. The amplitude of the measured EOG signals also depends on several factors like the size of the measurement electrodes, the placement of the electrodes, the distance of the electrodes from the eye as well as from each other. Moreover, the skin-electrode contact impedance imposes another challenge, introducing DC drifts and deteriorating the EOG signal quality during measurement. In most experimental setups, electrodes are connected to the EOG hardware via long wires, which may also introduce power-line interferences. Motion during EOG measurement may also further contribute artifacts to the measured signal and deteriorates its quality. All these factors mentioned above cause inevitable challenges in selecting a good quality EOG electrode as well as in designing a good EOG measurement system [14].

An ideal biopotential measurement electrode (be it for EOG, EEG, or ECG applications) should be comfortable to wear for long term measurement (e.g. sleep study) and should have very low skin-electrode impedance to acquire a good quality biopotential signal which is generally in a few microvolts to millivolts range. The conventional commercially available electrodes for biopotential measurements are silver, silver-chloride, and gold electrodes, known for their relatively low skin-electrode contact impedances and DC drifts [14]. The electrodes can be set up

in either dry or wet configuration. In dry electrode setup, there is no need for skin preparation or use of electrode gels and the electrodes can be directly placed on the patient for measurement. However, most of the reported dry electrodes are large in size, since larger area compensates for the impedance developed at the skin-electrode contact interface. For wet electrode configuration, saline solution based electrode gels are generally used with the electrode setup to lower the skin-electrode contact impedance and improve signal measurement [15]. However, due to their rigid structure, the commercial electrodes are not generally preferred for long-term measurements as they cause discomfort to the wearer.

To overcome this obstacle, several flexible electrodes have been developed and reported by researchers. In recent technology, fabric based wearable electrodes have been developed for many biopotential measurement applications. Arnin *et. al.* [16] combined dry silver electrodes with conductive silver/nylon fabric and then attached to a headband for EOG application. Vehkaoja *et. al.* [17] developed an embroidered, conductive silver-coated fiber based wearable wet electrode for EOG and facial EMG measurements. A graphene textile based dry flexible electrode for EOG measurement have also been designed by Golparvar and Yapici [18]. Another silver/polyamide compound based flexible fabric sensor, by Liang *et. al*., is also reported in [19] for EOG based sleep study. Polymer composite based flexible electrodes are also designed and reported for similar applications. Guo *et. al.* [20] also designed ultra-thin gold wire mesh printed on a patchable elastic tape and used it as EOG electrodes. Chlaihawi *et. al.* [21] also reported multi-walled carbon nanotube (MWCNT)/PDMS composite based flexible conductive polymer based dry electrodes for ECG application. In another manuscript, a silver nano-wire (Ag NW)/PDMS composite based flexible dry EEG electrodes have been designed by Chen *et. al*. [22]. Each of these flexible electrode involves specific fabrication and design processes, which will add extra cost to the manufacturer along with the cost for the EOG measurement system design.

Interfacing the measurement electrodes with the hardware may introduce another limitation when it comes to patient's comfort during long term monitoring. The flexible electrodes maybe comfortable to wear, but most of the commercial EOG hardware are generally rigid, bulky and

kept at a distance from the patient. Long wires are used to connect the electrodes with the EOG system. The use of long wires is also undesirable, because it forces the patient to stay still for the entire duration of monitoring as wire movements may introduce motion artifacts in the measurement which may saturate the input amplifier stage of the measurement unit [23]. In some dry electrodes, some part of the instrumentation is implemented on the opposite side of the skin-electrode contact plate [23]–[25]. But again, those active electrodes are generally made of rigid boards to accommodate the recording hardware and cause discomfort when placed on a subject's body. In some applications, the rigid hardware unit is housed in a plastic case and then attached with the wearable device itself (e.g. goggles and headbands), which can be uncomfortable to wear [10], [16], [26]. Flexible printed circuit boards (PCB boards) have garnered sufficient attention in recent trends and have potential for designing the recording hardware which could be wearable. Printing measurement electrodes on one side of the flexible PCB while implementing the hardware on the other side of the flexible PCB will eliminate the requirement of long wires. The flexible PCB boards are generally very light in mass and can be worn very comfortably due to their flexibility. In a recent work, by Dabbaghian *et. al.*, a wireless, eight channel EEG system implemented on flexible PCB with printed capacitive dry electrodes was reported [27]. Although the circuit characterization was thoroughly performed and reported, the work did not report any real time measurement of EEG signals using their hardware.

In this manuscript, we present a flexible wireless biopotential measurement system for EOG application. The EOG hardware is implemented on a flexible polymide substrate with printed gold electrodes. A low power Bluetooth module is used for wireless data transmission. The entire unit is powered with a Li-ion coin battery. The measured mass of the flexible board, along with the implemented EOG unit (except the battery) and the battery with its holder are around 3.35 g and 4.35 g, respectively, making the total mass of the entire unit 7.7 g. Thus, the light mass along with the flexibility of the EOG system makes it easy to use on any human subject, without causing any discomfort. If needed, the system can also be integrated in any type of head cap or head band for long term monitoring. The system performance is validated on eight healthy human subjects by

acquiring their EOG data wirelessly. The EOG data are later processed on a computer for feature extraction. The system is able to detect different types of eye activities efficiently, for all the eight healthy subjects, and has potential for long term comfortable EOG monitoring.

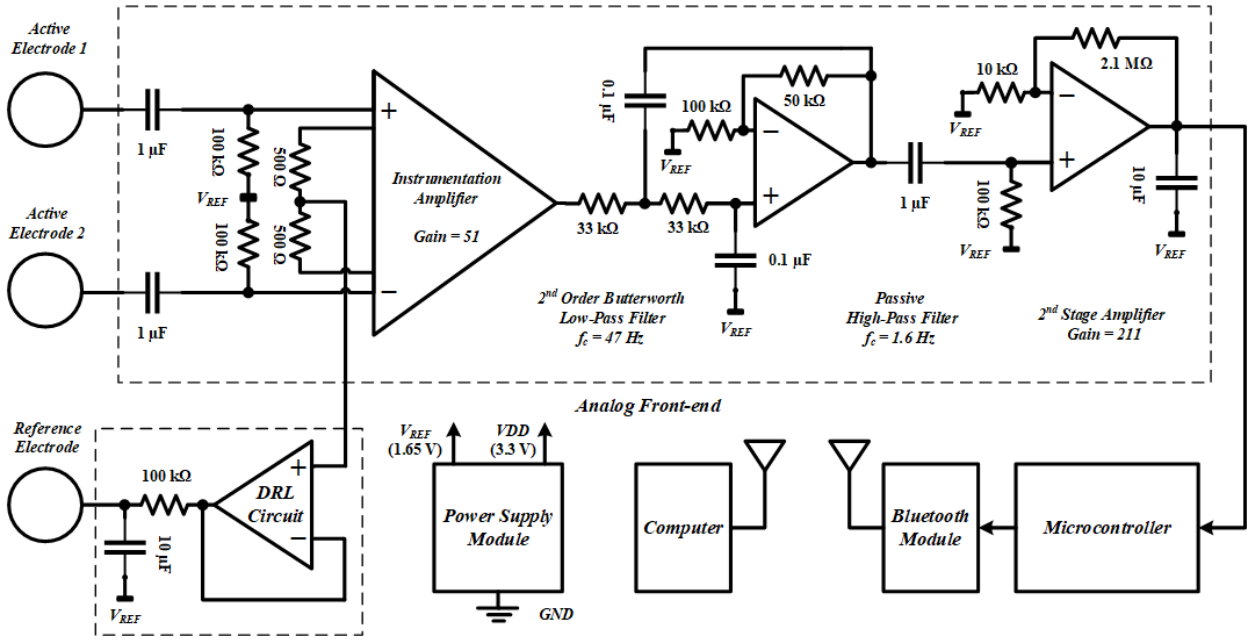

Fig. 2.2. The complete block diagram of the implemented EOG measurement unit.

2.3 System Design and Implementation

The complete EOG system block diagram is presented in Fig. 2.2. The system has a single EOG channel in this prototype with a three electrode (two active electrodes and one reference electrode, as shown in Fig. 2.1) configuration for the measurement. The system has the following blocks: a power supply module, an analog front-end with the two active electrodes as inputs, a driven right leg (DRL) circuit interfaced with the reference electrode, and a microcontroller interfaced with a Bluetooth module for wireless data transmission. The dimension of the flexible polymide PCB board is approximately 12.5 cm × 1.8 cm. The flexible board has four layers. The top layer is used to implement all the off the shelf components for the EOG instrumentation blocks. The second layer is used as the ground plane and routing plane for overlapping PCB tracks. The third layer is used for implementing active shielding. The fourth (or the bottom) layer is used to print the gold

measurement electrode. The entire module is powered with a Li-ion coin battery. The EOG system design is explained with in-depth detail in the following subsections.

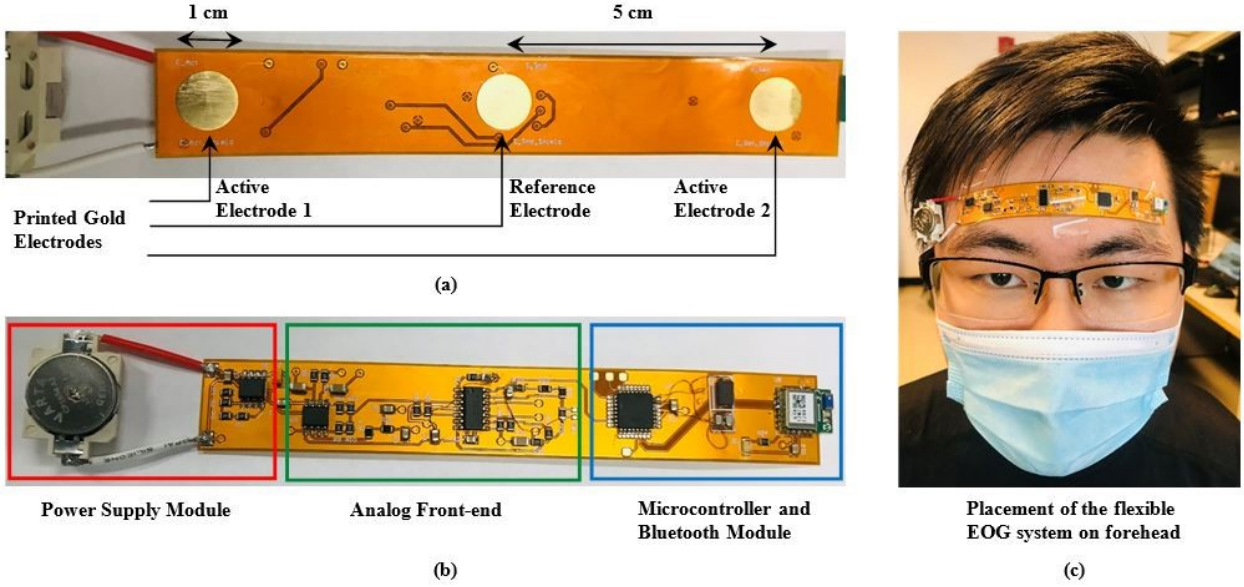

Fig. 2.3. The EOG measurement unit – (a) three printed gold electrodes at the bottom layer of the flexible PCB, (b) the EOG measurement circuit on the top layer of the flexible PCB, and (c) the placement of the flexible system for EOG measurement.

2.3.1 The Power Supply Block

The power supply block in this unit uses a rechargeable Li-ion coin battery (manufactured by VARTA), a low-dropout voltage regulator IC TPS7333 (by Texas Instruments), and a general purpose op-amp LMC6484 (CMOS Quad Op-Amp IC, by Texas Instruments). The battery has a capacity of 120 mAh and its nominal voltage varies between 4.2 V to 3.7 V. This battery power ups the voltage regulator IC which generates a constant supply 3.3 V used for powering up the subsequent analog and digital circuit blocks. A general purpose op-amp circuit is also used to generate a constant voltage of 1.65 V to act as a reference voltage (or analog ground V_{REF}, as shown in Fig. 2.2) for the analog front-end block and the DRL circuit. When powered up, the entire EOG system consumes 47.85 mW of power while transmitting data wirelessly using the Bluetooth. A battery life test is performed for the system by connecting it to the Li-ion coin battery when fully

charged. The overall battery life of the EOG unit is found out to be around 7 hours 40 minutes. The implemented power supply module on the flexible board is also shown in Fig. 2.3b.

2.3.2 The Electrode Configuration

The EOG system has one EOG channel which uses three electrode configuration: two active electrodes and one reference electrode. The electrodes are directly printed with gold on the fourth layer (or bottom layer) of the flexible board as soldering pads. The printed electrodes have a diameter of 1 cm and is printed 5 cm center-to-center apart from each other, as shown in Fig. 2.3a. The left and right electrodes of the board act as the active electrodes (Electrode 1 and Electrode 2, with reference to Fig. 2.2) and used as differential inputs to the analog front-end block. The middle electrode (as shown in Fig. 2.3a) acts as the reference electrode of the system, which is connected with the DRL block. It should be noted that the EOG signal amplitude can be increased by increasing the size of the electrodes and the distance between them [2].

2.3.3 The Analog Front-End

The analog front-end is the most important part of the EOG system since this block helps in sensing and picking up the EOG potential and sending it to the analog-to-digital converter (ADC) of the microcontroller through various signal conditioning stages. This unit is also responsible for amplification of the measured EOG signal in an acceptable range and sufficient suppression of noise and common-mode signals. The signal conditioning stages of the analog front-end are an instrumentation amplifier (IA) as a first stage amplifier, followed by a 2^{nd} order Butterworth low-pass filter (LPF), a first order passive high-pass filter (HPF), and a second stage amplifier, as shown in Fig. 2.2. Since the entire analog front-end block is powered with a single 3.3 V supply voltage, its output voltage swing is also limited from 0 V to 3.3 V with analog ground set at 1.65 V by the power supply block. The analog front-end block of the EOG system is implemented on the top layer of the flexible board and is shown in Fig. 2.3b. Each of these analog signal conditioning stage is discussed in detail in the next subsections.

2.3.3.1 The Instrumentation Amplifier (IA, as 1st Stage): The first instrumentation amplifier stage of the analog front-end block is a very crucial component as this block is directly connected to the EOG measurement electrodes. When the measurement electrodes are placed on the skin, high skin-electrode impedances are introduced. The skin-electrode contact interface also develops pretty large DC offsets and DC drifts, known as the common-mode signals [14]. Such DC signals are undesirable and if not removed, they may saturate the output of the first stage IA. Therefore, the IA component should also have very high common-mode rejection ratio (CMRR) in order to reject common-mode signals (like DC offset and DC drifts) coming from the skin-electrode interfaces. The EOG signal, like other biopotentials, also operates near DC as its useful bandwidth ranges from 0.1 to 40 Hz [10]. To further minimize the impact of common-mode signals, both the input active measurement electrodes are coupled with a 1 μF input capacitor and a 100 kΩ input resistor (as shown in Fig. 2.2) before feeding them to the input stages of the instrumentation amplifier. The capacitor-resistor network forms a high-pass filter (HPF) with a cut-off frequency ($f_{c,HPF}$) of 1.6 Hz and helps in reducing the skin-electrode DC offset. It should be noted that considering the bandwidth of EOG signals, the loss of information between 0.1 Hz to 1.6 Hz is negligible. This HPF at the input terminals along with differential configuration at the IA inputs reduce a significant portion of the skin-electrode DC offset and prevents the first amplification stage from saturation. Some residual components of the EOG signal below 1.6 Hz may still remain at the output of the IA because of the first order input high-pass network. The requirement of using large resistor at the input high-pass network makes it imperative to have a very high input impedance (above 10 GΩ or more) at the input of the first stage amplifier to avoid loading effect. An IA generally has a very large input impedance and is an optimal choice for the first stage amplification in such applications. For this prototype, we have used low-power instrumentation amplifier INA818 (by Texas Instruments) as the first stage amplifier. It has an input impedance around 100 GΩ, low offset voltage around 35 μV, and its gain formula is given by,

$$Gain_{IA} = 1 + \frac{50000}{R_G} \tag{2.1}$$

where R_G is an external resistor used with the IA to set a specific gain for amplification. Although the electrodes at the differential inputs of the IA are coupled with capacitor and resistor for DC offset minimization, the gain of the first stage amplifier is still kept small to make sure the amplifier output does not saturate. For this prototype the gain at the first stage amplifier is kept at 51 by selecting R_G as 1 kΩ.

2.3.3.2 The 2nd Order Butterworth Low-Pass Filter: The second order low-pass active Butterworth filter is implemented using the LMC6484 Quad Op-Amp IC after the first stage amplifier, shown in Fig. 2.2. The gain of the low-pass filter (LPF) is kept around 1.5, whereas, the low-pass cut-off frequency ($f_{c,LPF}$) for this stage is kept around 47 Hz. This makes the effective bandwidth for this EOG measurement system from 1.6 Hz to 47 Hz, bounded by the input high-pass network and this low-pass stage, thus covering the useful EOG bandwidth as given in [10].

2.3.3.3 The Passive High-Pass Filter: After the LPF, a first-order passive high-pass filter (HPF), with $f_{c,HPF}$ around 1.6 Hz, is implemented just by using another 1 μF capacitor and a 100 kΩ resistor, shown in Fig. 2.2. This is done as a precautionary step to minimize the impact of the DC offsets coming from the previous stages, as the gain of the next stage, which is the second stage amplifier, is very high and having a large amplified version of DC offset at the output is not desirable. Although, some DC offset may still remain at the output because of the order chosen for this passive HPF.

2.3.3.4 The 2nd Stage Amplifier:

The second stage amplifier is implemented in a non-inverting configuration, as shown in Fig. 2.2, using the same general purpose LMC6484 Quad Op-Amp IC and its gain is set at 211 for this system. The second stage gain is kept relatively high to achieve a faithful amplification of the detected EOG signals coming from the previous stages and this gain value is selected empirically.

2.3.4 The Driven Right Leg (DRL) Circuit

A driven right leg or DRL circuit is a circuit arrangement which is normally used in many biopotential measurement hardware with differential input configuration. In this arrangement, the

common mode signal of the differential input stage is sensed from a subject using the active electrodes and then the common-mode signal is fed back to the subject's body using the reference electrode. This arrangement further helps in minimizing the DC error that may have been introduced at the first stage IA inputs by the DC offset and the DC drifts generated at the skin-electrode contact interface [28]. In this system, the DRL circuit is implemented using the same general purpose LMC6484 Op-Amp IC. A current limiting resistor of 100 kΩ is also at the output of the DRL circuit before interfacing it with the reference electrode, as shown in Fig. 2.2. This is done to meet the safety standards set by IFCN for biopotential measurements involving human subjects [29].

2.3.5 Active Shielding

Since the flexible polymide substrate is very thin, there is always a chance that the EOG system components implemented on the top layer of the flexible board may introduce capacitive coupling around the electrodes printed on the bottom layer of the flexible board [27]. To avoid this issue, the flexible board is made of four layers and on the third layer, the layer just above the bottom layer, the active shielding scheme is implemented. This is done by printing three more metal plates of similar dimension of the electrodes on the third layer and aligned them exactly on top of the measurement electrodes at the bottom layer, so that it can couple an exact replica of the EOG potentials picked up at the skin-electrode interface. The second layer of the flexible board is used for implementing ground planes and routing overlapping PCB tracks.

2.3.6 The Microcontroller and the Bluetooth Module

The microcontroller and the Bluetooth module are the digital part of the EOG system. This signal acquisition block uses an analog-to-digital converter (ADC) to convert the output of the analog front-end block to digital data and transmit them wirelessly. The microcontroller Atmega328P IC (by Microchip Technology) is used for this implementation. The Atmega328P IC has eight ADC channels with resolution of 10 bits. The output of the analog front-end is fed to one of ADC channels of the microcontroller. The input signal at ADC is sampled at 200 Hz considering the signal bandwidth, thus meeting the Nyquist criteria. The microcontroller is then interfaced with a

low-energy Bluetooth module RN4871 (by Microchip Technology, BLE 5.0 transceiver, with built-in antenna), to transmit the EOG data wirelessly.

2.3.7 Computer With the Bluetooth Transceiver

Another RN4871 Bluetooth module is interfaced with a computer as the receiver module to acquire the ADC data sent by the EOG system wirelessly. The data is collected in real-time and then analyzed in MATLAB. The transmitted ADC data always have a DC offset, which is removed in MATLAB during signal processing and then a smoothening filter is also employed to remove the high frequency glitches generated from the ADC. The filtered signal is then processed for feature extraction indicating various eye activities performed during the measurement.

2.4 System Characterization

After the complete implementation of the EOG measurement system, the system is tested to evaluate its effective gain, and common-mode rejection responses. The EOG measurement unit has filters (a 2^{nd} order Butterworth LPF and a passive HPF) which generally attenuate the incoming signals during filtering. Therefore, the effective gain of the system cannot be calculated directly by using the gain of the first and second stage amplifiers. To measure the gain of the EOG unit, the three printed electrodes of the system are interfaced to three external individual electrodes (of same size) printed on another board in such a way that the electrodes on the EOG system faces and touches their corresponding external electrodes. The external electrodes are fabricated such that they can be excited with external source from the back side. Next, an AC (alternating current) signal source is setup with a simple voltage division network to feed input signals to the external electrodes. The resistances of the voltage division network are selected such that the input electrodes experience only (1/1000) fraction of the actual signal set at the source. Then, the differential input terminals of the IA in the EOG system are fed with two sinusoid inputs using the external electrodes. The reference electrode is connected to the signal ground of the AC source. The amplitude of the input sinusoidal signals is varied until a clear sinusoidal waveform is observed at the output of the analog front-end block of the EOG system. Once a clear sinusoidal

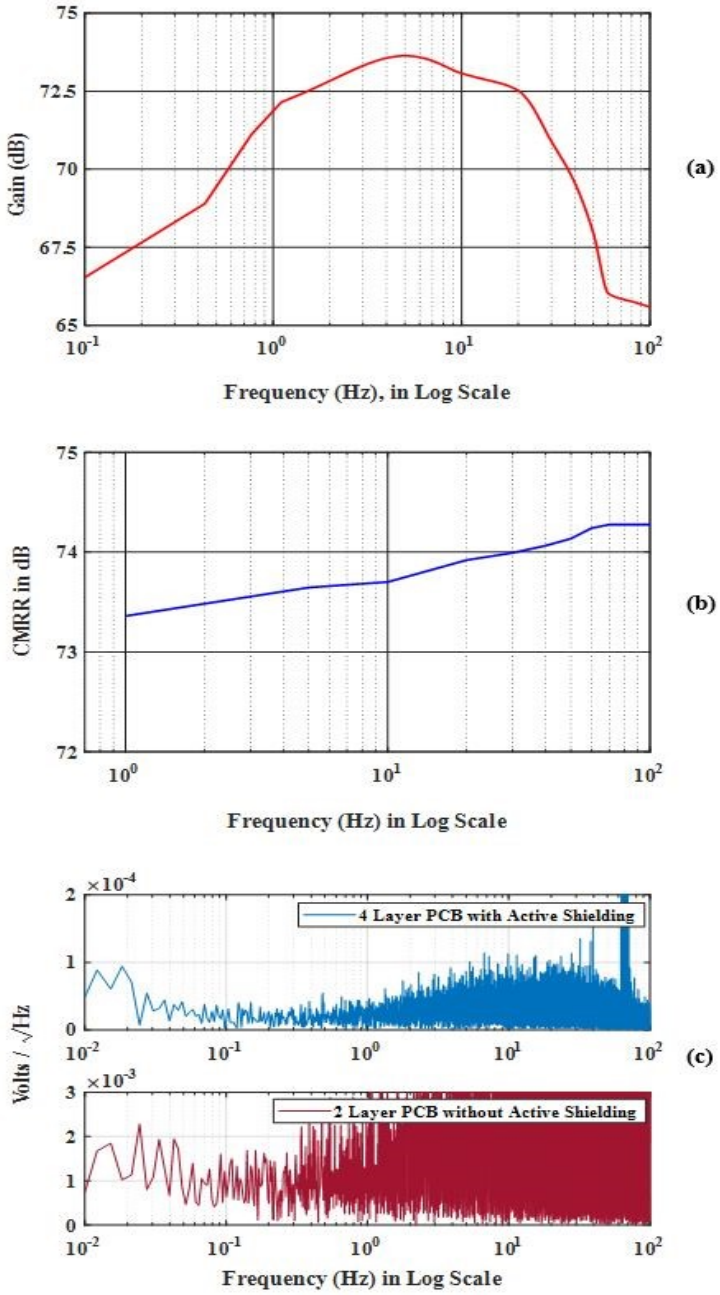

Fig. 2.4. The EOG system characterization – (a) gain-vs-frequency response and (b) CMRR-vs-frequency response, (c) noise-vs-frequency response of the EOG systems (4 layer PCB with active shielding in Blue and 2 layer PCB without active shielding presented in [30]).

TABLE 2.1
A DETAILED COMPARISON BETWEEN THIS PROPOSED FLEXIBLE SYSTEM AND SOME OTHER SYSTEMS FOR BIOPOTENTIAL MEASUREMENT APPLICATION

	BSN'19 [10]	TITS'20 [12]	EMBC'05 [17]	TIM'15 [19]	SENS. J.'19 [22]	TBCAS'19 [27]	THIS WORK
Electrode Design and Specifications:-							
Electrode Type	Rigid	Flexible	Flexible	Flexible	Flexible	Flexible	Flexible
Contact/non-contact	Contact	Contact	Contact	Contact	Contact	Non-contact (Capacitive)	Contact
Electrode Material	Metal (Silver)	Silver Coated Nylon	Silver Coated Fibers	Dry Fabric (Silver/ polymide)	Silver NWs/ PDMS	Metal	Metal (Gold)
Electrode Size	—	1.7 cm × 1 cm	2 cm × 2 cm	—	—	2 cm diameter	1 cm diameter
Interface with the System	Wired	Wired	Wired	Wired	Wired	Integrated with the system	Integrated with the system
System Design and Specifications:-							
PCB Board Type	Rigid	Rigid	Rigid	Rigid	Rigid	Flexible	Flexible
System Weight	—	—	—	84.2g	—	9.2g	7.7g
Number of Channels	2	4	6	1	8	8	1
Power Supply (Volts)	3.3	3.3	3.3	3.3	3.3	3.3	3.3
Power Consumption (Watts)	~ 30 mA (Current)	—	~ 25.6 mA (Current)	—	—	~ 26 mW	~ 48.75 mW
Data Trasmission	Bluetooth	Bluetooth	Zigbee	Bluetooth	Bluetooth	Bluetooth	Bluetooth
System Gain	1100 (EOG) 40000 (EEG)	12	40 (EOG) 1000 (fEMG)	—	—	> 53 dB	> 68.5 dB
System Bandwidth	0.5 – 40 Hz (EOG) 0.5 – 50 Hz (EEG)	4 – 30 Hz	0 – 400 Hz (EOG) 10 – 400 Hz (fEMG)	0.3 – 35 Hz	—	1 – 300 Hz	1.6 – 47 Hz
Application	EOG/EEG	EOG	EOG/fEMG	EOG	EEG/ECG/ Respiration	EEG	EOG

output is observed, the frequency of the input signals is swept from 0.1 Hz to 100 Hz and the amplitude of the analog front-end output is observed. The gain-vs-frequency response curve for the EOG system is presented in Fig. 2.4a. The overall effective gain of the system is found out to be greater than 68.5 dB for the input bandwidth (from 1.6 Hz to 47 Hz) bounded by the HPF and LPF networks.

The common-mode rejection (CMR) response of a system is another crucial metric. The CMR response quantify the ability of rejecting common-mode signals and interferences by the system [30]. Here, the EOG system is also tested for CMR response. A common-mode signal (with same amplitude, phase, and frequency) is applied to both the inputs of the IA in the EOG system to quantify the common-mode rejection ratio (CMRR) of the system. The CMRR is found out to be greater than 70 dB. Hence, it is confirmed that the EOG system has an excellent rejection response to common-mode input signals. The CMRR-vs-frequency of the system is presented in Fig. 2.4b. The noise-vs-frequency response of the EOG circuit is evaluated and presented in Fig. 4c (in Blue). The noise response of this circuit is then compared with the noise response of our previous prototype (in Red) [31]. In this work, a four layer PCB is implemented with active shielding for reducing noise in the system. As we can see in Fig. 2.4c, the noise of the new prototype is indeed less than the prototype presented in [31]. The proposed flexible system is compared in details with some other biopotential measurement systems from the literature in Table 2.1. After the evaluation of the EOG system characteristics is completed, it is used to measure EOG signals for different eye activities.

2.5 Measurement Results and Analysis

The experimental procedure in this study is in accordance with the Deceleration of Helsinki and was approved by Institutional Review Board of McGill University (study number: A04-M21-19B, approval date: 04/17/2019). As shown in Fig. 2.3c, the flexible EOG board, along with its battery unit, is placed on the forehead of a human subject just above the eyebrows to monitor EOG signals. The EOG system is attached to the forehead of the human subject using transparent adhesive tapes.

It should be noted that the entire EOG unit with its battery can be easily integrated in a head cap or head band, if needed.

2.5.1 Detection of Different EOG Signals

The EOG system is validated for feature extraction during various eye activities like eye-blink, eye wink, and horizontal eye movements. The system is placed in such a way so that the reference electrode in the middle is positioned horizontally almost in the middle but a bit shifted towards the left side and vertically just above the eyebrows. A saline-solution based electrolytic gel is also used to reduce the skin-electrode contact impedance during EOG monitoring. Then the three eye activities: eye-blink, eye wink, and horizontal eyeball movements are performed and the respective EOG signals are captured, as shown in Fig. 2.5. The printed electrodes are configured with the analog front-end of the EOG system in such a way that the right electrode is connected to the positive input terminal and the left electrode is connected to the negative input terminal of the first stage IA of the analog front-end block. Therefore, any eye- activity to the right side will result in a positive or upward) deflection in the measured EOG potential and any eye-activity to the left side will result in a negative (or downward) deflection in the measured EOG potential, w.r.t. the baseline of the EOG signal. The baseline of the EOG signal is nothing but the common-mode signal of the two active electrodes observed by the DRL circuit block, which is fed back to the human body using the reference electrode. The first three eye activities, presented in Fig. 2.5a, are eye-blink activities. As mentioned earlier, because of the experimental electrode setup, we see a downward change followed by an upward change for every eye blinking. The downward change marks the eye-close event, followed by the upward change which marks the eye-open event in the signal. In Fig. 2.5b, two eye wink activities are presented. In eye wink activity, since there is only one eye is involved, the captured signal is generally large in amplitude. The EOG signal morphology for eye wink activities remains similar just as eye blink activities, but the peak-to-peak response for eye winks are generally higher than the eye blink activities. By inspecting the polarity of the captured EOG signal we can also tell which eye is involved during the eye-wink activity. For example, in this setup we know that the reference electrode is positioned slightly

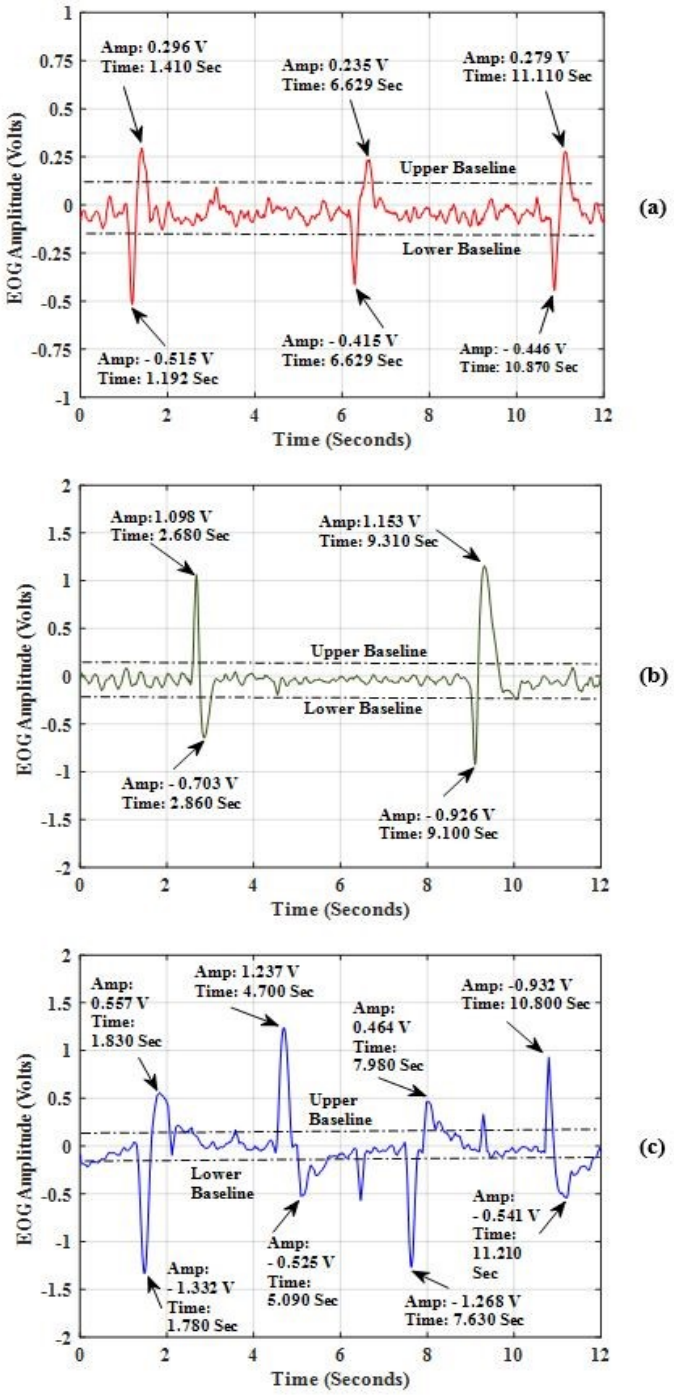

Fig. 2.5. Measurement of the amplified EOG signals – (a) eye blinking activity, (b) eye winking activity, and (c) horizontal eyeball movement.

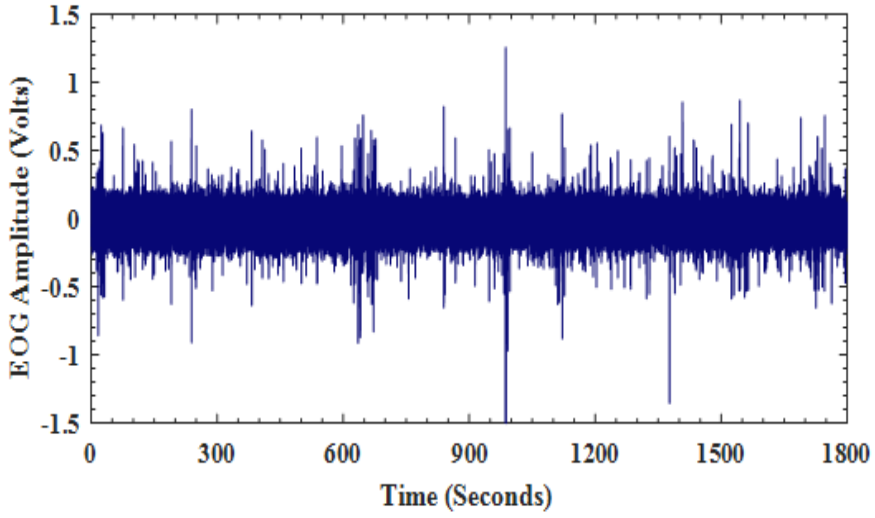

Fig. 2.6. The EOG data measured for a duration of 30 minutes.

towards the left of the middle of the eye brows, the left active electrode is connected to the negative input terminal and the right active electrode is connected to the positive input terminal of the first stage IA in the analog front-end block. Therefore, an EOG signal with a negative (or downward) deflection followed by a positive(or upward) deflection represents a left eye wink activity. Whereas, an EOG signal with a positive (or upward) deflection followed by a negative (or downward) deflection represents a right eye wink activity (again, as presented in Fig. 2.5b). In Fig. 2.5c, the horizontal eyeball movements are presented. Given the EOG system placement configuration, a negative (or downward) deflection represents an eyeball movement towards the left and a positive (or upward) deflection represents an eyeball movement towards the right w.r.t. an initial position. As mentioned earlier, given its light weight and flexibility, this EOG system is suitable for longterm monitoring. One such EOG data is presented in Fig. 2.6, recorded for a duration of 30 minutes (long term monitoring) using this flexible EOG unit. As we can see, the EOG signal has relatively stable baseline ranging around ± 0.15 volts (approximately). Therefore, it can be said that the EOG system is less sensitive to DC drift. This could be due to the cut-off frequency (1.6 Hz) of the high pass network which limits the DC baseline variation upto some extent.

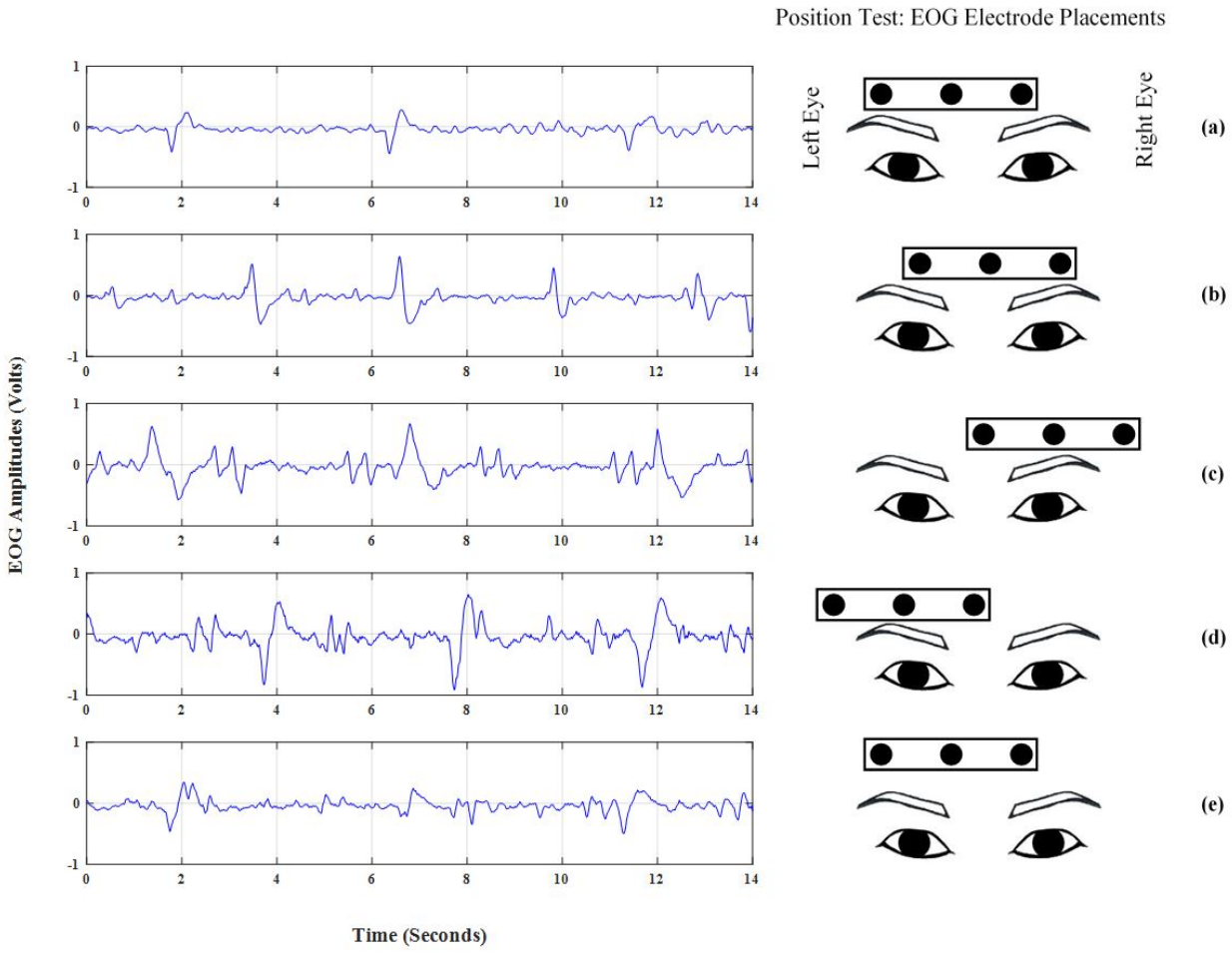

Fig. 2.7. The EOG system position tests – (a) reference electrode's center aligned a bit left from the middle of the eyebrows and vertically the center of the electrodes was in the middle of the forehead just above the eyebrows (the lower part of the forehead), (b) reference electrode's center aligned a bit right from the middle of the eyebrows and vertically the center of the electrodes was in the middle of the forehead just above the eyebrows (the lower part of the forehead) (c) reference electrode's position shifted to the right w.r.t. to the position in (b), (d) reference electrode's position shifted to the left w.r.t. to the position in (a), and (e) the EOG system placed to the upper side of the forehead w.r.t. the position in (a).

2.5.2 EOG System Placement Position Testing

In the EOG system, the left and right printed electrodes are the active electrodes for EOG measurement, as shown in Fig. 2.3a. The middle electrode, as shown in Fig. 2.3a, acts as the

reference electrode and is connected to the DRL block of the system. All the three electrodes are of same size. The left and right electrodes are printed at same distance w.r.t. the middle electrode and their center-to-center distance is only 5 cm. Since the size of the measurement electrodes are same and the active electrodes (left and right) are printed in equidistance w.r.t. the reference electrode (in the middle), there may be a position where both the left and right measurement electrodes develop equal potential w.r.t. the reference electrode and in such case the measured EOG potential will be zero. Therefore, this flexible EOG circuit have to be placed on the forehead in such a way that the two left and right measurement electrodes never experience same potential w.r.t. the reference electrode. In the experimental setup (as shown in Fig. 2.3c), the flexible EOG system is positioned in such a way that horizontally the center of reference electrode (the middle electrode) is aligned a bit left/right from the middle of the eyebrows and vertically just above the eyebrows (closer to the eyes, as much as possible). In this configuration, the left and right measurement electrodes can never develop equal potential w.r.t. the reference electrode. Next we performed a position testing of the flexible EOG system and the test results are presented in Fig. 2.7.

In this test, the system is initially placed such that horizontally the center of reference electrode (the middle electrode) is aligned a bit left from the middle of the eyebrows and vertically just above the eyebrows (closer to the eyes, as much as possible). Three eye blinking activities, where both the eyes are closed and then opened immediately, are performed and captured clearly, as shown in Fig. 2.7a. The eye-blinking activity results in a negative (or downward) deflection followed by a positive (or upward) deflection w.r.t. the EOG baseline. The negative (or downward) deflection at the beginning proves that the reference electrode is positioned slightly left w.r.t. the middle of the eyebrows. Next, the circuit is placed with the reference electrode positioned horizontally almost in the middle but a bit shifted towards the right side of the middle of the eyebrows. Again, the three eye-blinking activities are repeated and as we can see in Fig. 2.7b, the polarity of the eye-blinking activity is reversed. This time we see a positive (or upward) deflection first and then a negative (or downward) deflection in the EOG measurement. Next, the system is

shifted to the right so that the left active electrode is positioned at the middle of the eyebrows. Again the three eye-blinking activity is repeated. We can see in Fig. 2.7c that the EOG response from the right eye is larger than the response captured in the previous configuration in Fig. 2.7b. It can be also seen that the left EOG electrode can barely pick up the left eye-blink activity because of its distance.

Next, the EOG system is shifted to the left so that the right active electrode is positioned at the middle of the eyebrows. The captured EOG data is presented in Fig. 2.7d. In this case, the polarity response of the EOG signal during eye-blink activities are similar to the ones we have seen in Fig. 2.7a, but with higher amplitude for the left eye blink. Also the right EOG electrode can barely pick up the right eye-blink activity because of its distance. Next, the EOG system is placed similar to the position described for Fig. 2.7a, but this time the circuit is placed vertically further up w.r.t. the eyebrows. In this configuration, the captured EOG signals for eye-blink activities have similar pattern like in Fig. 2.7a. But this time, the EOG amplitude is reduced as the EOG measurement unit is placed far from the eyes, as shown in Fig. 2.7e. After this study, it can be concluded that the best position for placing this EOG system is either (a) or (b) configuration, as presented in Fig. 2.7. For measurements of section 2.5.1, configuration (a) is used.

2.5.3 The EOG Feature Extraction

To further validate the efficacy of the EOG system performance, the EOG system unit is tested on eight healthy individuals. For all of them, the EOG system unit is positioned in such a way so that the reference electrode in the middle is positioned horizontally almost in the middle but a bit shifted towards the left side and vertically just above the eyebrows (in short, the placement position (a) in Fig. 2.7). All the subjects are asked to perform the following eye activities: ten eye-blinks, ten eye winks (five left eye wink and five right eye wink), and ten horizontal eyeball movement activities (five times towards the left side and five times towards the right side). The collected data are then processed to remove DC offset generated from the analog-to-digital converter of the microcontroller and then passed through a smoothening filter of order 10 to minimize noise. The EOG signal pattern for different eye activities may remain similar for all the subjects, but their

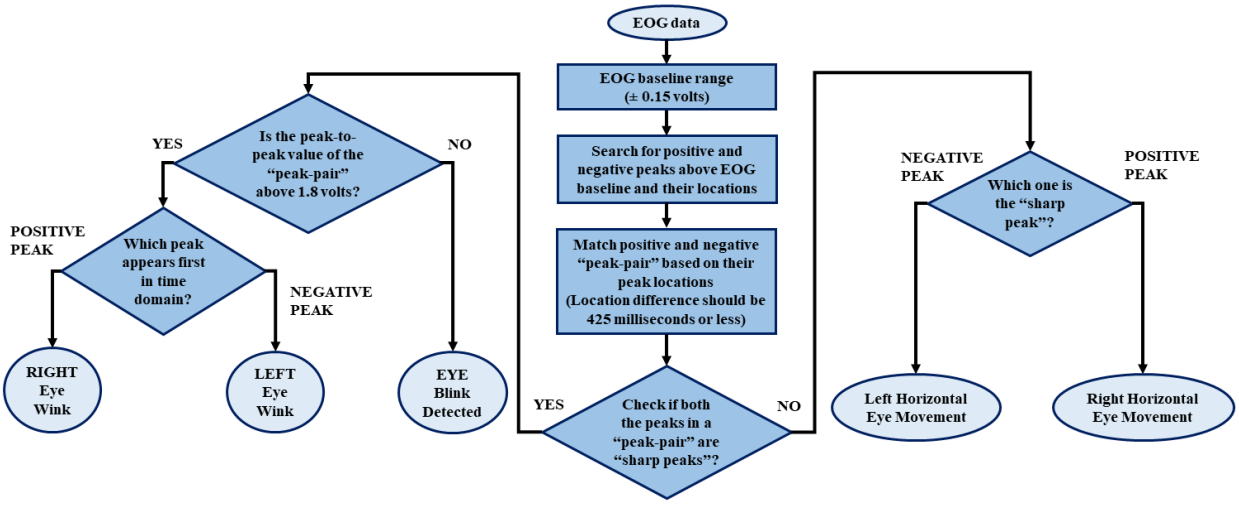

Fig. 2.8. The EOG feature extraction algorithm flowchart.

amplitude range vary significantly from person-to-person due to several reasons. For example, the head size and the forehead surface area varies from person-to-person. The EOG signals amplitude levels for subjects with smaller forehead surface area are found out to be higher as the flexible EOG substrate are able to cover a larger area above the eyes, where the system is placed. Even the shape of the eyebrows determines the distance between the eye and position above the eyebrows where the EOG system is to be placed. And we know, the peak-to-peak EOG amplitudes reduces with distance from the eyes. The EOG baseline signals also change across the subjects depending on their skin composition, sweat etc. which modulates the skin-electrode contact impedances. Therefore, it is challenging to classify different eye activity features using algorithm based on simple amplitude versus time data. Several assumptions have to be made for automated EOG feature extraction to achieve an acceptable range of accuracy. After analyzing the EOG data taken from the eight volunteers, feature extraction parameter values are chosen empirically (they are also shown in Fig. 2.5) and an EOG feature extraction algorithm, as shown in flowchart of Fig. 2.8, is proposed for automatic eye activity detection based on those basic signal parameters (like the EOG baseline range, the minimum peak-to-peak distance for a peak-pair, and minimum peak-to-peak amplitude for eye wink activities). Then the filtered EOG data of from another 8 subjects are

analysed using the EOG feature extraction algorithm (flowchart presented in Fig. 2.8) for automatic eye activity detection. The algorithm is written in MATLAB.

One of the important step of this algorithm is to determine if the peaks in "peak-pairs", identified by the algorithm, are "sharp peaks" or not. Since the amplitude for eye blinks, eye winks, and horizontal eye movements may appear in similar range, it is impossible to classify them based on only amplitude values. Therefore, the widths of each peak in a peak-pair are also quantified to check their sharpness. As we can see in Fig. 2.5a and 2.5b, for the eye blink and the eye wink activities, the positive and the negative peaks have fast rise and fall time. Therefore, their widths are smaller. Whereas for horizontal eye movements (see Fig. 2.5c), one peak (either positive or negative) has fast rise and fall time, but the corresponding peak in the opposite direction has relatively slow rise or fall time. This happens because the EOG signal tends to go back to baseline range after a horizontal eye movement event in one direction (left or right). Therefore, one of the peaks has smaller width, and the corresponding peak has relatively larger width. For calculating the width of the peak, the absolute value of the peaks are analyzed. If the peak amplitude is greater than 0.6 volts, both its rising and falling edges (in either direction of a peak) are checked for a point where the amplitude value drops by 0.3 volts from its peak value in the either direction and the corresponding time locations of those points are selected. Then the time difference of those two points is calculated to quantify the width of the peak. For EOG peaks with absolute amplitude greater than 0.3 volts and less than 0.6 volts, the two points are selected on the either side of the peak when the amplitude value drops by 0.15 volts from the peak value. Next, the width of the peaks are assessed. If any peak has a width of 15 milliseconds or less, it is considered to be a "sharp" peak. If there is only one "sharp" peak is present in a peak-pair, it is classified as a horizontal eye movement. If the "sharp" peak for horizontal eye movement is a positive peak, it is classified as a right horizontal eye movement (w.r.t. placement configuration Fig. 2.7a). If the "sharp" peak for horizontal eye movement is a negative peak, it is classified as left horizontal eye movement (w.r.t. placement configuration Fig. 2.7a). If both the peaks are identified as "sharp", their peak-to-peak amplitude is calculated. If the peak-to-peak amplitude lies between 0.3 – 1.8

TABLE 2.2

THE EOG FEATURE EXTRACTION ALGORITHM PERFORMANCE VALIDATION OF DIFFERENT EYE ACTIVITY DETECTION FOR EIGHT SUBJECTS

Subject ID	Eye Blink		Eye Wink				Horozontal Eyeball Movement			
			Left		Right		Left		Right	
	Counted by hand	Detected by Algorithm	Counted by hand	Detected by Algorithm	Counted by hand	Detected by Algorithm	Counted by hand	Detected by Algorithm	Counted by hand	Detected by Algorithm
1	10	9	5	4	5	4	5	4	5	5
2	10	8	5	3	5	5	5	3	5	4
3	10	7	5	4	5	4	5	3	5	2
4	10	10	5	4	5	3	5	4	5	3
5	10	7	5	4	5	4	5	3	5	3
6	10	8	5	3	5	4	5	5	5	3
7	10	7	5	3	5	2	5	4	5	3
8	10	10	5	4	5	5	5	5	5	5
Total	**80**	**66**	**40**	**29**	**40**	**31**	**40**	**31**	**40**	**28**
Accuracy	**82.5 %**		**72.5 %**		**77.5 %**		**77.5 %**		**70 %**	

volts, it is classified as the eye blink activity. If the peak-to-peak amplitude is above 1.8 volts, it is classified as eye wink activity. For eye wink activity, if the positive peak appears first in the time domain for a peak-pair, it is classified as a right eye wink, otherwise it is a left eye wink. The EOG data of all eight subjects are analyzed using this algorithm and the results are presented in Table 2.2. The EOG feature extraction algorithm was able to detect 185 out of 240 different eye-activities correctly, making the overall accuracy of the algorithm around 77.08 %.

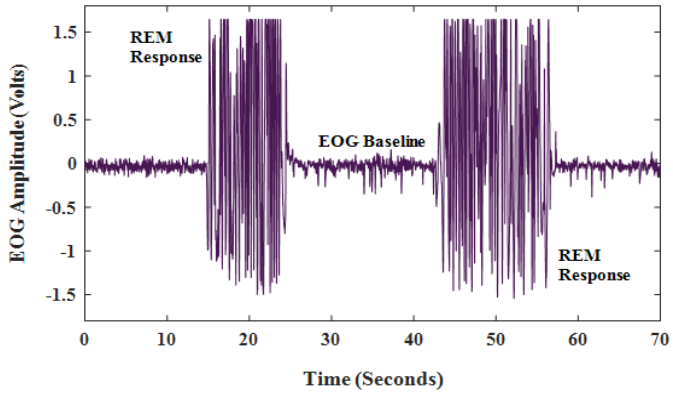

Fig. 2.9. Repetitive eye movement (REM) test, depicting the REM sleep stage, using the flexible EOG circuit.

In future, this flexible EOG system is expected to be used in in sleep stage classification during sleep study. Therefore, a very simple experiment is performed where one volunteer is asked to lie down in supine position and keep the eyelids closed. Then the person is asked to rapidly move his eyeballs while keeping his eyelids closed, to simulate the REM (repetitive eye movement) sleep stage condition. REM sleep stage condition is a condition of deep sleep where the subject under study is said to be dreaming, which leads to REM activity [7]. The flexible EOG circuit is able to detect the REM activity, as shown in Fig. 2.9, thus validating the applicability of the system.

2.6 Conclusion and Future Scope

A flexible, wireless, wearable biopotential measurement system for EOG monitoring is presented in this manuscript. The single channel flexible EOG system has printed gold electrodes on the

bottom side of the flexible board, whereas the biopotential measurement instrumentation is implemented on the top side of the flexible board. The flexible board is made of four layers with the inner two layers used for ground plane and active shielding. The system is characterized for its gain and CMRR characteristics. The effective gain of the EOG system is over 68.5 dB for its effective bandwidth limited from 1.6 Hz to 47 Hz. The system also has an excellent CMRR response, greater than 70 dB. The system performance is then evaluated for capturing different eye activities (e.g. eye blink, eye wink, and horizontal eyeball movement) from eight healthy subjects. It shows an accuracy of 95.83% for detecting different eye activities. The EOG prototype is very light (mass only 7.7 g) and very comfortable to wear because of its flexible polymide substrate and printed electrodes. Moreover, the printed electrodes in the system eliminates the use of long wire during EOG measurement, which makes this system ideal for long term monitoring. The system can also be easily integrated in head caps, head bands, and eye masks.

Currently the electrodes need some electrolytic gel to be placed in between the electrodes and the skin to pick up good EOG signal. Otherwise the collected EOG is not clear enough to detect many eye activities. The size of the printed electrodes is small with only a diameter of 1 cm. In most of the cases, active dry electrodes are larger in size, with diameter (or dimension) of at least 2 cm or more, as reported in many research works [19] – [25], [27]. Sweat also has an impact on skin-electrode contact impedance during biopotential measurement. The chemical composition of sweat helps in conductivity and the presence of sweat during biopotential measurement further helps in reducing the skin-electrode contact impedance and capturing a better quality signal with higher amplitude [32]. However, given the small size of printed electrodes and application of electrode gel during EOG measurement using this system, the effect of the sweat test was not tested separately. In future the size of the printed electrodes will be increased to remove the necessity of the electrolytic gel. Moreover, with larger size printed dry electrodes we will test the effects of sweat. The EOG feature extraction algorithm will also be further refined in future, to improve its accuracy in classifying the different EOG signals. Then, the EOG system will also be used in sleep studies.

2.7 Bridging Text

This work presents a lightweight, battery-operated, wireless, wearable, flexible EOG measurement system. This is also the first reported flexible EOG prototype with integrated flexible gold electrodes printed on the bottom layer of the board. The sensitivity of the flexible gold electrodes has been tested and found out to be similar like the commercial rigid gold electrodes. However, the system still requires electrode gel to lower the impedance at the skin-electrode contact interface for a good quality EOG measurement which is a known fact for any kind of contact electrode based systems. However, the gel dries up with time making the system not suitable for long-term monitoring. The skin-electrode contact impedance can be relaxed by increasing the present size of the printed gold electrodes. But this increases the dimensions of the entire flexible board. Moreover, one of the participants was found out to be allergic to gold during EOG data acquiring. This has led us to think the possibility of using non-contact (or capacitive) electrodes for our next prototype design. The device presented in this chapter was also found out to be sensitive to motion artifacts, which imposed another limitation on the system performance. Therefore, we investigated the possibilities of a smart way to mitigate this motion artifact issue in our next prototype. It is worth to mention that this device has been validated for EOG measurement based sleep stage classifications using machine learning algorithm, implemented by one of the graduate students in our lab [33]. Therefore, it can be concluded that this EOG wearable along with a MAD has a potential to monitor sleep stages and treat OSA patients effectively.

References

[1] A. Bulling, J. A. Ward, H. Gellersen, and G. Troster, "Eye movement analysis for activity recognition using electrooculography," *IEEE Trans. Pattern Anal. Mach. Intell.*, vol. 33, no. 4, pp. 741–753, 2010.

[2] H. Manabe, M. Fukumoto, and T. Yagi, "Direct Gaze Estimation Based on Nonlinearity of EOG, " *IEEE Trans. Biomed. Eng*., vol. 62, no. 6, pp. 1553-1562, June 2015.

[3] L. Popa, O. Selejan, A. Scott, D. F. Mureşanu, M. Balea, and A. Rafila, "Reading beyond the glance: eye tracking in neurosciences," *Neurol. Sci*., vol. 36, pp. 683–688, 2015.

[4] R. Ouyang, Z. Lv, X. Wu, C. Zhang, and X. Gao, "Design and Implementation of a Reading Auxiliary Apparatus Based on Electrooculography, " *IEEE Access*, vol. 5, pp. 3841-3847, 2017.

[5] N. N. J. Rommelse, S. der Stigchel, and J. A. Sergeant, "A review on eye movement studies in childhood and adolescent psychiatry," *Brain Cogn.*, vol. 68, no. 3, pp. 391–414, 2008.

[6] A. Larson, J. Herrera, K. George, and A. Matthews, "Electrooculography based electronic communication device for individuals with ALS," *2017 IEEE Sens. Appl. Symp. (SAS)*, 2017, pp. 1–5.

[7] J. Virkkala, J. Hasan, A. Värri, S.-L. Himanen, and K. Müller, "Automatic sleep stage classification using two-channel electro-oculography," *J. Neurosci. Methods*, vol. 166, no. 1, pp. 109–115, 2007.

[8] E. Trull, J. Mize, A. Sadeghian, and M. Sadeghian, "Implementation and use of the electrooculogram in sleep monitoring," *2015 IEEE Virtual Conf. Appl. Commercial Sens. (VCACS)*, Raleigh, NC, 2015, pp. 1-13.

[9] R. G. Lupu, R. G. Bozomitu, A. Păsărică, and C. Rotariu, "Eye tracking user interface for Internet access used in assistive technology, " *2017 E-Health and Bioeng. Conf. (EHB)*, Sinaia, 2017, pp. 659-662.

[10] N. Kosmyna, C. Morris, U. Sarawgi, T. Nguyen, and P. Maes, "AttentivU: A wearable pair of EEG and EOG glasses for real-time physiological processing," *2019 IEEE 16th Int. Conf. on Wearable and Implantable Body Sens. Netw. (BSN)*, 2019, pp. 1–4.

[11] M. A. D. Sucres, S. S. F. Pérez, I. V. G. Zavala, D. L. I. Ramírez, and N. R. Hernández, "EOG-based interface and speech recognition for wheelchair control," *2019 IEEE Int. Conf. on Engg. Veracruz (ICEV)*, Boca del Rio, Mexico, 2019, pp. 1-4.

[12] W. Zheng, K. Gao, G. Li, W. Liu, C. Liu., J. Q. Liu, G. Wang, and B. L. Lu, "Vigilance Estimation Using a Wearable EOG Device in Real Driving Environment," *IEEE Trans. Intell. Transp. Syst.*, vol. 21, no. 1, pp. 170-184, Jan. 2020.

[13] M. Lin and B. Li, "A wireless EOG-based human computer interface," *2010 3rd Int. Conf. Biomed. Engg. and Inform.*, 2010, vol. 5, pp. 1794–1796.

[14] W. Heide, E. Koenig, P. Trillenberg, D. Kömpf, and D. S. Zee, "Electrooculography: technical standards and applications. The International Federation of Clinical Neurophysiology," *Electroencephalogr. Clin. Neurophysiol. Suppl.*, vol. 52, p. 223—240, 1999, [Online]. Available: http://europepmc.org/abstract/MED/10590990.

[15] B. Taji, A. D. C. Chan and S. Shirmohammadi, "Effect of Pressure on Skin-Electrode Impedance in Wearable Biomedical Measurement Devices," *IEEE Trans. Instrum. and Meas.*, vol. 67, no. 8, pp. 1900-1912, Aug. 2018.

[16] J. Arnin et al., "Wireless-based portable EEG-EOG monitoring for real time drowsiness detection," *2013 IEEE 35th Annu. Int. Conf. Engg. Medicine and Biol.*, 2013, pp. 4977-4980.

[17] A. T. Vehkaoja, J. A. Verho, M. M. Puurtinen, N. M. Nojd, J. O. Lekkala, and J. A. Hyttinen, "Wireless head cap for EOG and facial EMG measurements," *2005 IEEE 27th Annu. Conf. Engg. Medicine and Biol.*, 2006, pp. 5865–5868.

[18] A. J. Golparvar and M. K. Yapici, "Electrooculography by wearable graphene textiles," *IEEE Sens. J.*, vol. 18, no. 21, pp. 8971–8978, 2018.

[19] S. F. Liang et al., "Development of an EOG-based automatic sleep-monitoring eye mask," *IEEE Trans. Instrum. Meas.*, vol. 64, no. 11, pp. 2977–2985, 2015.

[20] X. Guo, W. Pei, Y. Wang, Y. Chen, H. Zhang, X. Wu, X. Yang, H. Chen, Y. Liu, and R. Liu, "A human-machine interface based on single channel EOG and patchable sensor," *Biomed. Signal Process. and Control*, vol. 30, pp. 98–105, 2016.

[21] A. A. Chlaihawi, B. B. Narakathu, S. Emamian, B. J. Bazuin, and M. Z. Atashbar, "Development of printed and flexible dry ECG electrodes," *Sens. Bio-Sens. Res.*, vol. 20, pp. 9–15, Sep. 2018.

[22] C. Chen et al., "Novel Flexible Material-Based Unobtrusive and Wearable Body Sensor Networks for Vital Sign Monitoring," *IEEE Sens. J.*, vol. 19, no. 19, pp. 8502-8513, 1 Oct.1, 2019.

[23] D. Svärd, A. Cichocki, and A. Alvandpour, "Design and evaluation of a capacitively coupled sensor readout circuit, toward contact-less ECG and EEG," *2010 Biomed. Circuits and Syst. Conf. (BioCAS)*, 2010, pp. 302–305.

[24] F. N. Guerrero and E. M. Spinelli, "A Two-Wired Ultra-High Input Impedance Active Electrode," *IEEE Trans. Biomed. Circuits and Syst.*, vol. 12, no. 2, pp. 437-445, April 2018.

[25] T. Tang et al., "An Active Concentric Electrode for Concurrent EEG Recording and Body-Coupled Communication (BCC) Data Transmission," *IEEE Trans. Biomed. Circuits and Syst.*, vol. 14, no. 6, pp. 1253-1262, Dec. 2020.

[26] A. Chaudhuri, A. Dasgupta, S. Chakrborty and A. Routray, "A low-cost, wearable, portable EOG recording system," *2016 Int. Conf. Syst. Med. and Biol. (ICSMB)*, 2016, pp. 102-105.

[27] A. Dabbaghian, T. Yousefi, S. Z. Fatmi, P. Shafia, and H. Kassiri, "A 9.2-g Fully-Flexible Wireless Ambulatory EEG Monitoring and Diagnostics Headband With Analog Motion Artifact Detection and Compensation," *IEEE Trans. Biomed. Circuits and Syst.*, vol. 13, no. 6, pp. 1141-1151, Dec. 2019.

[28] M. Guermandi, E. F. Scarselli and R. Guerrieri, "A Driving Right Leg Circuit (DgRL) for Improved Common Mode Rejection in Bio-Potential Acquisition Systems," *IEEE Trans. Biomed. Circuits and Syst.*, vol. 10, no. 2, pp. 507-517, April 2016.

[29] M. R. Nuwer et al., "IFCN standards for digital recording of clinical EEG," *Electr. Clin. Neuroph.*, vol. 106, no. 3, pp. 259–261, Mar. 1998.

[30] A. S. Sedra and K. C. Smith, Microelectronic Circuits, 7th ed., New York: Oxford University Press, 2015, pp. 627–636.

[31] S. Debbarma, S. Nabavi, and S. Bhadra, "A wireless flexible electrooculogram monitoring system with printed electrodes," in *Proc. IEEE Int. Instrum. Meas. Technol. Conf. (I2MTC)*, Glasgow, Scotland, May 2021, pp. 1–6.

[32] L. Kalevo et al., "Effect of Sweating on Electrode-Skin Contact Impedances and Artifacts in EEG Recordings With Various Screen-Printed Ag/Agcl Electrodes," *IEEE Access*, vol. 8, pp. 50934-50943, 2020.

[33] M. Hamza, S. Bhadra, and Z. Zilic, "Sleep Stage Detection on a Wearable Headband Using Deep Neural Networks," *2022 Global Internet of Things Summit (GloTS)*, Dublin, Ireland, 2022, pp. 187-198.

Chapter 3

A Flexible Wearable Electrooculogram System With Motion Artifacts Sensing and Reduction

3.1 Abstract

Electrooculogram (EOG) is a well-known physiological metric picked up by placing two or more electrodes around the eyeball. EOG signals are known to be extremely susceptible to motion artifacts. This paper presents a single channel, wireless, wearable flexible EOG monitoring system with motion artifacts sensing and reduction feature. The system uses two non-contact electrode pairs for EOG/motion artifacts detection and motion artifacts reduction. It is implemented on a four-layer flexible polyimide substrate. It is light-weight (only 8.75 gram), battery operated, and uses a microcontroller and a BLE 5.0 transceiver for wireless EOG data transmission, while consuming only 56 mW of power. The system metrics such as gain around 37 dB, bandwidth from 1 Hz to 40 Hz, and noise are evaluated. The system is tested for different electrode configurations and it is demonstrated that horizontally parallel electrode pairs achieve an acceptable motion artifact reduction at the output, while preserving perfect EOG features (such as eye-blinking). The average sensitivity for horizontally parallel non-contact electrodes is found out to be more than 50 times with respect to commercial gold electrodes, whereas the average response time of the sensor is around 380 mS. The flexible EOG system is comfortable to wear and the use of non-contact

electrode eliminates the need of skin preparation. Therefore, the system can be easily integrated with eye-masks and headbands, thus making it an excellent prototype for many smart applications.

Index Terms— Analog front-end, electrooculography, eye activity, flexible, motion artifacts reduction, noncontact electrodes, skin conformable, wearable.

3.2 Introduction

Electrooculography (or EOG) is one of the well- renowned and standard technique used in biomedical research and in various applications such as psychiatry, sleep study, gaze estimation, human-computer interface (HCI) [1]–[7]. EOG sense the biopotential developed during eye blinking and eye movement activities [5], [8]. The amplitude of EOG signal can have a spread from a few microvolts (~ 50 μVolts) up to a few millivolts, depending upon the placement of the measurement electrodes around the eyes and the distance between them [9]. The useful bandwidth of EOG signal can be limited from 0.1 Hz to 40 Hz [10]. The features of EOG signal strongly depend on the physical attributes (e.g., type, size etc.) of the measurement electrodes and their placement around the eyes.

The EOG (or any biopotential) measurement electrodes are generally classified into two categories: contact electrodes and non-contact electrodes (also known as capacitive electrodes) [10]. The contact electrodes make contact with the skin during biopotential measurement [9]–[11] and are the most common type. Non-contact electrodes, on the other hand, use an insulating layer as a dielectric between the skin and the metal electrode plate, creating a capacitor between the skin-electrode interfaces [10], [12]. Contact electrodes generally require skin preparation and electrode gel during the measurement [10], [11]. Non-contact electrodes do not require any skin preparation/electrode gel during measurement which is advantageous [10], [12]. Since EOG potentials can get contaminated easily by other biopotential signals, such as electroencephalogram (EEG) and electromyogram (EMG), it is recommended to place EOG electrodes as close to the eyes as possible to achieve a faithful detection of EOG signal during eye activities.

Flexible electrodes are generally preferred over rigid electrodes. Flexible contact printed electrodes have already been reported to have similar sensitivity like the standard rigid electrodes [13]. In some latest applications, the EOG/EEG system is developed on flexible printed circuit boards (PCBs) with the instrumentation implemented on one side and the electrodes printed on the other side of the flexible board [11], [12]. Such acquisition systems are suitable for long-term monitoring due to their flexibility, light weight, skin conformability, and capability of providing comfort to the wearer.

Biopotential measurements are susceptible to random motion artifacts [12], [14]–[17]. Such artifacts get introduced due to nearby environmental vibrations and movement of the subject under test. The non-contact (or capacitive) electrodes are extremely sensitive to motion artifacts. The gap between the skin and the metal plate changes due to motion which in turn impacts the overall capacitance offered by the non-contact electrode at the skin-electrode interface [12]. Motion artifacts may have a large dynamic range in comparison to the measured biopotential. The bandwidth of the motion signals may fall well within the biopotential signal bandwidth itself, which makes it more difficult to remove motion artifacts using conventional signal processing. Given its large dynamic range, the motion artifacts also demand to have an acquisition system with large supply voltage in order to capture the motion signals and avoid output saturation. In one report, by Ottenbacher *et al.* [15], a sensor-fusion is performed using an accelerometer and electrocardiogram (ECG) electrodes. The accelerometer picks up the motion artifacts and the ECG electrodes measures the motion contaminated ECG signal. The accelerometer signal is used as the reference signal in a complex adaptive filter to estimate and remove the motion artifacts from the ECG output. Another research group has designed an ECG/ETI (or electrode-tissue impedance) system, where the same electrode is employed to sense both ECG and ETI signals [16]. This time, ETI signal is used as the reference motion signal. In another work, the same concept has been adapted for an EEG/ETI system to estimate and remove motion artifacts from the EEG signal [17]. The works in [16] and [17] use DSP for motion suppression algorithm which consumes large power to operate. This results in smaller battery life which is undesirable. Moreover, the systems

reported in [15]–[17] use contact electrodes which need skin preparation and gel. One recent work, by Dabbaghian *et al.* [12], also reports an EEG measurement circuit which is capable of sensing both EEG and motion artifacts using a pair inter-digitated non-contact electrodes. One of the inter-digitated electrodes is treated as the signal path and the other as the motion path. The signal sensed at the motion path is used to control a variable gain module present at the signal path, thereby estimating and effectively reducing motion artifacts from the measured EEG signal. While they report a detailed validation of their circuits, no basic EEG recording using their system was reported. Moreover, their circuitry is complex to implement. The motivation of our work is to overcome some of the limitations of these existing works.

In this manuscript, we report a wireless wearable EOG acquisition system consisting of two pairs of flexible printed non-contact electrodes for EOG sensing, and motion artifacts sensing and reduction. The complete system is implemented on a four-layer flexible polyimide substrate. The EOG acquisition unit is implemented on the top layer whereas the flexible non-contact measurement electrodes are printed on the bottom layer. The second layer is used as the ground plane, and the third layer is used as the active shielding layer of the system. The flexible EOG system is battery operated and transmits the recorded data wirelessly using BLE 5.0 transceiver. The novelty of the system is that it does not require any skin preparation/gel and uses a simple approach of two electrode pairs and differential amplifier to sense and minimise the impact of motion. The system requires less number of components when compared to the state of the art and does not use any DSP chip or algorithm for motion artifacts reduction. Moreover, the system is flexible, light weight (i.e., 8.75 gram) and comfortable to wear. It is extensively tested with different shapes of non-contact electrodes under different placement configurations for robust motion artifacts estimation and reduction. The impact of sweat and motion on the printed non-contact electrodes are also investigated. It is shown that the system is capable to reduce the motion artifacts effectively while the EOG features can be preserved by using the optimal electrode configuration.

3.3 Non-contact Electrode Design Considerations and Motion Artifacts

Unlike contact electrodes, non-contact electrodes (or capacitive electrodes) generally do not make any direct contact with skin where the electrode is placed. Apart from the advantage of no requirement of skin preparation, another advantage of noncontact electrodes is that they do not suffer from polarization effect like the contact ones [10], [12]. Fig. 3.1 presents generic skin-electrode contact impedance models for contact electrodes with electrode gel, dry contact electrodes, and non-contact electrodes [12], [18].

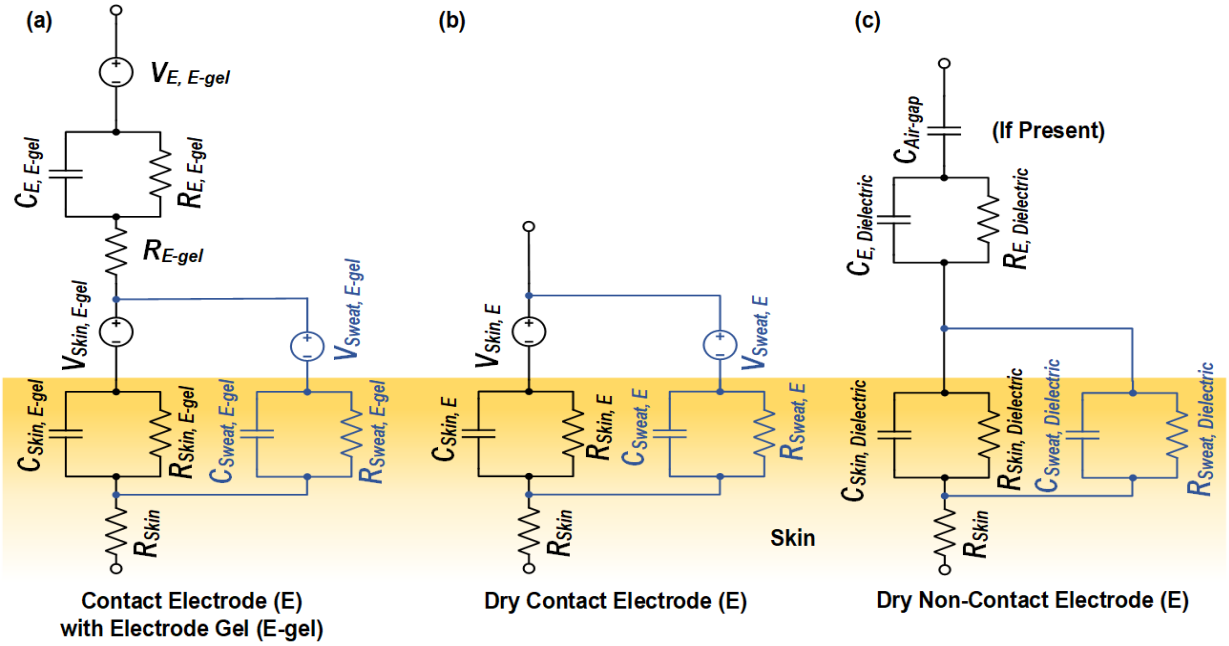

Fig 3.1. Generic skin-electrode contact impedance models with the impact of sweat: (a) contact electrode with electrode gel ($V_{E,\,E\text{-}gel}$, $V_{Skin,\,E\text{-}gel}$, and $V_{Sweat,\,E\text{-}gel}$ are polarization voltages at respective interfaces [18]; (b) dry contact electrode ($V_{Skin,\,E}$ and $V_{Sweat,\,E}$ are polarization voltages at respective interfaces, based on [12], [18]); and (c) non-contact electrode (no polarization effect, based on [12] and the sweat model of contact electrode).

3.3.1 Skin-Electrode Contact Capacitance Measurement

The capacitance of the non-contact electrodes generally depends upon the size of the metal electrode, the skin property, and the thickness and dielectric property of the insulating layer [10], [12], [13]. In our work, three different non-contact gold electrodes: circular, rectangular, and

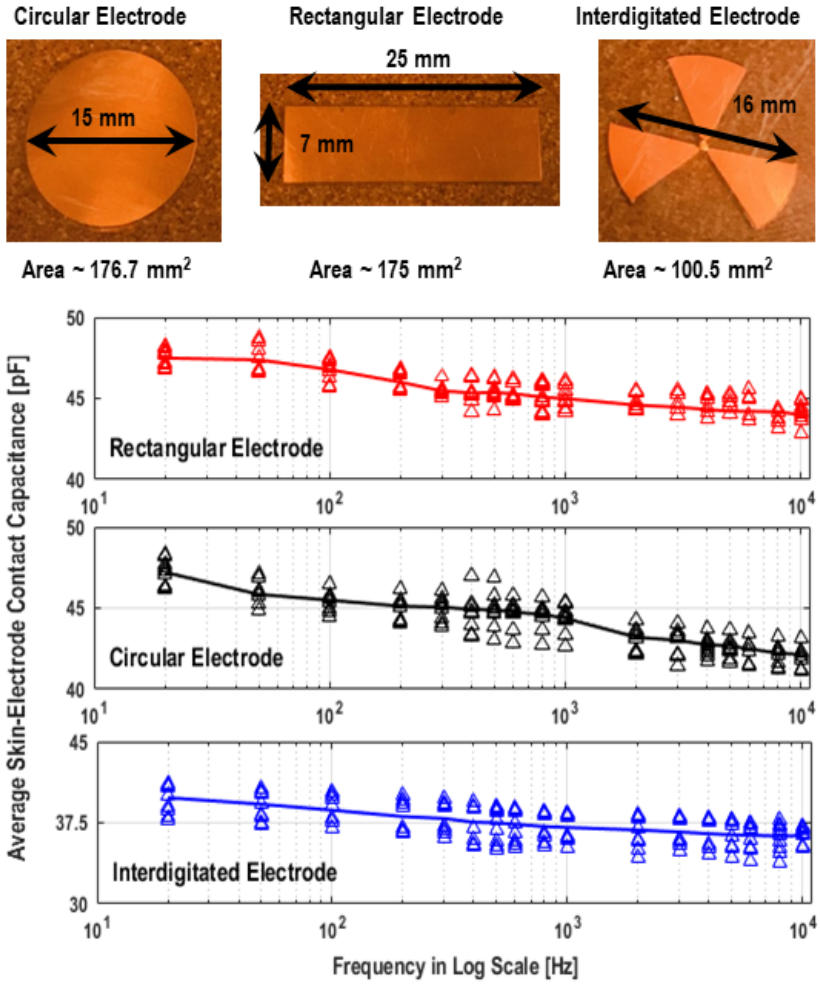

Fig. 3.2. Skin-electrode contact capacitance measurement for the three types of non-contact electrodes: circular, rectangular, and interdigitated. The solid lines show the average of 10 measurements.

interdigitated as shown in Fig. 3.2, are printed as contact pads by the PCB manufacturer on the flexible polyimide PCB (printed circuit board) substrate. A kapton film (with a thickness of approximately 127 µm) is used as the dielectric material between the skin and the metal plate for all the electrodes. The effective skin-electrode contact capacitance for all three electrodes are measured using a Keysight E4980A LCR meter. For the skin-electrode contact capacitance measurement, a contact gold electrode with electrode gel and one of the non-contact electrodes are placed closely on the forehead of one subject [19]. The effective skin-electrode contact capacitance

is measured by measuring the capacitance between the two metal terminals of the contact and noncontact electrodes connected with the LCR meter. For a better accuracy, the experiment is repeated ten times for each type of electrodes and the average skin-electrode contact capacitance ($C_{Skin\text{-}Electrode}$) along with the measured values are reported in Fig. 3.2. The experimental data are summarized in third column of Table 3.1. As we can see from the presented data, the circular and the rectangular electrodes have almost same area and their measured capacitances are also very close. Whereas, the interdigitated one has smaller capacitance because of its smaller area. The maximum difference found in the skin-electrode contact capacitances from their average values is defined as the uncertainty band in all three measurements. It should be noted that the measured skin-electrode contact capacitances for all three types non-contact electrodes are considerably small. Therefore, they are highly sensitive to even the slightest movements and vibrations around them or small displacement. This is one major drawback of non-contact electrodes [10], [12].

3.3.2 Impact of Sweat on Skin-Electrode Contact Capacitance

The skin-electrode contact impedance also gets modulated in the presence of sweat. Sweat is considered to be a good medium for biopotential measurement, which helps in decreasing the overall skin-electrode contact impedance for contact electrodes and enhancing the biopotential recording capability [18]. Therefore, the impact of sweat is modelled as an additional capacitance-resistance pair along with its respective polarization voltage (see, Fig. 3.1a and 3.1b) in contact electrodes [12], [18]. Non-contact electrodes have very small capacitance and the change in capacitance due to sweat may impact the sensed biopotential. Therefore, following the sweat models of contact electrodes, the impact of sweat on non-contact electrodes can be modelled as an additional capacitance-resistance pair in the model of non-contact electrode reported in [12]. Since non-contact electrodes do not suffer from polarization effect, no polarization voltage is present in the non-contact electrode model. The model for non-contact electrode with the impact of sweat is shown in Fig. 3.1c. The overall dielectric property at the skin-insulating layer interface will change due to the presence of sweat, which in-turn will increase (as assumed in the model) the overall

skin-electrode contact capacitance. However, the impact of the added capacitance will be small due to the presence of the series capacitance at electrode-dielectric interface.

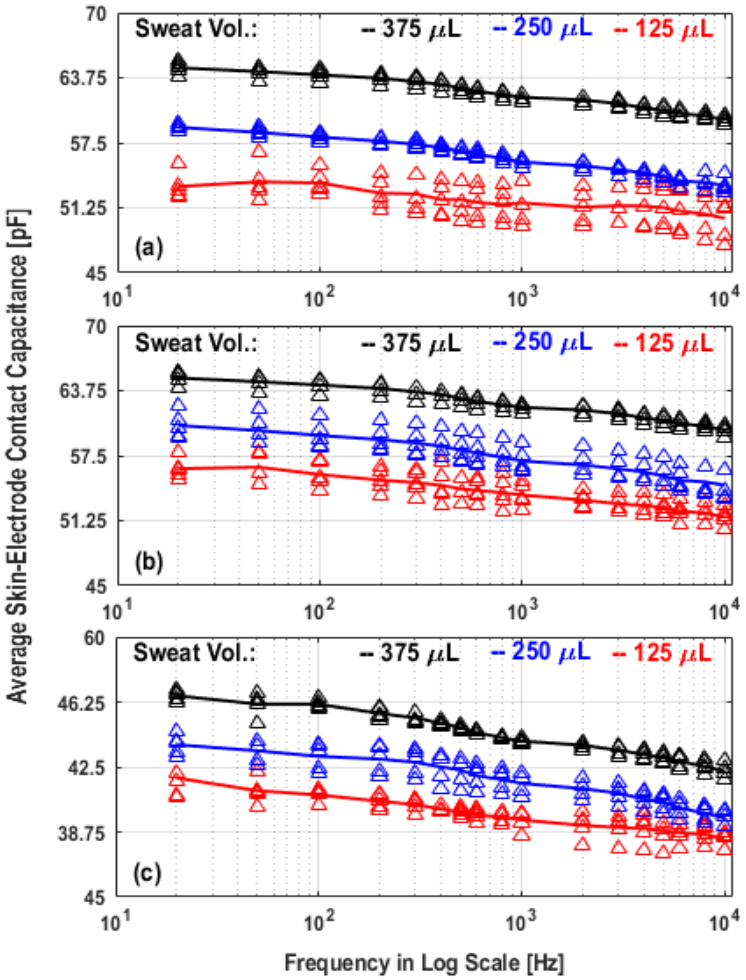

Fig. 3.3. The impact of sweat on the skin-electrode contact capacitance measured for the three types of non-contact electrodes: (a) circular, (b) rectangular, and (c) interdigitated electrode. The solid lines show the average of 5 measurements.

To do a qualitative study of the impact of sweat on non-contact electrodes, a sweat test is performed. In the test, a saline solution (with 0.9% $Na^{+}Cl^{-}$ concentration) is used as a substitute of sweat on the non-contact electrodes. A sprayer is used to spray the solution on the test electrodes before placing it on the skin for measurement. The average solution volume is 125 µL per spray.

Three sweat volume tests are performed (with one spray i.e., 125 µL, two sprays i.e., 250 µL, and three sprays i.e., 375 µL of sweat) on each type of electrodes. The measurements are repeated five times for each test cases. The average skin electrode contact capacitances along with the measured values are presented in Fig. 3.3. The experimental data are summarized in fourth, fifth and sixth column of Table 3.1. If we compare the data in Table 3.1, we can see that the effective skin-electrode contact capacitances indeed increase by small amount as the volume of sweat increases. These results align with predictions from the model in Fig. 3.1c. Overserving the amount of change in capacitance for different types of electrodes, it can be said that the capacitance increase due to sweat is proportional to the sweat volume as well as the area of the electrodes.

TABLE 3.1

NON-CONTACT ELECTRODE DESIGN, MEASUREMENT, AND SWEAT TESTING

Electrode Geometry	Electrode Area	No Sweat	Sweat Volume 125 µL	Sweat Volume 250 µL	Sweat Volume 375 µL
		Avg. $C_{Skin\text{-}Electrode}$ Spread ± Uncertainty (20 Hz – 10 kHz)	Avg. $C_{Skin\text{-}Electrode}$ Spread ± Uncertainty (20 Hz – 10 kHz)	Avg. $C_{Skin\text{-}Electrode}$ Spread ± Uncertainty (20 Hz – 10 kHz)	Avg. $C_{Skin\text{-}Electrode}$ Spread ± Uncertainty (20 Hz – 10 kHz)
Circular	176.7 mm^2	47.2 pF ± 0.75 pF to 42.1 pF ± 1.18 pF	53.2 pF ± 2.25 pF to 50.3 pF± 2.61 pF	59.0 pF ± 0.33 pF to 53.4 pF ± 1.15 pF	64.7 pF ± 0.87 pF to 59.7 pF ± 0.5 pF
Rectangular	175 mm^2	47.5 pF ± 1.06 pF to 43.9 pF ± 1.02 pF	56.3 pF ± 1.60 pF to 51.6 pF ± 1.21 pF	60.4 pF ± 1.88 pF To 54.7 pF ± 1.50 pF	65.0 pF ± 1.04 pF to 60.0 pF ± 0.68 pF
Interdigitated	100.5 mm^2	39.8 pF ± 2.02 pF to 36.3 pF ± 1.11 pF	41.9 pF ± 2.06 pF to 38.4 pF± 0.71 pF	43.8 pF ± 0.80 pF To 39.6 pF ± 0.45 pF	46.6 pF ± 0.40 pF to 42.3 pF ± 0.59 pF

3.3.3 Impact of Motion on Skin-Electrode Contact Capacitance

In biopotential acquisition systems, motion artifacts can be considered as the most challenging interference during signal measurement. Motion artifacts get introduced to the measured signal during recording due to several reasons, like improper electrode placements, patient's voluntary/involuntary movements during normal activities (e.g., talking, chewing, breathing etc.), and nearby environmental vibrations [12]. Non-contact electrodes are more prone to motion

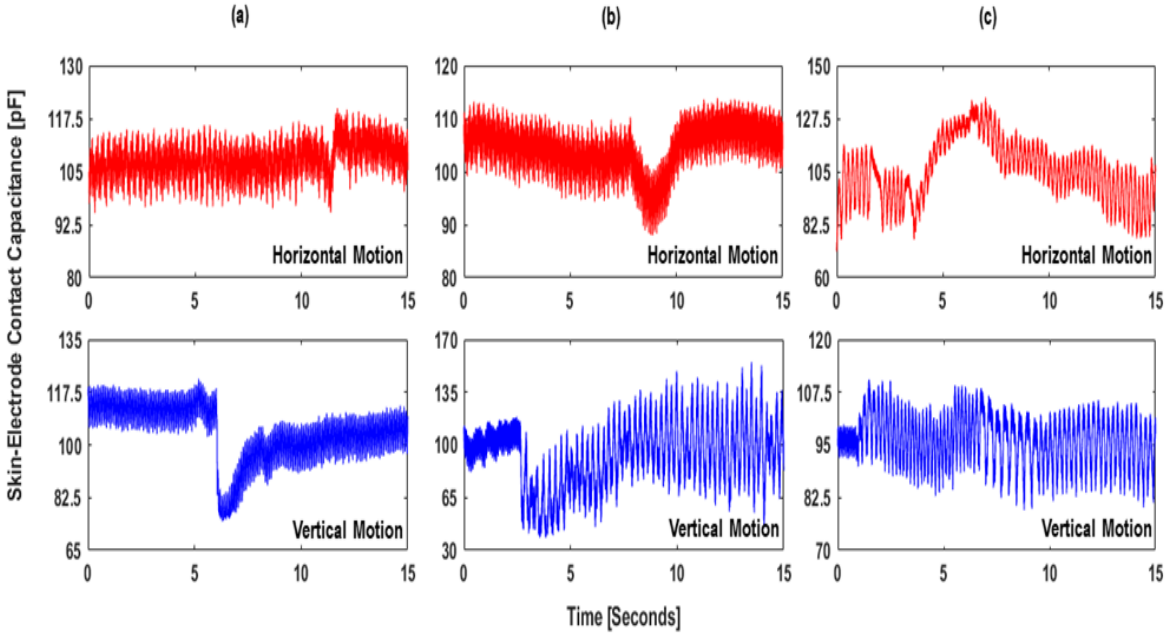

Fig. 3.4. Impact of motion artifacts on the skin-electrode contact capacitance: (a) circular electrode, (b) rectangular electrode, and (c) interdigitated electrode.

artifacts. Motion artifacts may create an air-gap at the skin-electrode contact interface. Sometimes, improper placement of measurement electrodes also creates air-gap at the skin-electrode contact interface. As a result of air-gap, the distance between the electrode plate and the skin increases and the overall skin-electrode contact capacitance reduces at the contact interface, thus making the electrode more sensitive to motion. Such variation in input capacitance also changes the amplitude and phase of the recorded biopotential, thereby degrading the overall output of the system. When it comes to two or more recording electrodes, all the electrodes do not experience the same amount of motion artifacts at the same time, which causes DC drifts at the input of the measurement unit, degrading the overall common-mode rejection ratio (or CMRR) of the measurement unit [20]. Therefore, it is important to have a proper contact between the skin and the dielectric layer of measurement electrodes for a good quality signal detection. The high-pass cut-off frequency, at the input stages of the biopotential measurement system, also gets easily affected by skin-electrode contact capacitance variation. The high-pass cut-off frequency variation can be stabilized by

choosing large load resistance at the input terminal. But such designs will need an ultra-high input impedance (> 1 TΩ) amplifier as the first stage amplifier of the measurement unit, to avoid loading effect [14], [21] – [23]. These system design considerations will be discussed in detail in the next section.

To simulate the impact of motion on skin-electrode contact capacitance, a capacitive-feedback amplifier circuit is implemented [12]. The gain of the amplifier is set at 1 by selecting the input and feedback capacitor values, both as 100 pF. The high-pass cutoff of the circuit is set around 0.16 Hz by selecting a resistor of 10 GΩ at the feedback path. Two electrode plates of similar shape (circular or rectangular or interdigitated) and the kapton film as the insulation layer are used to form the test capacitive electrode (measured value ~ 10 pF). The test electrode is configured in parallel with the 100 pF input capacitance. The setup is fed with a sinusoid input of 10 Hz. The entire test setup is placed on a platform. Then random motions and vibrations of various intensities are introduced during the output recording both in horizontal and vertical directions on the platform. The overall capacitance variations, due to motion, are computed for the three types of electrodes and presented in Fig. 3.4. The variation in the measured capacitance also appeared to be random due to both type (horizontal/vertical) of induced random motions. It is also clearly seen from the graph that the capacitance at the input terminal of the amplifier varies around the fixed input capacitance value of 100 pF. In some cases, the capacitance variation even goes below 100 pF, stating the possibility that even the small constant capacitors (here 100 pF) may suffer from environmental vibrations and motions when they are used in low frequency (near DC) applications like biopotential measurements.

3.4 System Design and Implementation

3.4.1 System Architecture and Design

The EOG board is implemented on a four-layer flexible polyimide substrate, as shown in Fig. 3.5a. The top layer of the board is used to implement the EOG measurement unit with commercial off-the-shelf ICs and components. The entire system is battery operated and uses a microcontroller

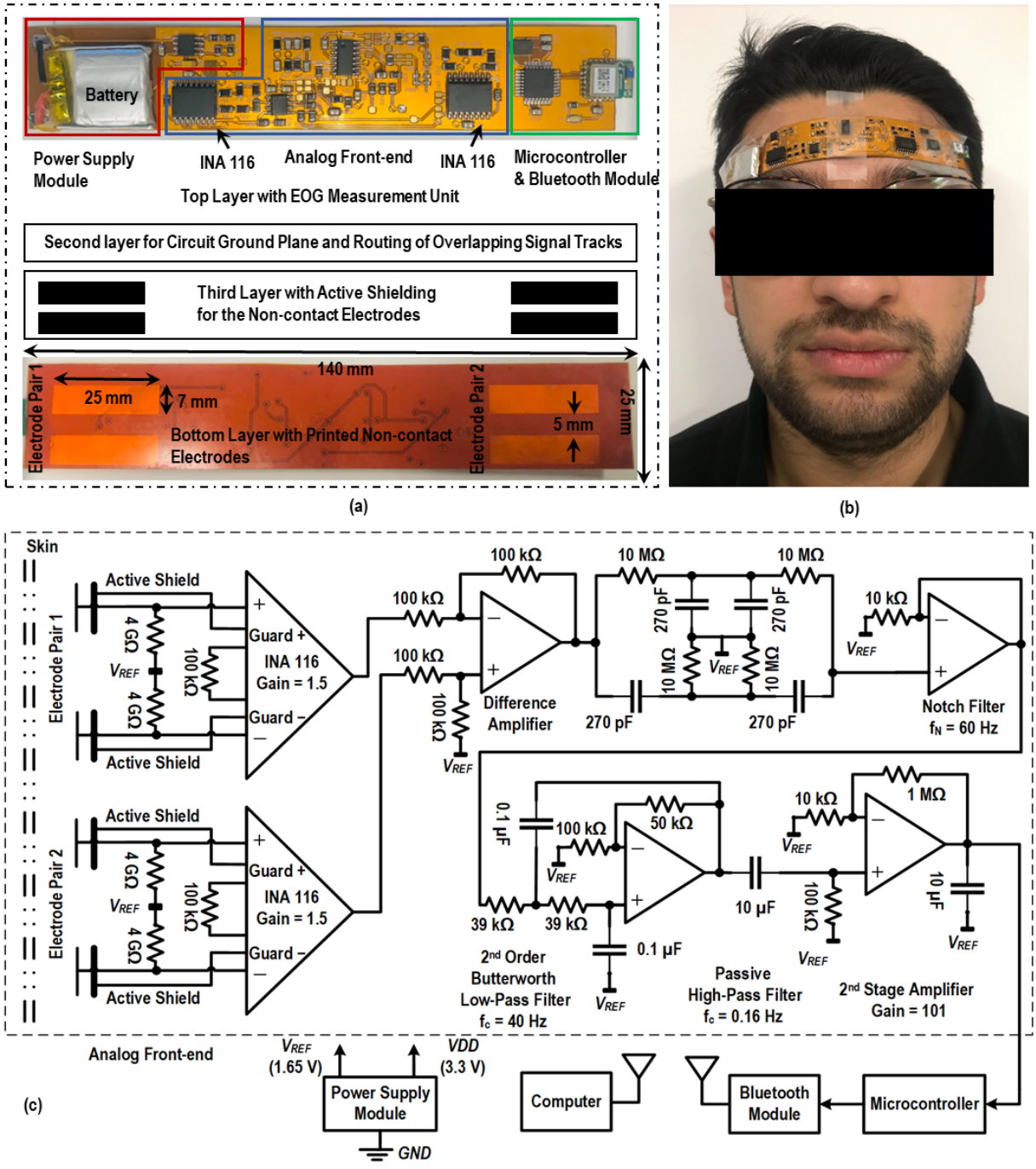

Fig. 3.5. The proposed wearable flexible EOG system: (a) four layers of the flexible board with EOG measurement system, (b) the experimental setup for EOG recording, and (c) a detailed block diagram of the EOG measurement circuit.

and BLE 5.0 transceiver for wireless EOG data transmission. The bottom layer is used for printing the measurement electrodes (circular, rectangular, or interdigitated type) and one of them is shown in Fig. 3.5a. The printed electrodes are covered with a biocompatible kapton film [24], thus forming non-contact measurement electrodes. The second layer is used for routing overlapping PCB tracks and ground plane for the entire system. The third layer is used for active shielding in order to reduce capacitive coupling effect between the discreet component on the top layer and the printed electrodes on the bottom layer [11]–[13]. The experimental setup for EOG measurement is presented in Fig. 3.5b.

In this EOG system, two pairs of measurement electrodes are used for EOG detection and motion artifacts sensing, as shown in Fig. 3.5a. The two electrodes in each pairs are placed vertically or horizontally or in interdigitated configurations (discussed in detail in the next section). The EOG potential sensed by the two electrodes of each pair are different in terms of their positions and distance from the eyes [11]. On the other hand, motion artifacts have stronger intensity than the EOG signals. Therefore, it is assumed that the motion signals picked up by the two electrodes of an electrode pair will be almost similar as they are printed very close to each other. Therefore, subtracting the signals picked up by both the electrodes in an electrode pair will help in reduction of the motion artifacts, thereby compensating for the DC drifts and improving the overall CMRR of the system. Whereas, after subtraction of motion signals, some portion of the EOG potential will still be present. To improve the EOG signal detection, two dedicated ultra-high input impedance instrumentation amplifiers (or IAs) are used as the first stage amplifiers for each electrode pair. The IAs are positioned on the top layer of the board in such a way that they are very close to the printed electrode pairs in the bottom layer. This sort of placement has been generally done in several dry electrode designs for better biopotential detection [21]–[23]. Once the EOG signal is detected, it needs to be amplified up to a desired level through various analog signal conditioning stages and then digitized into data-stream through digital circuitry for wireless data transmission, which are discussed in the next subsection.

3.4.2 Circuit Level Implementation

A detailed block diagram of the analog front-end, power supply module, and digital circuitry for the implemented EOG system is presented in Fig. 3.5c. The power supply module uses a 125 mAh Li-ion battery with 3.7 V of nominal voltage and a voltage regulator IC to generate a 3.3 V supply voltage for the rest of the circuit block, while consuming only 56 mW of power. The battery life of the system is approximately 7 hours and 15 minutes, which is good enough for long-term monitoring. This module also uses an op-amp to generate an analog ground (or V_{REF}) of 1.65 V for the analog front-end block, thus limiting the signal swing of the analog front-end to ± 1.65 V.

The most important circuit block in an analog front-end is the first stage amplifier, as it is directly connected to the measurement electrodes as its inputs. The first requirement of the first stage amplifier is having a very large input impedance, so that it can handle near DC high-pass cut-off frequency (~0.1 Hz) of biopotential measurements [14], [21]–[23]. When it comes to applications involving non-contact electrodes, given their small skin-electrode contact capacitance values (in the range of pico-farads), the requirement of input impedance of the amplifier can exceed above 1 TΩ (~ 10^{12} Ohms). The second requirement of the first stage amplifier is to have a large CMRR to reject the common-mode DC drifts generated at the skin-electrode contact interfaces [20], [25]. Instrumentation amplifier (IA) ICs can be an ideal solution to meet such specifications mentioned above. For this application, the famous Burr-Brown's IA INA116 (with input impedance ~ 10^{15} Ohms and CMRR ~ 90 dB) is selected [26]. Given the measured skin-electrode contact capacitances of the printed non-contact electrodes and the impact of sweat and motion artifacts on them (assuming the average skin-electrode contact capacitance as 40 pF), a load resistance of 4 GΩ is selected to set the input high-pass cut-off close to 1 Hz and limit the overall baseline variation for this EOG application, as shown in Fig. 3.5c. It should be noted that the input high-pass cut-off frequency of the system will change with motion. The motions will mostly create an air gap between the skin and the kapton film interface, thus increasing the effective distance between the skin and the metal electrode plate. This will further decrease the overall capacitance at the skin-electrode contact interface and shift the high-pass cut-off of the system towards higher

frequency. To stabilize the high-pass cut-off frequency against capacitance variations, ultra-high value resistors (around 100 GΩ) can be used. But this will increase the cost, thermal noise, and sensitivity of the overall system. The two electrodes in an electrode pair are used as the inputs of the IA. The electrode pair as inputs will supress the impact of motion artifacts in the first stage IA itself. The performance of non-contact electrodes also degrades in the presence of power-line interferences due to capacitive coupling [14], [27]. To control the impact of such interferences, active shielding is implemented on the third layer of the flexible board and later interfaced with guard pins of the IA, as shown in Fig. 3.5c. Two IAs are used for the two electrode pairs. Given the high sensitivity of the non-contact electrodes towards the system non-linearity mentioned above, the gain of the first stage amplifier is set at 1.5 only, to avoid any output saturation [28]. In the next stage, the outputs of the two IAs are fed in a difference amplifier, implemented using one of the op-amps. In the next stage, a notch filter is implemented to further supress any power-line interferences present in the sensed signal spectrum. The notch frequency (f_N) of this block is set at 60 Hz. After that, a second order low-pass Butterworth filter is designed with a low-pass cut-off ($f_{c,LPF}$) at 40 Hz. Thus, the overall EOG bandwidth of the system is limited from 1 Hz (assumed) to 40 Hz. In the next step, a first order passive high-pass filter (with high-pass cut-off, $f_{c,HPF}$ of 0.16 Hz) is implemented to reduce the impact of DC offsets coming from the previous signal conditioning stages. Therefore, the poles of the system can be located at 0.16 Hz (due to the passive high-pass network), around 1 Hz (at the inputs of the system), and at 40 Hz (due to the low-pass Butterworth filter). Given the first order of the high-pass networks, the zeros of the system simply stay at 0 Hz. The next stage of the analog front-end is the second stage amplifier. The second stage amplifier is responsible for amplifying the sensed EOG signal up to a desired level. The gain of this block is determined empirically and set to 101 for the final analog output amplification. The output of the analog-front end is then fed to the digital circuitry part for digitization.

The digital circuitry of the system uses a microcontroller and a BLE 5.0 transceiver. One of the analog-to-digital converter (ADC) channel of the microcontroller unit is used to digitize the EOG signal (sensed by the analog-front end block) at a rate of 200 samples per second. The

digitized data are then transmitted using a BLE 5.0 transceiver. The data are acquired in a nearby computer using another BLE 5.0 transceiver module and then processed in MATLAB to extract EOG information for eye-blinking activities. The flexible EOG system is also compared with some state-of-the-art systems discussed in the previous sections and presented in Table 3.2. As we can see from Table 3.2, this work can be directly compared with respect to (w.r.t.) the recent state-of-the-art flexible biopotential measurement systems [11] and [12]. This work uses non-contact electrodes for EOG measurement whereas [11] uses contact electrodes and requires skin preparation and gel. This work has relatively less gain w.r.t. [11] and [12]. Since, non-contact electrodes are generally very sensitive, even small gain is good enough to detect large biopotentials like EOG. The system is slightly heavier than the system reported in [11] and lighter than the system reported in [12]. Although this work consumes higher power than the systems reported in [11] and [12], it is still suitable for long term monitoring, as proven from the battery life mentioned before. Like this work, the system in [11] does not have motion artifact reduction feature. Although [12] has motion artifact reduction feature, it has not been validated for biopotential measurement from human subjects properly. This work is extensively validated for biopotential measurements in the presence/absence of motion artifacts (discussed in the next section). Lastly this work uses a simpler circuit concept than [12] for motion artifacts sensing and reduction.

3.5 System Characterization and Measurement Results

The experimental procedure in this study is in accordance with the Declaration of Helsinki and was approved by Institutional Review Board of McGill University (study number: A04-M21-19B, approval date: 04/17/2019). In the first step, the analog front-end part of EOG system is characterized to evaluate its gain-vs-frequency response, noise, and CMRR. In the next step, the EOG system is validated for EOG measurement and its capability of motion artifacts reduction. The experiments are done with all three types of electrodes (circular, rectangular, and interdigitated) in different placement configurations and the results are discussed in more detail.

TABLE 3.2

SOME OF THE STATE-OF-THE-ART BIOPOTENTIAL MEASUREMENT APPLICATIONS WITH/WITHOUT MOTION ARTIFACTS SENSING AND REDUCTION

	EMBS'08 [15]	BIOCAS'10 [14]	TBCAS'12 [16]	JSSC'14 [17]	TBCAS'19 [12]	SENS. J.'21 [11]	THIS WORK
ELECTRODE DESIGN AND SPECIFICATIONS							
Electrode Type	Rigid	Rigid	Rigid	Rigid	Flexible	Flexible	Flexible
Contact/Non-contact	Wet Contact	Non-contact	Wet Contact	Dry Contact	Non-Contact	Wet Contact	Non-Contact
Electrode Design	Square	Square	—	—	Interdigitated	Circular	Various*
Electrode Area	400 mm^2	625 mm^2	—	—	~ 157 mm^2	78.54 mm^2	Various*
MOTION ARTIFACTS DETECTION AND REDUCTION METHODS							
Motion Artifacts Detection	Yes	No	Yes	Yes	Yes	No	Yes
Sensing Method	Accelerometer	—	ETI	ETI	Parallel	—	Parallel
Motion Artifacts Reduction	Digital	—	Digital	Digital	Analog	—	Analog
SYSTEM DESIGN AND SPECIFICATIONS							
PCB board type	Rigid	Rigid	Rigid	Rigid	Flexible	Flexible	Flexible
System weight	—	—	—	—	9.2 gram	7.7 gram	8.75 gram
Number of channels	5	—	3	4	8	1	1
Power Supply (Volts)	—	±5 V, 3 V	1.2 V	1.8 V	3.3 V	3.3 V	3.3 V
Power Consumption (Watts)	—	116 mW	200 µW	170 µW	26 mW	48.75 mW	56 mW
Input impedance of the first stage amplifier (Ω)	—	~ 10^{15} Ω	~ 10^{9} Ω	~ 1.2×10^{9} Ω	—	~ 10^{11} Ω	~ 10^{15} Ω
System Gain (maximum)	—	~ 58 dB	~ 50 dB	~ 70 dB	~ 48.3 dB	~ 68.5 dB	~ 37 dB
System Bandwidth	—	3 – 42 Hz	0.2 – 250 Hz	0.5 – 200 Hz	1 – 300 Hz	1.6 – 47 Hz	1 – 40 Hz
Application	ECG	ECG/EEG	ECG/ETI	EEG/ETI	EEG	EOG	EOG

*Three different shape and sizes of electrodes are tested in this work, see Figure 3.2 for details.

3.5.1 System Characterization

Being the crucial signal conditioning block, the analog frontend of the EOG measurement unit should have a stable gain over the range of interested signal bandwidth, minimal noise generated by the discreet components, and acceptable CMRR to reject the unwanted DC drifts coming from the skin-electrode contact interface. All these characteristics for the proposed system are evaluated and presented in Fig. 3.6. To evaluate the gain-vs-frequency response of the analog front-end, a constant capacitor of 40 pF (assuming the average skin-electrode contact capacitance value) is used as the input capacitor. The EOG unit has four inputs (two IAs), see Fig. 3.5c. Three of them are connected to the analog ground and a sinusoid is fed to the fourth input with the capacitance of 40 pF and a load resistance of 4 GΩ. The effective gain-vs-frequency response of the system is recorded and presented in Fig. 3.6a. The gain of the system is found out to be around 37 dB over the signal bandwidth of 1 Hz to 10 Hz. Then the gain response drops as the frequency approaches to 40 Hz. The variation in the gain response can be attributed to the order of the notch filter present in the analog front-end. However, the bandwidth of EOG signals for basic eye activities such as eye blinking and eyeball movements can be limited up to 10 Hz. Therefore, the system still performs well for basic eye activity detection with this gain variation over the signal bandwidth. Moreover, the capacitance at the actual skin-electrode interface can vary, which will result in a slightly different gain-vs-frequency response for the system. It should be noted that the gain variability of the system can be stabilized by removing the notch filter from analog front-end.

The input-referred noise response of the circuit is presented in Fig. 3.6b. In this test, all the inputs of the IAs were shorted to the analog ground and the input-referred noise is quantified from the recorded noise output and the gain of the system. The input-referred noise remains below 1 μVrms at any frequency over the system bandwidth of 1 – 40 Hz, thus meeting the noise specification (less than 1.5 μVrms over the interested signal bandwidth) for biopotential measurement applications as per IFCN standards [25]. To further improve the noise response of the system, the large resistances at the input stages can be reduced, which would require larger size capacitive electrodes to maintain the high-pass cut-off frequency around 1 Hz. For the CMRR

calculation, a common-mode sinusoid was fed to the positive terminals of the IAs of the system and the negative terminals were shorted to the analog ground. The overall CMRR of the system is found out to be above 74 dB, as presented in Fig. 3.6c.

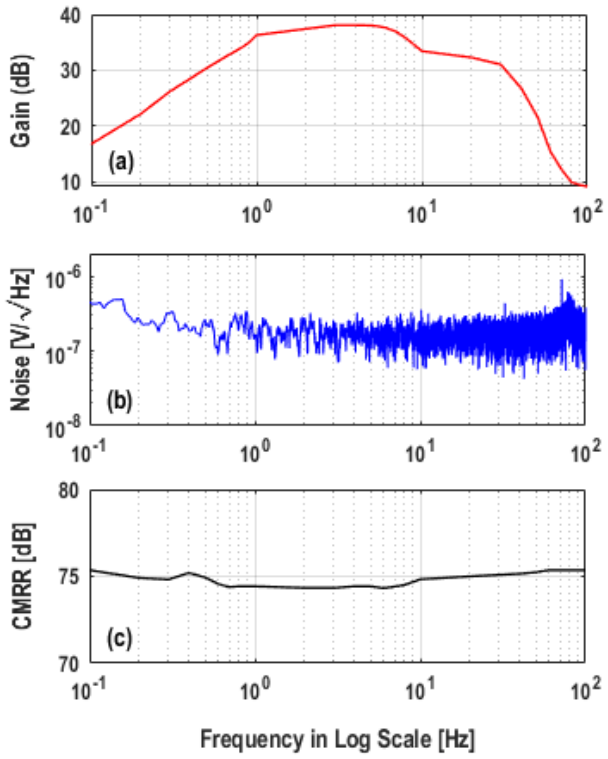

Fig. 3.6. The analog front-end characterization: (a) gain-vs-frequency response, (b) input-referred noise response, and (c) CMRR response.

3.5.2 Detection of EOG Signals With Different Electrode Configuration for Motion Artifacts Reduction (MAR)

The three types of electrodes (circular, rectangular, and interdigitated) are arranged in five different configurations to form an electrode pair for parallel EOG/motion sensing and motion artifacts reduction (MAR). The five different electrode arrangements (termed as circular electrode pair in horizontally parallel configuration, circular electrode pair in vertically parallel configuration, rectangular electrode pair in horizontally parallel configuration, rectangular electrode pair in

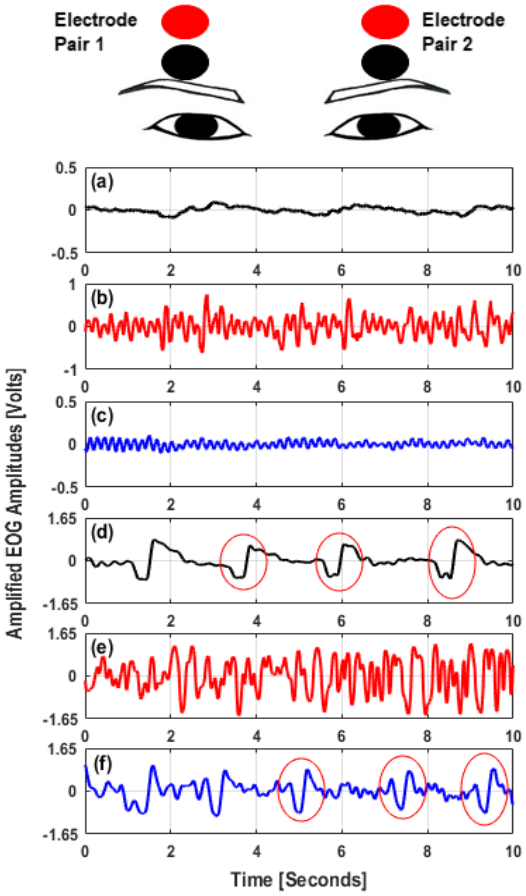

Fig. 3.7. EOG recording using circular electrodes in horizontally parallel configuration– (a) EOG baseline recording in the absence of motion artifacts, (b) EOG baseline recording in the presence of motion artifacts and without motion artifact reduction (MAR), (c) EOG baseline recording in the presence of motion artifacts and with MAR, (d) eye-blinks recording in the absence of motion artifacts, (e) eye-blinks recording in the presence of motion artifacts and without MAR, and (f) eye-blinks recording in the presence of motion artifacts and with MAR.

vertically parallel configuration, and interdigitated electrode pair) are shown in Figs. 3.7 –3.11, respectively. The distance between the two electrodes in an electrode pair are chosen empirically and set at 5 mm edge-to-edge, except for the interdigitated configuration (Fig. 3.11). Five different flexible EOG boards are made for the five different electrode arrangements. The flexible boards are placed on the forehead, just above the eyebrows and as much closer to the eyes as possible, and attached using transparent adhesive, as shown in Fig. 3.5b. After that, the EOG baseline and

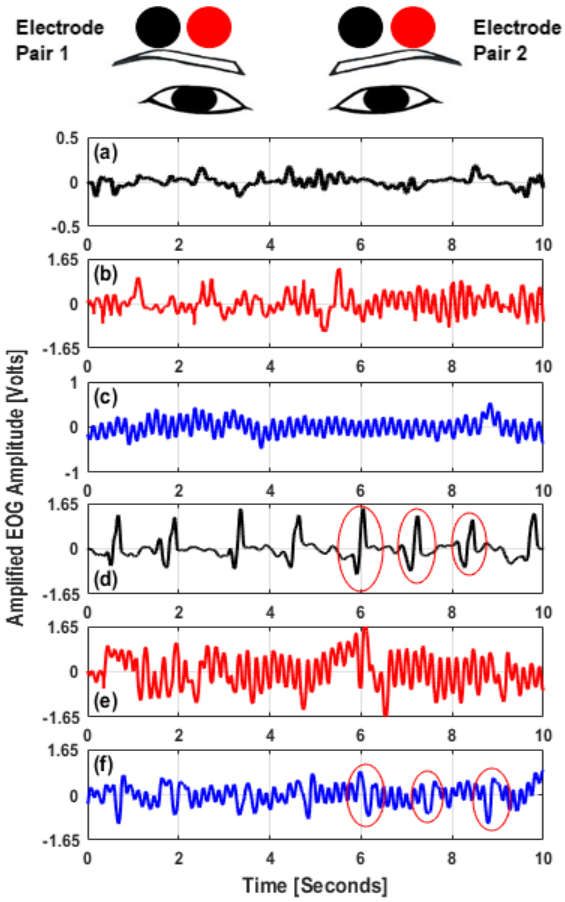

Fig. 3.8. EOG recording using circular electrodes in vertically parallel configuration– (a) EOG baseline recording in the absence of motion artifacts, (b) EOG baseline recording in the presence of motion artifacts and without MAR, (c) EOG baseline recording in the presence of motion artifacts and with MAR, (d) eye-blinks recording in the absence of motion artifacts, (e) eye-blinks recording in the presence of motion artifacts and without MAR, and (f) eye-blinks recording in the presence of motion artifacts and with MAR.

eye-blinking activities are recorded in the presence and absence of motion. The motion artifacts are introduced by asking the subject to shake the legs during data recording. The results for all five electrode configurations are presented in the Figs. 3.7–3.11. The EOG measurement conditions for all five set of data (Figs. 3.7–3.11) are as follows: (a) EOG baseline recording in the absence of motion artifacts, (b) EOG baseline recording in the presence of motion artifacts and without motion artifact reduction (MAR), (c) EOG baseline recording in the presence of motion artifacts and with

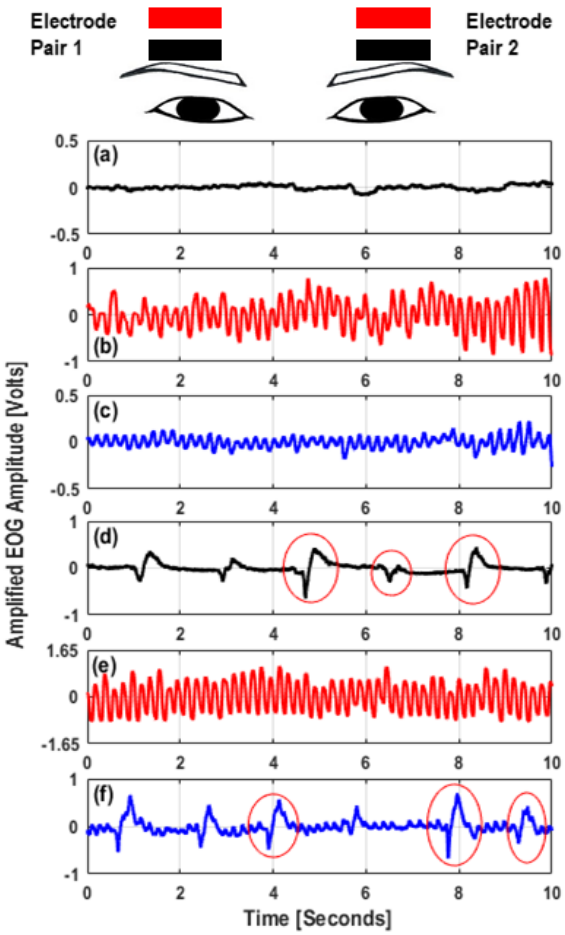

Fig. 3.9. EOG recording using rectangular electrodes in horizontally parallel configuration– (a) EOG baseline recording in the absence of motion artifacts, (b) EOG baseline recording in the presence of motion artifacts and without MAR, (c) EOG baseline recording in the presence of motion artifacts and with MAR, (d) eye-blinks recording in the absence of motion artifacts, (e) eye-blinks recording in the presence of motion artifacts and without MAR, and (f) eye-blinks recording in the presence of motion artifacts and with MAR.

MAR,(d) eye-blinks recording in the absence of motion artifacts, (e) eye-blinks recording in the presence of motion artifacts and without MAR, and (f) eye-blinks recording in the presence of motion artifacts and with MAR. For measurement conditions (b) and (e), the load resistance (as shown in Fig. 3.5c) of one of the measurement electrodes in an electrode pair (the RED electrodes, shown in Figs. 3.7–3.11) are directly shorted to the analog ground (or V_{REF}).

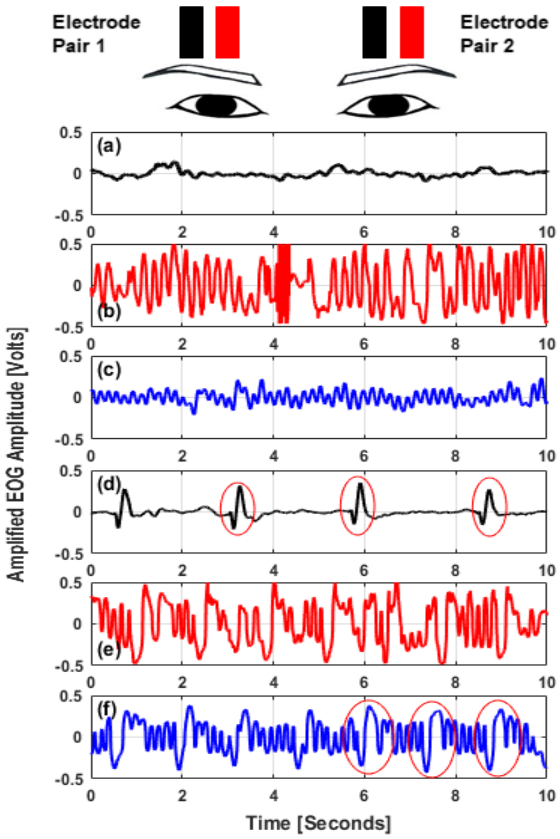

Fig. 3.10. EOG recording using rectangular electrodes in vertically parallel configuration– (a) EOG baseline recording in the absence of motion artifacts, (b) EOG baseline recording in the presence of motion artifacts and without MAR, (c) EOG baseline recording in the presence of motion artifacts and with MAR, (d) eye-blinks recording in the absence of motion artifacts, (e) eye-blinks recording in the presence of motion artifacts and without MAR, and (f) eye-blinks recording in the presence of motion artifacts and with MAR.

3.5.3 Discussion

The first step of measurement in EOG is to study the pure baseline signal and its variation, in the absence of motion artifacts. The EOG baseline represents the low-frequency components of the EOG signal with a range from DC to 1 Hz. The EOG baseline should have a limited range of variation in order to avoid saturation at the output during eye-activities, which is controlled by the high-pass cut-off frequency at the inputs of the system. For this system, the high-pass cut-off is set around 1 Hz and a stable EOG baseline is observed for all five electrode configurations, as shown

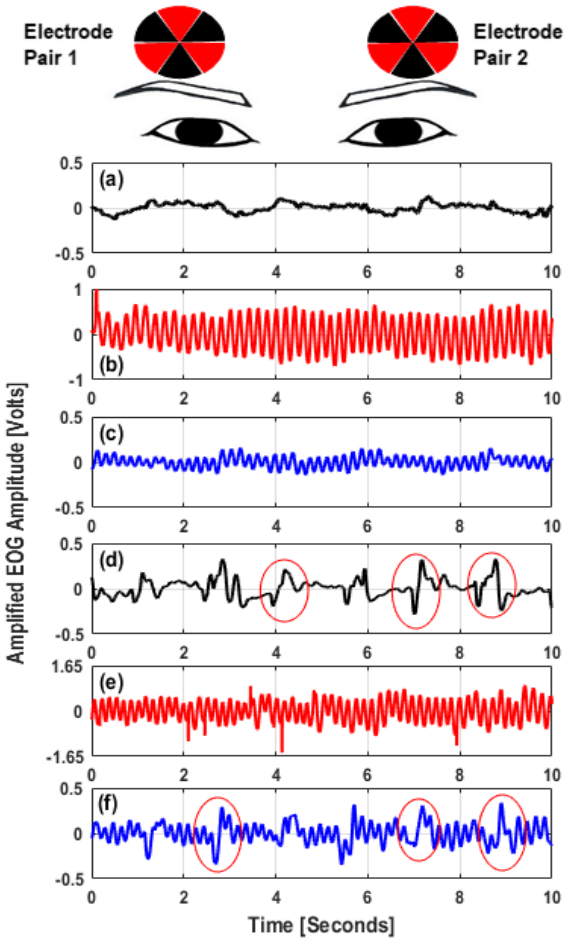

Fig. 3.11. EOG recording using interdigitated electrode configuration– (a) EOG baseline recording in the absence of motion artifacts, (b) EOG baseline recording in the presence of motion artifacts and without MAR, (c) EOG baseline recording in the presence of motion artifacts and with MAR, (d) eye-blinks recording in the absence of motion artifacts, (e) eye-blinks recording in the presence of motion artifacts and without MAR, and (f) eye-blinks recording in the presence of motion artifacts and with MAR.

in Figs. 3.7a–3.11a. In Figs. 3.7b–3.11b, the EOG baseline is recorded in the presence of motion artifacts and without MAR. For all five cases, the EOG baseline gets distorted severely. In Figs. 3.7c–3.11c, again the EOG baseline signal is recorded in the presence of motion artifacts and with MAR implementation. The MAR technique indeed reduced the impact of motion artifacts on the EOG baseline signal. However, by looking at the amplitude levels of the EOG baseline after MAR, it can be said that the MAR worked better for the horizontally parallel electrode configurations

and the interdigitated ones (Figs. 3.7c, 3.9c, and 3.11c). Each electrode in an electrode pair senses different levels of EOG signals based on their placement configurations [11]. The EOG signals sensed by each electrode in an electrode pair in horizontally parallel configurations (Figs. 3.7 and 3.9) will be different. The RED electrodes, in Figs 3.7 and 3.9, will sense a weaker EOG signal than the BLACK ones, because of their distance from the eye [11]. In case of electrode pairs with vertically parallel configurations (Figs. 3.8 and 3.10), the electrodes (both the BLACK and RED ones) in an electrode pair will sense EOG signals of almost similar strength because of same distance from the eye but with different phases (because of the electrode placement locations). These phase differences in the EOG potential maybe contributing a larger amplitude variation in the EOG baseline even after MAR for vertically parallel configurations (as presented in Figs. 3.8c and 3.10c). In case of the interdigitated electrode pairs, the EOG sensed by the electrodes (both the BLACK and RED ones) in an electrode pair will be almost similar, resulting in a stable EOG baseline after MAR implementation, as shown in Fig. 3.11c. It should be noted that, the strong motion artifacts experienced by the electrodes (both BLACK and RED) in an electrode pair are assumed to be almost same in this study. In the next study, eye-blinking activities are recorded in the absence of motion artifacts for all five electrode configurations and presented in Figs. 3.7d–3.11d. The eye-blinking activities are detected clearly for all electrode configurations and some of them are circled in RED. The eye-blinking activities are also captured in the presence of motion artifacts and without MAR technique, as presented in Figs. 3.7e–3.11e. As expected, none of them are visibly recognizable. Next, eye-blinking activities are captured (circled in RED) in the presence of motion artifacts and with MAR technique, shown in Figs. 3.7f–3.11f. As we can see, the eye-blinks are detected very clearly for horizontally parallel electrode configurations and for the interdigitated configurations (Figs. 3.7f, 3.9f, and 3.11f). It is expected since these configurations also worked better for motion artifacts estimation and reduction during EOG baseline recording. For the vertically parallel electrode configurations (Figs. 3.8f and 3.10f), the baseline variation range is appeared to be almost as strong as the eye activity signals detected. The explanation for such behavior can be attributed to the similar reasoning given for the EOG baseline signal in Figs. 3.8c and 3.10c. The amplitude level of the eye-blinks detected by the interdigitated electrode pairs

TABLE 3.3

QUALITATIVE RESULT SUMMARY OF THE FIVE TYPES OF ELECTRODE PLACEMENTS FOR EOG DETECTION IN THE PRESENCE/ABSENCE OF MOTION ARTIFACTS (MA) AND WITH/WITHOUT MOTION ARTIFACTS REDUCTION (MAR)

Electrode Pair Type	Placement Configuration	Presence of Motion Artifacts (MA)			Detectable Eye Blinks		
		EOG Baseline without motion	EOG Baseline with Motion and without MAR	EOG Baseline with Motion and with MAR	Eye Blinks without motion	Eye Blinks with Motion and without MAR	Eye Blinks with Motion and with MAR
Circular	Horizontally Parallel	MA absent	Strong MA	Weak MA	Yes	No	Yes (large amplitudes)
	Vertically Parallel	MA absent	Strong MA	Medium MA	Yes	No	Not Clear
Rectangular	Horizontally Parallel	MA absent	Strong MA	Weak MA	Yes	No	Yes (large amplitudes)
	Vertically Parallel	MA absent	Strong MA	Medium MA	Yes	No	Not Clear
Interdigitated	Interdigitated	MA absent	Strong MA	Weak MA	Yes	No	Yes (small amplitudes)

(Fig. 11f) are smaller in comparison to the ones detected in Fig. 3.7f and 3.9f, as because the EOG potential sensed by the interdigitated electrodes in an electrode pair are of almost same amplitude and phase and they nearly cancel each other at the very first stage of amplification. Therefore, it can be concluded that horizontally parallel electrode configurations (be it rectangular or circular) are better for this proposed EOG application with MAR. The qualitative performance summary of all these electrode configurations is reported in Table 3.3.

The sensitivity and response time of the different electrode configurations are calculated w.r.t. a reference eye blink. Two commercial contact gold electrode pairs in horizontally parallel configurations are used to acquire the reference eye blink. The contact electrode pairs are interfaced with four 40 pF capacitors at the input stage to set the input high pass cut-off at 1 Hz. Contact electrodes are less sensitive and, therefore, the gain of the circuit is increased 30 times than before to amplify the eye blink signal. Therefore, a gain multiplication factor (GMF) of 30 is used for sensitivity calculations. The eye blink data for all non-contact electrode configurations are presented in Fig. 3.12. The sensitivity is calculated by taking the average ratio of negative and positive peaks of the eye blink w.r.t. the amplified reference negative and positive peaks, respectively. The average ratio is then multiplied by GMF to compute the sensitivity of the electrode pairs. The response time is calculated by taking the average rise and fall times of the eye-blink signals. The calculated data are presented in Table 3.4.

From Table 3.4, it can be seen that the calculated sensitivity for all non-contact electrodes, except interdigitated ones, are 50 times higher than the contact ones. This validates the fact that non-contact electrodes are indeed more sensitive than the contact ones. The interdigitated pairs have the least sensitivity among all configurations, thus proving the fact that interdigitated configuration is not optimal for biopotential measurement. The response time for horizontally parallel configurations (both circular and rectangular) are found out to be larger than the other non-contact electrode configurations.

TABLE 3.4

SENSITIVITY & RESPONSE TIME CALCULATIONS OF THE NON-CONTACT ELECTRODES AND THEIR DIFFERENT PLACEMENT CONFIGURATIONS

	Gold Contact Electrodes H.P.C. (Ref. Signal × GMF)	Non-contact Electrode Pairs Placement Configurations				
		Circular (H.P.C.)	Circular (V.P.C.)	Rectangular (H.P.C.)	Rectangular (V.P.C.)	Interdigitated
EYE BLINK PARAMETERS FOR SENSITIVITY CALCULATIONS						
Positive Peak (Volts)	0.529 (GMF = 30)	0.885	1.065	0.910	1.058	0.319
Negative Peak (Volts)	– 0.506 (GMF = 30)	– 0.876	– 0.678	– 0.934	– 0.885	– 0.282
Sensitivity w.r.t. Ref.	1	51.06	50.30	53.49	56.24	17.41
EYE BLINK PARAMETERS FOR AVERAGE RESPONSE TIME CALCULATIONS						
Negative Peak Rise Time from Baseline	75 mS	340 mS	170 mS	280 mS	165 mS	80 mS
Positive Peak Fall Time to Baseline	155 mS	420 mS	110 mS	340 mS	190 mS	125 mS
Avg. Response Time	115 mS	380 mS	140 mS	310 mS	177.5 mS	102.5 mS

* H.P.C. means Horizontally Parallel Configuration, V.P.C. means Vertically Parallel Configuration, and GMF is gain multiplication factor

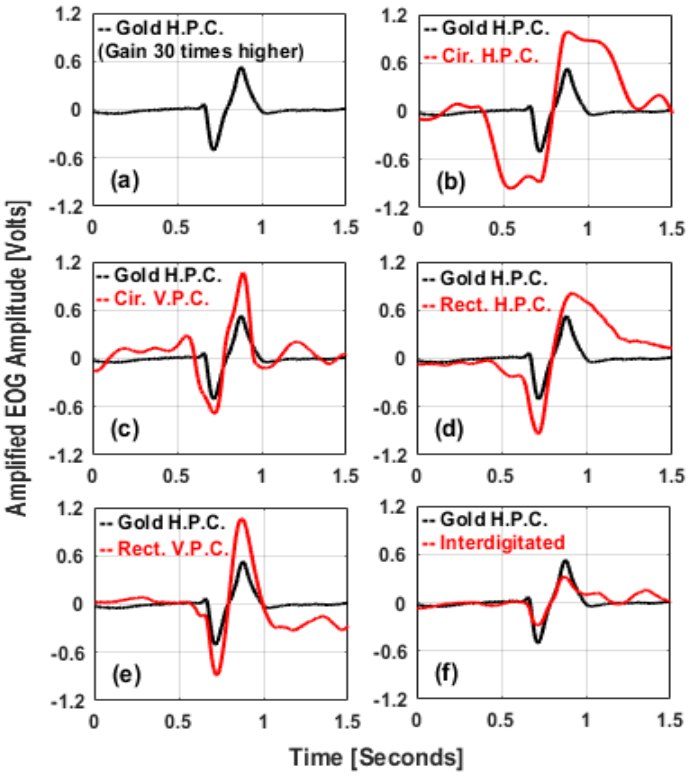

Fig. 3.12. Eye blink signals from the different electrode pair configurations for sensitivity measurement: (a) gold contact as reference in horizontally parallel configuration (H.P.C.), (b) circular in H.P.C., (c) circular in vertically parallel configuration (V.P.C.), (d) rectangular in H.P.C., (c) rectangular in V.P.C., and (f) interdigitated non-contact.

3.6 Conclusion

In this manuscript, a wireless, wearable, EOG measurement system, implemented on a flexible polyimide substrate, is presented. The system is capable of sensing and reducing motion artifacts using two pairs of parallel non-contact electrodes. The flexible board has four layers with: (a) EOG measurement system on the top layer, (b) kapton film covered non-contact measurement electrode pairs on the bottom layer for EOG and motion artifacts sensing, (c) the system ground plane on the second layer, and (d) active-shielding on the third layer. The system uses a microcontroller and BLE 5.0 transceiver for transmitting EOG data wirelessly. The performance and properties of the non-contact electrodes are tested thoroughly for their size, shape (circular, rectangular, and interdigitated), skin-electrode contact capacitance, impact of sweat, and motion artifacts. The

crucial system metrics of the EOG acquisition system such gain and CMRR are found out to be around 37 dB and 74 dB, respectively, which meet biopotential measurement standards. The system is tested for different electrode configurations for effective reduction of motion artifacts during EOG signal measurement. It is found out that with horizontally parallel electrode pairs the system is capable of reducing low frequency motion artifacts from EOG signals and detecting eye activities. The entire system is lightweight (only 8.75 gram), skin conformable, and can be mounted on any head-shape and size because of its flexibility, thus making it ideal for smart applications.

3.7 Bridging Text

This work presents our second wearable, flexible EOG prototype that employs parallel non-contact electrode pairs for motion artifacts sensing and reduction. The electrodes are printed on the bottom layer of the board. The use of non-contact electrodes eliminates the risk of allergic reactions during EOG measurement. Non-contact electrodes are highly sensitive and do not require gel for a good quality EOG detection, thus eliminating another limitation of our previous EOG prototype. The use of parallel non-contact electrode pairs does reduce the impact of motion artifacts effectively and the system is capable of sensing EOG signals in the presence of motions. However, a slight impact of motion artifacts still persists as ripples visible in the EOG baseline. EOG signals have specific time-domain features which can be identified easily using sophisticated signal processing algorithms and the baseline ripples can be removed. But, wearables like headbands and eye-masks may also get displaced easily due to body or head movements during sleep, which may compromise the measurement system placements and corrupt the measured EOG data. Despite the usage of soft materials and the effort of minimizing the device size, the prototypes presented in the form of headband are still uncomfortable for some people to wear during sleep, which sarcastically reduces their sleep quality. Intra-oral devices such as mouthguards, MAD are quite common these days to be worn during sleep for different health issues. For example, mouthguards are commonly used to prevent or reduce bruxism or snoring [29], [30]. MAD is used for sleep apnea treatment if the sleep apnea is mild [31]. Therefore, a biopotential-measuring MAD that can

be worn during sleep will be beneficial for sleep monitoring of OSA patients without causing discomfort to the users. Among various biopotentials EEG signals were successfully acquired intraorally from palate region [32], [33].

In the above contexts, we propose a smart MAD device to acquire intra-oral EEG data for our next work. This smart MAD design eliminates the requirement of having a separate smart headband and a MAD for OSA patients. Only a single, smart MAD should be sufficient for treating OSA and monitor intra-oral EEG for sleep study. However, intra-oral EEG measurements can also suffer from various intra-oral motions (e.g. tongue movement, teeth grinding, and gulping) which is considered in our design. The parallel electrode-pair based approach used in this chapter for motion artifact reduction in EOG cannot be employed for motion artifacts reduction involving EEG measurements. This parallel electrode-pair based approach has noise ripples along the baseline signals during EEG measurements. EEG signals are generally studied in frequency domain. Therefore, presence of baseline ripple due to motion artifacts may appear well within the EEG signal bandwidth which is undesirable. Moreover, intra-oral palate region is small and cannot accommodate enough electrodes for multichannel EEG systems. Therefore, our next work focuses on the development of a single channel intra-oral EEG system. and exercises the possibility smart sensor-fusion based approach to address the issue of intra-oral motion artifacts during intra-oral EEG measurements.

References

[1] L. Popa *et al.*, “Reading beyond the glance: eye tracking in neurosciences,” *Neurol. Sci.*, vol. 36, pp. 683–688, 2015.

[2] R. Ouyang *et al.*, "Design and implementation of a reading auxiliary apparatus based on electrooculography," *IEEE Access*, vol. 5, pp. 3841-3847, 2017.

[3] N. N. J. Rommelse, S. der Stigchel, and J. A. Sergeant, “A review on eye movement studies in childhood and adolescent psychiatry,” *Brain Cogn.*, vol. 68, no. 3, pp. 391–414, 2008.

[4] E. Trull *et al.*, "Implementation and use of the electrooculogram in sleep monitoring," *2015 IEEE Virtual Conf. Appl. Commercial Sens. (VCACS)*, Raleigh, NC, 2015, pp. 1-13.

[5] H. Manabe, M. Fukumoto, and T. Yagi, "Direct gaze estimation based on nonlinearity of EOG," *IEEE Trans. Biomed. Eng.*, vol. 62, no. 6, pp. 1553-1562, June 2015.

[6] A. Larson *et al.*, “Electrooculography based electronic communication device for individuals with ALS,” *2017 IEEE Sens. Appl. Symp. (SAS)*, 2017, pp. 1–5.

[7] R. G. Lupu *et al.*, "Eye tracking user interface for Internet access used in assistive technology," *2017 E-Health and Bioeng. Conf. (EHB)*, Sinaia, 2017, pp. 659-662.

[8] A. Bulling *et al.*, “Eye movement analysis for activity recognition using electrooculography,” *IEEE Trans. Pattern Anal. Mach. Intell.*, vol. 33, no. 4, pp. 741–753, 2010.

[9] N. Kosmyna *et al.*, “AttentivU: A wearable pair of EEG and EOG glasses for real-time physiological processing,” *2019 IEEE 16th Int. Conf. on Wearable and Implantable Body Sens. Netw. (BSN)*, 2019, pp. 1–4.

[10] Y. M. Chi, T. Jung, and G. Cauwenberghs, "Dry-contact and noncontact biopotential electrodes: methodological review," in *IEEE Rev. Biomed. Eng.*, vol. 3, pp. 106–119, 2010.

[11] S. Debbarma and S. Bhadra, "A lightweight flexible wireless electrooculogram monitoring system with printed gold electrodes," *IEEE Sens. J.*, vol. 21, no. 18, pp. 20931–20942, 15 Sept.15, 2021.

[12] A. Dabbaghian *et al.*, "A 9.2-g fully-flexible wireless ambulatory EEG monitoring and diagnostics headband with analog motion artifact detection and compensation," *IEEE Trans. Biomed. Circuits & Syst.*, vol. 13, no. 6, pp. 1141–1151, Dec. 2019.

[13] S. Debbarma, S. Nabavi, and S. Bhadra, “A wireless flexible electrooculogram monitoring system with printed electrodes,” *2021 IEEE Int. Instrum. & Meas. Technol. Conf. (I2MTC)*, 2021, pp. 1–6.

[14] D. Svärd *et al.*, “Design and evaluation of a capacitively coupled sensor readout circuit, toward contact-less ECG and EEG,” *2010 Biomed. Circuits and Syst. Conf. (BioCAS)*, 2010, pp. 302–305.

[15] J. Ottenbacher *et al.*, "Reliable motion artifact detection for ECG monitoring systems with dry electrodes," *2008 30th Annu. Int. Conf. IEEE Eng. Medicine & Biol. Soc.*, 2008, pp. 1695–1698.

[16] N. Van Helleputte *et al.*, "A 160 μA biopotential acquisition IC with fully integrated IA and motion artifact suppression," *IEEE Trans. Biomed. Circuits & Syst.*, vol. 6, no. 6, pp. 552–561, Dec. 2012.

[17] J. Xu *et al*., "A wearable 8-channel active-electrode EEG/ETI acquisition system for body area networks," *IEEE J. Solid-State Circuits*, vol. 49, no. 9, pp. 2005–2016, Sept. 2014.

[18] L. Kalevo *et al.*, "Effect of sweating on electrode-skin contact impedances and artifacts in EEG recordings with various screen-printed Ag/Agcl electrodes," *IEEE Access*, vol. 8, pp. 50934-50943, 2020.

[19] W. Jia *et al.*, "Characteristics of skin-electrode impedance for a novel screw electrode," *2014 40th Annu. Northeast Bioengg. Conf. (NEBEC)*, 2014, pp. 1-2.

[20] M. Guermandi, E. F. Scarselli, and R. Guerrieri, "A driving right leg circuit (DgRL) for improved common mode rejection in bio-potential acquisition systems," *IEEE Trans. Biomed. Circuits and Syst.*, vol. 10, no. 2, pp. 507-517, April 2016.

[21] J. Xu *et al.*, "Active electrodes for wearable EEG acquisition: review and electronics design methodology," *IEEE Rev. Biomed. Engg.*, vol. 10, pp. 187-198, 2017.

[22] F. N. Guerrero and E. M. Spinelli, "A two-wired ultra-high input impedance active electrode," *IEEE Trans. Biomed. Circuits and Syst.*, vol. 12, no. 2, pp. 437-445, April 2018.

[23] T. Tang *et al*., "An active concentric electrode for concurrent EEG recording and body-coupled communication (BCC) data transmission," *IEEE Trans. Biomed. Circuits and Syst.*, vol. 14, no. 6, pp. 1253–1262, Dec. 2020.

[24] C. P. Constantin *et al.*, “Biocompability of Polyimides: A Mini-Review,” *Materials (MDPI)*, vol. 12, no. 3166, pp. 1–27, Sep. 2019, doi:10.3390/ma12193166.

[25] M. R. Nuwer *et al.*, “IFCN standards for digital recording of clinical EEG,” *Electr. Clin. Neuroph.*, vol. 106, no. 3, pp. 259–261, Mar. 1998.

[26] Texas Instruments, “Ultra low input bias current instrumentation amplifier,” INA116 datasheet, May 1995 [Revised Sept. 2000].

[27] W. Heide *et al.*, “Electrooculography: technical standards and applications. The International Federation of Clinical Neurophysiology,” *Electroencephalogr. Clin. Neurophysiol. Suppl.*, vol. 52, p. 223–240, 1999.

[28] T. J. Sullivan, S. R. Deiss, and G. Cauwenberghs, "A low-noise, non-contact EEG/ECG sensor," *2007 IEEE Biomed. Circuits and Syst. Conf. (BioCAS)*, 2007, pp. 154-157.

[29] "Whole You: Live Out Loud Live Whole," wholeyou.com. https://www.wholeyou.com/sleeper/ (accessed Mar. 20, 2023).

[30] "SomnoMed Patient: The Comfortable Alternative to CPAP," somnomed.com/en/. https://somnomed.com/en/patients/effective-cpap-alternative/ (accessed Mar. 21, 2023).

[31] D. J. Bratton, T. Gais, A. M. Wons, and M. Kohler, "CPAP vs mandibular advancement devices and blood pressure in patients with obstructive sleep apnea: a systematic review and meta-analysis," J. Amer. Med. Assoc. (JAMA), vol. 314, no. 21, pp. 2280–2293, 2015.

[32] M. S. Cohen, "EEG Data Collection Intrabuccal Method and Apparatus," WO Patent 107446A1, 2014, Jul. 10, 2014.

[33] R. Radmand, "Intra-oral Electroencephalography Device and Method," U.S. Patent 0 060 611 A1, 2020, Feb. 27, 2020.

Chapter 4

A Sensor-Fusion Method for Motion Artifacts Reduction in Intra-oral EEG Signals

4.1 Abstract

In recent studies, Electroencephalography or EEG signals are acquired intra-orally from the palate region. However, intra-oral EEG study is a less explored research area and its challenges are yet to be investigated. In this study, we look into the possibility of studying EEG signals from various intra-oral locations and investigate the sources of motion artifacts during intra-oral EEG measurements. Later we propose a sensor-fusion of EEG electrodes and accelerometer module to monitor intra-oral EEG signal and intra-oral motions simultaneously. The EEG electrodes, accelerometer, and the sensor read-out circuitry are integrated with a mandibular advancement device (MAD). The system is battery-operated and uses a Bluetooth 5.0 transceiver to send data wirelessly. The smart MAD is used to acquire intra-oral EEG and accelerometer data and a MATLAB based algorithm is implemented using empirical mode decomposition (EMD) and independent component analysis (ICA) to decompose the EEG signal components. The decomposed ICA components containing intra-oral motion artifacts are then mapped with the motion events extracted from the accelerometer data to identify the motion corrupted data segments. The ICA components containing intra-oral motions are then denoised by nullifying the motion corrupted data segments. A motion artifacts reduced intra-oral EEG is reconstructed from

the denoised ICA components. The efficacy of the sensor-fusion and the proposed algorithm are demonstrated by quantifying the signal-to-noise ratio (SNR) difference and percentage artifacts reduction based on correlation analysis from the EEG signals before and after motion artifacts reduction. Later, the processed intra-oral EEG signals are also analyzed for the detection of 'eye open' and 'eye close' activities in the presence of intra-oral motions. The device along with the algorithm will have potential applications for motion artifacts free intra-oral EEG monitoring.

Index Terms— Intra-oral, wearable, flexible, mandibular advancement device, sensor-fusion, electroencephalogram, eye open-close activities, accelerometer, motion-artifacts, empirical mode decomposition, independent component analysis.

4.2 Introduction

Electroencephalography (or EEG) is a well-established, versatile technique known for studying neural activities of brain for clinical and commercial applications [1]–[4]. Electroencephalogram or EEG signals are small electrical impulses, from 0.5 μVolts to 100 μVolts of amplitudes, elicited during various brain activities [5]–[7]. These electrical impulses (also known as biopotentials) can be recorded by placing one to many electrodes around the scalp of the subject in study either non-invasively [5], [7] or intracranially [6], which can be measured using a sophisticated biopotential measurement system [7]. EEG signals are generally classified into a few groups of signal bands namely: δ band (4 Hz and less), θ band (4 Hz to 8 Hz), α band (8 Hz to 13 Hz), β band (13 Hz to 30 Hz), and γ band (30 Hz and above).

In some recent studies, EEG signals have also been acquired intra-orally from the palate region [8]–[10]. The palate region inside the oral cavity is the closest surface to the hypothalamus the region of brain which controls sleep/awake states [8], [11]. Therefore, intra-oral EEG signals may have useful signatures related to different brain activities [11], [12]. The easiest way to access the intra-oral palate region of a subject is by using intraoral wearables such as mouthguard, mandibular advancement devices (or MADs). Intra oral devices are already popular for treating patients with conditions like teeth grinding (or bruxism) and snoring [13]–[15]. Cohen [8],

designed a special MAD with intra-oral EEG electrodes touching the palate inside the oral cavity. The device was used for acquiring intra-oral EEG data with eye-open/eye-close activities. A smart MAD with embedded EEG electrodes and a flexible EEG measurement board has also been reported in our previous work [10]. However, the possible sources of intra-oral motion artifacts and their impact on intra-oral EEG measurements were not investigated in this study. Another smart mouthguard was reported by Nguyen et al. [16] for acquiring electrooculogram (or EOG) signals intra-orally using fabric-based flexible electrodes. But their measurement system was implemented on a breadboard and the electrodes were interfaced with long wires, which is uncomfortable to use.

Motion artifacts are random interferences generally picked up by the measurement electrodes during physical movements of the subject under test and from surrounding environmental vibrations [17]–[22]. Such artifacts are typically stronger than EEG potentials and capable of saturating the measurement system's outputs. Motion artifacts may have wide amplitude/frequency range, and may lie within the EEG signal's band of interest, thus making it difficult to remove in-band noises using conventional band-pass filtering. Therefore, motion corrupted EEG data are generally discarded by visual inspections, which is a tiresome job for a large amount of EEG data [17]. Different techniques have already been implemented in system design as well as in signal processing for effectively tracking and reduction of motion artifacts present in biopotential measurements. An interdigitated electrode-pairs based system is developed by Dabbaghian et. al. [18], for simultaneous measurements of EEG and motion artifacts. Later, sensed motion artifacts is used to control the variable gain of the EEG sensing amplifier, thus suppressing the impact of motion artifacts on the measured EEG signal. However, their work does not report any real time EEG signal measurement using their system. Sensor-fusion techniques are also popular for motion artifacts removal which usually involve acquiring time synchronized multichannel sensor data digitally, preprocessing, signal analysis, extracting motion features, and then noise reduction algorithm for the signal of interest [19]. Beach et al. [20] used a sensor-fusion technique using an inertial measurements unit (or IMU) and EEG/ECG signals. The IMU is placed

in close proximity with the measurement electrodes to acquire accelerometric and gyroscopic motion signals, which are then cross-correlated with the measured EEG/ECG signals and the best match is selected as a reference for adaptive filtering. However, their adaptive filter did not perform optimally for EEG denoising and requires more detailed study. In another work for ambulatory EEG measurements reported by Islam et al. [21], EEG signals are decomposed using Discrete Wavelet Transform (DWT) into basic EEG bands. An accelerometer is used to acquire the motion signals which are correlated with the EEG signal to remove motion artifacts. However, their study reports that the EEG signals and the accelerometer data are not significantly correlated to each other.

For conventional multichannel EEG systems, statistical methods like Independent Component Analysis (ICA) [22]–[24] and Canonical Correlation Analysis (CCA) [24], [25] have already been used for EEG signal decomposition and noise reduction. Machine learning methods are also implemented in some works for identifying motion artifacts in multi-channel EEG data [17], [26], [27]. However, their learning models did not perform optimally and require more training datasets. For single channel EEG systems, other multi-resolution techniques such as DWT [21], [28], Singular Spectrum Analysis (SSA) [29], Empirical Mode Decomposition (EMD) [30], [31], and Ensemble EMD (EEMD) [32], [33] have been employed for noise reduction. In some approaches, single channel EEG data are decomposed to multichannel data matrix using DWT, EMD, EEMD and then employed in multichannel algorithms like ICA, CCA, and principle component analysis (PCA) for noise removal [28], [32], [33].

In this manuscript, we present a wearable smart MAD device with a sensor-fusion of flexible gold electrodes for intra-oral EEG measurements and an accelerometer for sensing intra-oral motions simultaneously. Given the limited space in the palate region of the oral cavity, our intra-oral EEG measurement systems captures a single channel EEG signal. The instrumentation for recording the intra-oral EEG signal and accelerometer outputs is implemented on a flexible polyimide board and attached with a customized MAD designed for this study. The system is battery operated and uses a BLE 5.0 transceiver to send the EEG and accelerometer motion data

wirelessly to a nearby computer. A MATLAB based algorithm is developed to identify the time locations and durations of the intra-oral motion events from the acquired accelerometer motion data. On the other hand, the single channel intra-oral EEG data is converted to a multichannel data using EMD technique and then ICA is implemented to separate the independent components containing the EEG and the motion artifacts. The motion artifacts related ICA components are then mapped with the motion events extracted from the accelerometer data and the motion contaminated segments are removed. Then the denoised ICA components are converted back to the motion artifacts reduced EEG signal which is then used for further processing. The novelty of the system is that it is the first prototype that analyzes the impact of intra-oral motions on intra-oral EEG measurement and removes them effectively using the proposed sensor-fusion based EMD-ICA algorithm. The smart MAD along with the proposed algorithm will have potential for intra-oral EEG monitoring applications.

4.3 Intra-oral EEG Study and Possible Challenges

In this study, different intra-oral locations are explored for intra-oral EEG detections. The objective of this study is to find an optimal configuration for intra-oral EEG electrodes placement and also to identify the possible challenges associated with such measurement setups. The experimental procedure in this study is in accordance with the Declaration of Helsinki and was approved by Institutional Review Board of McGill University (study number: A04-M21-19B, approval date: 04/17/2019). Flexible printed round gold electrodes (1 cm diameter) are chosen for the intra-oral measurements since they are comfortable to wear [10], [34]. These flexible gold electrodes are already reported to have similar sensitivity like commercial rigid gold electrodes [34]. The electrodes are printed as pads by PCB manufacturer on a flexible polyimide substrate. Gold is chosen as the printing material because of its biocompatible property [35].

4.3.1 Intra-oral EEG Measurements in Different Locations

After evaluating the skin-electrode contact impedance in different intra-oral locations, EEG signals are acquired from all these intra-oral locations with different electrode configurations, as presented

in Fig. 4.1. Three electrode configuration (also known as bipolar electrode configuration), with two active electrodes (E_{A1} and E_{A2}) and one reference electrode (E_R), is used to measure the intra-oral EEG potentials [7]. Here, the measurement electrodes are attached to the customized MAD using biocompatible adhesive and worn by a subject to achieve these intra-oral electrode configurations for the measurements. The EEG electrodes are then interfaced with a breadboard-based single channel EEG measurement system. The same system is later designed on a flexible polyimide substrate and integrated with the smart MAD. The system design approach is presented with detail in the next section. Forehead EEG data are also acquired as reference data for comparison with the intra-oral EEG, using the same breadboard-based single channel EEG system and three forehead EEG electrodes, as shown in Fig. 4.1(d).

In conventional scalp/forehead EEG study, the EEG signatures can be easily identified by a simple experiment involving 'eye open' and 'eye close' activities [7], [36]. The EEG spectrum, along alpha (8 to 13 Hz) and beta bands (13 to 30 Hz) spectrum, shows higher energy for 'eye close' activity in comparison to 'eye open' activity [7]. [36]. However, the EEG spectrum behavior along delta and theta bands are not always consistent for scalp/forehead EEG measurements during 'eye open' and 'eye close' activities and may vary depending on scalp electrode placements [36]. Therefore, in this study, only alpha band responses are investigated during intra-oral EEG measurements with different electrode placement configurations. Three subjects are asked to volunteer for the EEG data collection from those intra-oral locations and the forehead. The subjects are asked to perform 'eye open' and 'eye close' activities for 30 seconds during the experiment. Three sets of EEG data collected from each EEG test locations for all three subjects are reported here for repeatability test. The EEG data are acquired with a sampling rate of 200 Hz using a microcontroller module in a nearby computer. The spectrum of the EEG data are analyzed in MATLAB (version R2019a). Out of total nine datasets, two dataset of EEG spectrums for 'eye open' and 'eye close' activities are presented in Fig. 4.1 for all the test locations mentioned above. Here, each dataset contains four data collected from the four different EEG test locations. A qualitative summary of all nine datasets (from three subjects) for each EEG electrode

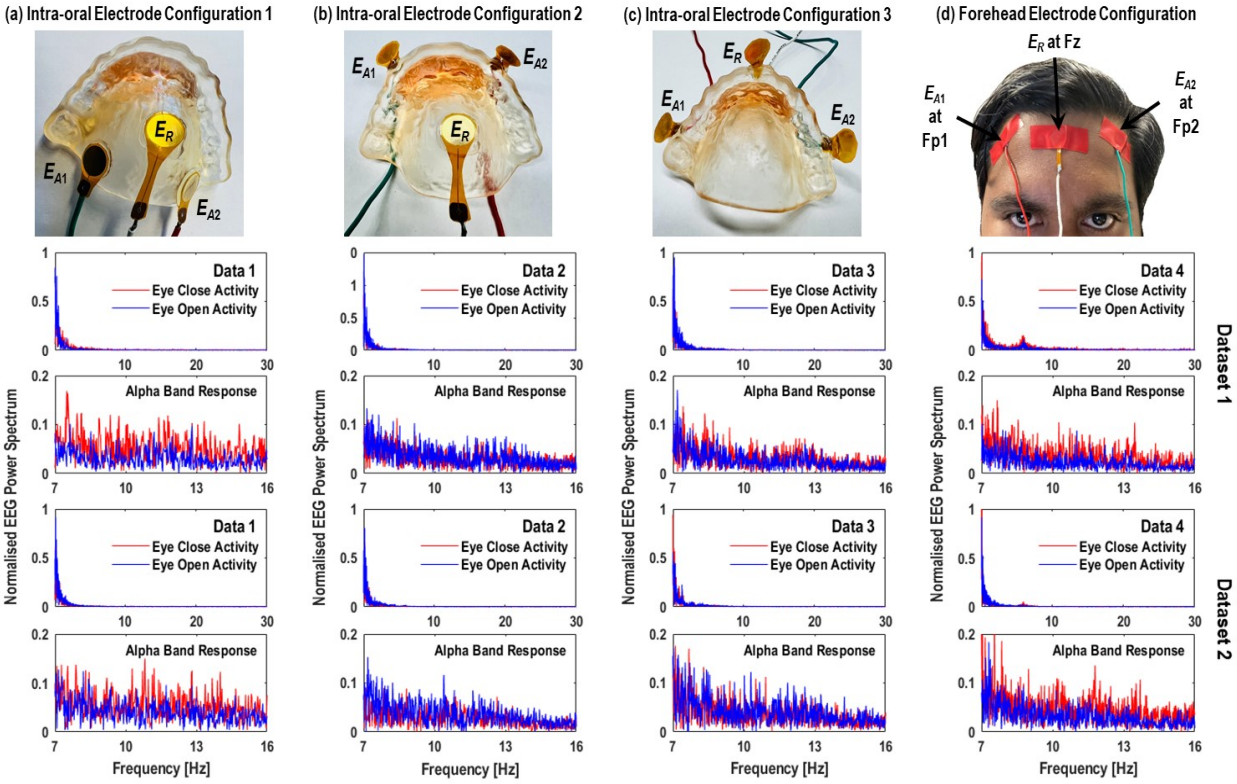

Fig. 4.1. Two dataset of EEG spectrums for 'eye open' and 'eye close' activities recorded in different intra-oral locations and forehead: (a) EEG electrode configuration 1 where all the electrodes are placed on the palate, (b) EEG electrode configuration 2 where the reference electrode is placed on the palate and the other two active electrodes on the outer gum above the teeth-line, (c) EEG electrode configuration 3 where all the electrodes are placed on the outer gum above the teeth-line, and (d) conventional forehead EEG electrode configuration.

configurations is also presented in Table 4.1. For Fig. 4.1(a) electrode configuration, the EEG spectrum for 'eye open' and 'eye close' activities in this electrode configuration are easily distinguishable. The alpha band shows higher spectrum energy for 'eye close' activities just like scalp EEG measurements, as reported in [7], [36]. For Fig. 4.1(b) configuration, no distinguishable differences or peaks are observed in alpha band EEG spectrum energy for 'eye open' and 'eye close' activities. Fig. 4.1(c) configuration could not capture any distinguishable differences or peaks in the alpha band EEG spectrum for 'eye open' and 'eye close' activities. The possible reason for such observation is that the outer gum area is far away from any of the sections of the

TABLE 4.1

A QUALITATIVE COMPARISON OF EEG SIGNAL SPECTRUMS ACQUIRED FROM DIFFERENT INTRA-ORAL LOCATIONS AND FOREHEAD DURING 'EYE OPEN' AND 'EYE CLOSE' ACTIVITIES

Subject	Meas.	Alpha Band (8 to 13 Hz) Spectrum Energy Comparison during 'Eye open' and 'Eye Close' activities			
		Forehead EEG	Intra-oral Config. 1 *	Intra-oral Config. 2 **	Intra-oral Config. 3 ***
1	1	**Higher for 'eye close'**	**Higher for 'eye close'**	Similar for both	Similar for both
	2	**Higher for 'eye close'**	**Higher for 'eye close'**	Similar for both	Similar for both
	3	**Higher for 'eye close'**	**Higher for 'eye close'**	Similar for both	Similar for both
2	4	**Higher for 'eye close'**	**Higher for 'eye close'**	Similar for both	Similar for both
	5	**Higher for 'eye close'**	**Higher for 'eye close'**	Similar for both	Similar for both
	6	**Higher for 'eye close'**	**Higher for 'eye close'**	Similar for both	Similar for both
3	7	**Higher for 'eye close'**	**Higher for 'eye close'**	Similar for both	Similar for both
	8	**Higher for 'eye close'**	**Higher for 'eye close'**	Similar for both	Similar for both
	9	**Higher for 'eye close'**	**Higher for 'eye close'**	Similar for both	Similar for both

* Intra-oral Electrode Configuration in Fig. 3(a) ** Intra-oral Electrode Configuration in Fig. 3(b) *** Intra-oral Electrode Configuration in Fig. 3(c)

brain in comparison to the palate region which is closer to hypothalamus. Therefore, it is unlikely to capture any EEG activities on the outer gum area. Fig. 4.1(d) presents the conventional scalp/forehead EEG with reference electrode ($\boldsymbol{E_R}$) connected at Fz location and the active electrodes ($\boldsymbol{E_{A1}}$ and $\boldsymbol{E_{A2}}$) at Fp1 and Fp2 locations [37]. The EEG signals collected from the forehead EEG show similar behavior in alpha band responses where higher spectrum energies are observed during 'eye close' activities. The alpha band activities also go up for 'eye close' activities during scalp/forehead EEG measurements [2], [36]. The EEG alpha band responses for all intra-oral and scalp EEG study for 'eye open' and 'eye close' activities are reported in Table 4.1 with the consistent results presented in bold. From this study, it can be concluded that the first EEG electrode configuration for intra-oral measurements is the best one as it is capable for capturing similar EEG signatures in alpha band like forehead (or scalp) EEG consistently for 'eye open' and 'eye close' activities.

4.3.2 Intra-oral Motion Artifacts & Accelerometer Sensor

Motion artifacts pose the most challenging issue during any kind of biopotential measurements. The common reasons of motion artifacts are patient's voluntary/involuntary movements during the measurement and any vibrations around the measurement devices [18]–[30], [32]. In the presence of motion, the measurement electrodes or the system may get displaced and the overall skin-electrode contact impedance may get altered along the measurement path. This affects the cut-off frequencies and the signal bandwidth of the biopotential measurement instrumentation. As a result, the motion artifacts appear within the signal bandwidth and are difficult to remove [18]. The possible sources of motion artifacts during intra-oral measurements are tongue movements, teeth grinding, gulping etc. The intra-oral motions are capable of impacting the entire MAD used for the intra-oral measurements. To study the impact of intra-oral motions on the MAD, an analog output 3-axial accelerometer MXR9500MZ module with ± 2g range, by Memsic Semiconductors, is used. The accelerometer sensor is capable of sensing motions along X, Y, and Z directions and produces three analog outputs, respectively. For this study, the accelerometer sensor module is first wrapped in a biocompatible cover to protect its electronic components from saliva and then

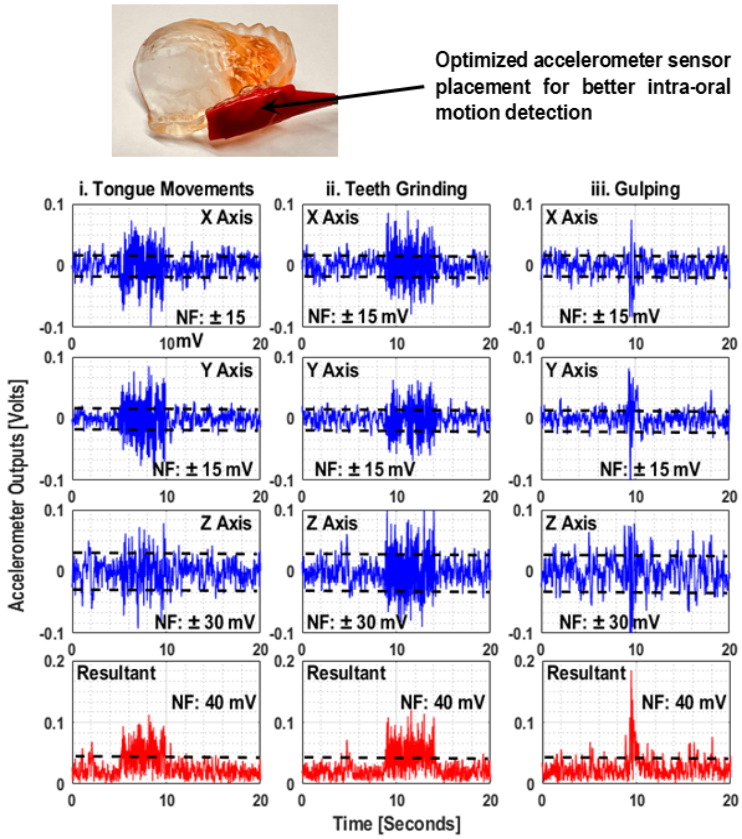

Fig. 4.2. Optimized accelerometer sensor placement for intra-oral motion detection: (i) tongue movements, (ii) teeth grinding, and (iii) gulping, respectively). Accelerometer noise floor (NF) are also presented in the figures (NF = ± 15 mVs for X and Y axes, NF = ± 30 mVs for Z axis, and NF = 40 mVs for the resultant data).

attached to a MAD using biocompatible adhesive. The subjects are asked to wear the MAD interfaced with the accelerometer and perform intra-oral motion activities (tongue movements, teeth grinding, and gulping) for measurement. The motion signals are recorded with a sampling rate of 200 Hz using a microcontroller module. The accelerometer sensor is tested in different locations along the outer curvature of the MAD to determine an optimal accelerometer placement for the system design. The optimized placement as shown in Fig. 4.2 of the accelerometer ensures a better detection of intra-oral motion sources (tongue movements, teeth grinding, and gulping). One accelerometer dataset for intra-oral motions is presented in Fig. 4.2. By looking at the resultant intra-oral motion data in Fig. 4.2, it can be said that the tongue movements are relatively weak

motion; whereas the teeth grinding and gulping are relatively strong motions. It should be noted that, given the size and the wiring complexity of the accelerometer sensor module, it was not considered to be placed/tested inside the oral cavity for this design.

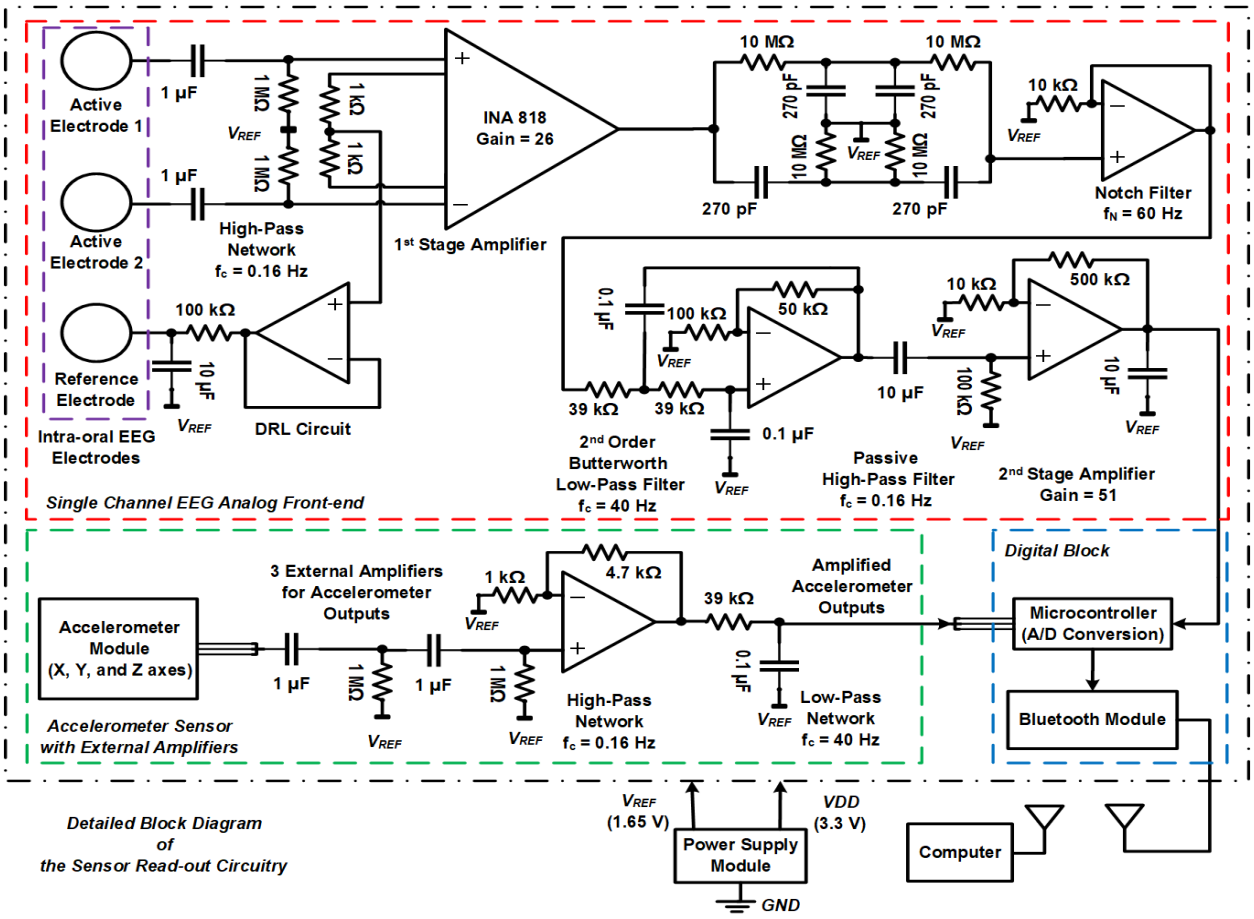

Fig. 4.3. A detailed block diagram of the sensor read-out circuitry with the single channel EEG analog-front end, accelerometer module with the three external amplifiers (here shown only one of them) for the three axes, the digital block with microcontroller and Bluetooth module, the power supply module, and the remote computer to acquire data.

4.4 The Sensor Read-out Circuitry Design

Using the optimal positions for intra-oral EEG electrodes and accelerometer placement, an intraoral EEG measurement system with accelerometer is implemented on a flexible polyimide board. The system is battery operated and capable of sending the EEG and accelerometer data over

a BLE 5.0 transceiver module to a nearby computer. A detailed block diagram of the sensor read-out circuitry is presented in Fig. 4.3. The entire sensor assembly and the circuit is attached to the MAD using biocompatible adhesive. The read-out circuitry, along with the battery, is covered with a saran wrap to protect the system from saliva before attaching it to the MAD. The sensor assembly and the circuit are shown in Fig. 4.4(a) and 4.4(b). Fig. 4.4(c) presents the experimental setup for the complete wearable smart MAD prototype. The read-out circuitry design approaches are discussed in detail in the following subsections.

4.4.1 The Power Supply Module

The entire circuit is powered with a rechargeable Li-ion battery with nominal voltage 3.7 Volts and capacity 200 mAh. The circuit then uses a 3.3 volts low dropout voltage regulator for powering up the EEG analog front-end, accelerometer with amplifier, and the digital part of the circuit. The power supply module also utilizes an op amp to generate an analog ground (or reference voltage V_{REF}) of 1.65 volts for the EEG analog front end and the accelerometer output amplifiers of the circuit. The sensor read-out circuitry consumes approximately 69.3 mW of power. The overall battery life of the current prototype is approximately 8 hours and 20 minutes, thus making the device suitable for long-term monitoring.

4.4.2 The Single Channel EEG Analog Front-end Circuit

The flexible EEG gold electrodes (diameter 1 cm) are interfaced with the EEG analog front-end (AFE) circuit for intra-oral EEG measurements. The active electrodes are connected with the two inputs of the first stage amplifier of the AFE through a high-pass network with capacitor 1 µF and resistor 1 MΩ, respectively. These high-pass networks at the input stage sets the high-pass cut-off frequency ($f_{c,HPF}$) at 0.16 Hz for the AFE. These high-pass networks also help in reducing the DC offsets and DC drifts generated at the skin-electrode contact interface [38]–[40]. The reference EEG electrode, on the other hand, is connected to a DRL (driven right leg) circuit. DRL circuits are generally used in many differential input (two active electrodes) biopotential measurement systems [41]. The DRL circuits are implemented to sense the common-mode signals of the active electrodes from the first stage amplifier of the AFE block. This signal is then buffered using an op amp and

fed back to the subject's body using the reference electrode. DRL arrangement helps in further minimizing the DC offsets and the DC drifts that may have been generated at the skin-electrode contact interface, thereby improving the overall bipotential sensing [39]. In this design, the DRL circuit is implemented using an op amp in unity gain configuration, as shown in Fig. 4.3. For safety purpose, a current limiting resistor of 100 kΩ is also placed before interfacing the DRL circuit output to the reference EEG electrode, as recommended by the IFCN for biopotential measurements involving human subjects [42].

The first amplification stage of the AFE is implemented using an instrumentation amplifier (IA) with a gain of 26. In the next stage of the AFE, a notch filter is implemented with cut-off frequency ($f_{c,Notch}$) of 60 Hz. This is done to reduce the impact of power-line interferences (if any) picked up during EEG measurements [38], [42]. In the next stage of the AFE, a second order Butterworth low pass filter, with cut-off frequency ($f_{c,LPF}$) of 40 Hz, is implemented to limit the upper EEG bandwidth to 40 Hz. In the next step, another passive high-pass network with capacitor 10 µF and resistor 100 kΩ ($f_{c,HPF}$) at 0.16 Hz (same as before), to minimize any DC offsets coming from the previous signal conditioning blocks of the AFE. Thus, the overall EEG bandwidth of the system becomes 0.16 Hz to 40 Hz. The last stage of the AFE is the second stage amplifier, responsible for the overall EEG amplification before sending it to an analog-to-digital converter (ADC) module of a microcontroller unit. The gain of the second stage amplifier is set to 51, thus making the overall gain of the AFE block 1326. The amplifier gains for the AFE block are determined empirically. The gain-vs-frequency response and common mode rejection ratio (CMRR) of the AFE are also evaluated using similar methods reported in [37], [38]. The effective gain-vs-frequency response of the AFE is found out to be above 57 dB over the EEG bandwidth of 0.16 Hz to 30 Hz. The overall common mode rejection ratio (or CMRR) is found out to be above 74 dB over the EEG bandwidth.

4.4.3 The 3-Axial Accelerometer with Amplifier

The 3-axial MXR9500MZ accelerometer module (capable of measuring motions along X, Y, and Z axes) is used to sense the presence of intra-oral motions during intra-oral EEG measurements.

To increase the sensitivity of the accelerometer outputs, three two stage high-pass networks (with capacitor 1 µF, resistor 1 MΩ, and cut-off frequency $f_{c,HPF}$ at 0.16 Hz) are implemented to remove the DC offsets generated by the accelerometer module at X, Y, and Z outputs. Then, three op-amp based amplifiers with gain 4.7 are used to amplify the accelerometer outputs. The high-pass networks are implemented to prevent the external amplifier outputs from saturation. The accelerometer outputs are also limited by a low-pass network with cut-off frequency ($f_{c,LPF}$) of 40 Hz to limit the accelerometer signal bandwidth, like the EEG bandwidth. The accelerometer outputs are recorded simultaneously with the intra-oral EEG signal and sent to three ADC modules of the same microcontroller unit.

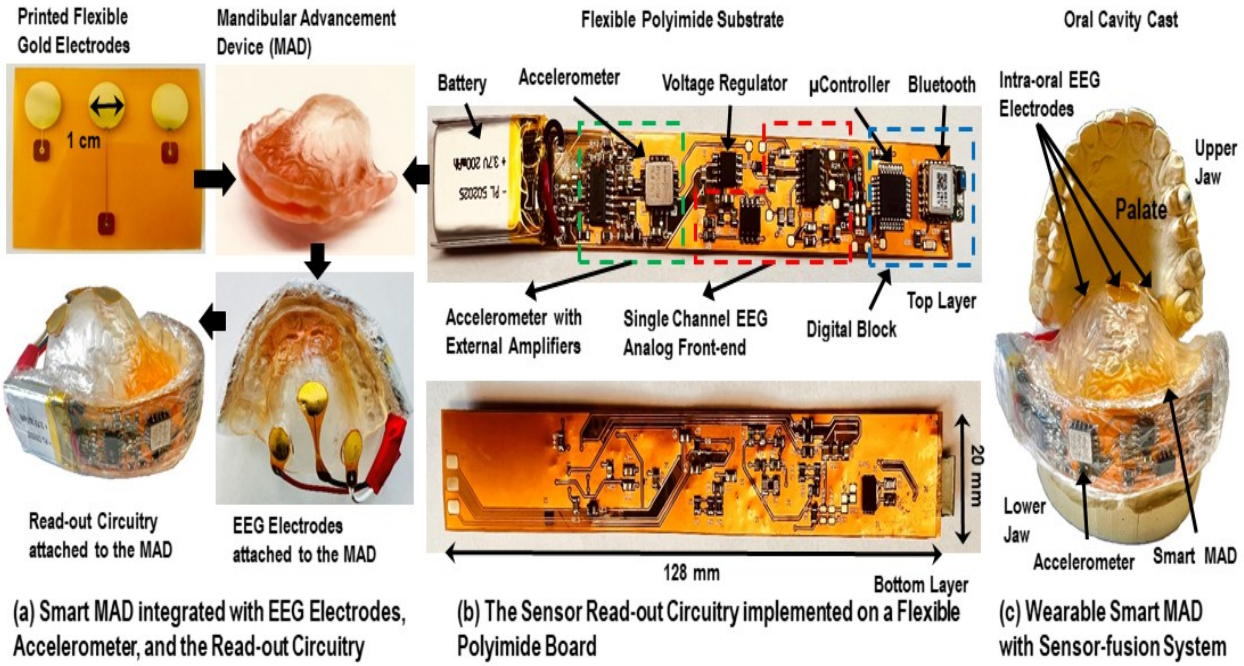

Fig. 4.4. The complete wearable smart MAD prototype: (a) the MAD integrated with the EEG electrodes, accelerometer, and the sensor read-out circuitry, (b) the sensor read-out circuitry with its circuit blocks, and (c) the wearable smart MAD placed on an oral cavity cast depicting the experimental setup.

4.4.4 The Microcontroller & Bluetooth Module

The digital part of the circuit uses a microcontroller unit Atmega328P interfaced with a low-power BLE 5.0 transceiver module RN4871 (by Microchip Technology). Four 10-bit analog-to-digital

converter (ADC) channels of Atmega328P (one for the single channel intra-oral EEG recording and three more for the accelerometer outputs) are used to digitize the intra-oral EEG signal coming from the AFE and the intra-oral motion signals coming from the accelerometer sensor. The sampling rate of the ADC channels are fixed at 200 Hz to meet the Nyquist criteria (> 2×EEG bandwidth) during analog to digital conversion. The digitized intra-oral EEG and the accelerometer data for intra-oral motions are then transmitted wirelessly using the Bluetooth module to a nearby computer.

4.4.5 The Computer Interface at the Receiving End

Another RN4871 BLE 5.0 transceiver is used to as receiver to acquire the transmitted data in a computer. The acquired intra-oral EEG and accelerometer data are then processed in a MATLAB (version R2019a) based algorithm to identify the timestamps of the intra-oral motions and then to remove the motion corrupted EEG data.

4.4.6 Comparative Study of the Proposed System with Other Intra-oral Biopotential Measurement Systems

Table 4.2 presents a comparative study of the proposed smart MAD system and other intra-oral biopotential measurement systems reported in scholarly articles. The system reported in [8] is the first reported study of intra-oral EEG measurements. This study uses rigid electrodes mounted on the dental retainer, which are then interfaced with a commercial EEG device using long wires coming out of the mouth. Such experimental setups are uncomfortable to use and suitable only for short term studies. Another smart mouthguard presented in [16] is the first reported study of intra-oral EOG signals. The mouthguard is integrated with flexible electrodes touching the inner walls of the upper and lower inner lips for EOG detection. The instrumentation, on the other hand, is implemented on a breadboard and the EOG electrodes are interfaced using long wires coming out of the mouth, thereby making the prototype suitable only for short term studies. The smart MAD reported in [10] is our first prototype made for intra-oral EEG measurements with integrated flexible electrodes and the measurement system, making the prototype comfortable to wear and suitable for relatively long term study. However, the prototype is sensitive to intra-oral motions

TABLE 4.2

A COMPARISION BETWEEN THIS PROPOSED SMART MAD AND OTHER SYSTEMS FOR INTRA-ORAL BIOPOTENTIAL MEASUREMENT

	PATENT [8]	SENSORS'21 [10]	FLEPS'23 [16]	THIS WORK
ELECTRODE DESIGN & SPECIFICATIONS:-				
Electrode Type	Rigid	Flexible	Flexible	Flexible
Electrode Size	—	1 cm diameter	1.5 cm × 1 cm	1 cm diameter
Interface with the System	Using Wire	Integrated with the Wearable	Using Wire	Integrated with the Wearable
INTRA-ORAL MOTION ARTIFACTS SENSING & REDUCTIONS:-				
Motion Sensing	No	No	No	Using Accelerometer
Motion Reduction	—	—	—	Sensor-fusion & Algorithm
SYSTEM DESIGN & SPECIFICATIONS:-				
Instrument Placement	Outside Oral Cavity	Integrated with the Wearable	Outside Oral Cavity	Integrated with the Wearable
PCB Board	Rigid	Flexible	Breadboard	Flexible
Number of Channels	—	1	4	1
Power Consump.	—	~49.5 mW	—	~ 69.3 mW
Data Trasmission	—	Bluetooth	Bluetooth	Bluetooth
System Gain	—	> 65 dB	—	> 57 dB
System Bandwidth	—	0.16 – 40 Hz	—	0.16 – 40 Hz
Wearable Platform	Dental Retainer	MAD	Mouthguard	MAD
Application	EEG	EEG	EOG	EEG

during signal measurements. This work is an improved version of our first smart MAD prototype and uses a sensor-fusion of intra-oral EEG electrode and accelerometer and capable of tracking intra-oral motions while measuring the EEG signal. The gain of the system is a bit low in comparison to our first prototype [10] to make sure that the EEG output does not saturate in the presence of motions. The addition of accelerometer also increases the overall power consumption of the system. But the prototype, along with the proposed algorithm, is able to reduce motion artifacts in intra-oral EEG signals. Therefore, it is safe to say that this proposed smart MAD is the most useful prototype reported so far for intra-oral biopotential measurement systems.

4.5 The Algorithm for Motion Artifacts Reduction in Intra-Oral EEG Data & Results

Intra-oral EEG measurements may suffer from motion artifacts due to intra-oral motions. Such motions can disturb the entire smart MAD device integrated with the intra-oral electrodes and may result in heavily distorted EEG measurements leading to output saturation in some cases [18], [39], [41]. In our work, we have used EMD-ICA method based algorithm for reducing motion artifacts in intra-oral EEG signals.

4.5.1 EMD-ICA Method

Empirical mode decomposition (or EMD) is nonlinear signal processing technique that decomposes a time series signals into a data matrix with each row containing an "intrinsic mode function" (or IMF) [30], [32]. The decomposed IMFs must satisfy the following conditions: (i) the total number of maxima and zero crossings over the full length time series data must be the same or differ by at most 1 and (ii) the mean value of the envelopes defined by the maxima and minima over the full length time series data must be zero [30].

A number of steps are implemented to decompose the IMFs from a time series signal ($\boldsymbol{x}$). In the first step, the maxima points all over the time series data ($\boldsymbol{x}$) are found and connected together using a cubic spline to create the upper envelop. Next, the same process is repeated for the minima points to create the lower envelop. Next, the average ($\boldsymbol{m}$) of upper and lower envelop are calculated and subtracted from the time series data to create a new signal $\boldsymbol{h} = \boldsymbol{r_0} - \boldsymbol{m}$, where $\boldsymbol{r_0} = \boldsymbol{x}$. Next, $\boldsymbol{h}$ is considered as the new signal and steps 1, 2, and 3 are repeated. This process is repeated until a $\boldsymbol{h}$ is found which satisfies the two conditions for IMFs mentioned above, which is considered as the first IMF ($\boldsymbol{c_1}$). Next, $\boldsymbol{c_1}$ is subtracted from $\boldsymbol{r_0}$ to obtain the residual signal ($\boldsymbol{r_1} = \boldsymbol{r_0} - \boldsymbol{c_1}$) and a new IMF ($\boldsymbol{c_2}$) is decomposed by repeating the entire process and so on. The decomposition process is stopped when the residual signal ($\boldsymbol{r_n}$) becomes a monotonic function. Once, all the IMFs ($\boldsymbol{c_j}$) are decomposed, the original signal ($\boldsymbol{x}$) can be reconstructed using the formula $\boldsymbol{x} = \sum_{j=1}^{n} \boldsymbol{c_j} + \boldsymbol{r_n}$, where $\boldsymbol{r_n}$ is the residual signal after decomposing $\boldsymbol{n}$ IMFs. In our

approach, EMD is used to decompose the single channel intra-oral EEG data into an IMF data matrix. However, the EEG and motion artifacts spectral components will be distributed over the decomposed IMFs which are needed to be separated. Independent component analysis (or ICA) can be a suitable choice to separate the EEG and motion artifacts components from the decomposed IMFs.

ICA, on the other hand, is a blind source separation (BSS) technique that assumes a recorded signal matrix ($\boldsymbol{X}$) constitutes a combination of independent components or sources [24], [43]. The criteria of using ICA algorithm is that the signal matrix must contain recorded data which is more than or equal to the number of unknown independent components, The ICA algorithm then utilizes a number of learning assumption like linear mixing, square mixing, stationary mixing etc. to estimate an unmixing matrix ($\boldsymbol{W}$) using higher order statistics (HOS) to separate the unknown independent components ($\widehat{\boldsymbol{S}}$) [32], [43]. These matrices can be related with each other using the formula $\widehat{\boldsymbol{S}} = \boldsymbol{WX}$. In our approach, by estimating $\boldsymbol{W}$, the independent components containing EEG and motion artifacts can be separated. The inverse of unmixing matrix ($\boldsymbol{W}$) is called the mixing matrix $\boldsymbol{A} = \boldsymbol{W}^{-1}$, which holds the following equation $\boldsymbol{X} = \boldsymbol{A}\widehat{\boldsymbol{S}}$ true. The independent components representing motion artifacts can be removed by setting them to zero and $\widehat{\boldsymbol{S}}$ matrix containing the independent components is modified. Later, denoised EEG IMFs can be reconstructed using the mixing matrix $\boldsymbol{A}$ and the modified $\widehat{\boldsymbol{S}}$ matrix. Later, the denoised IMFs can be added together along with the residual signal to reconstruct the artifacts free EEG signal. In this work, we have used fastICA algorithm simply because of its shorter computational time [43].

4.5.2 The Proposed Algorithm

The proposed algorithm uses the accelerometer X, Y, and Z axes outputs for intra-oral motion signals measurements during tongue movements, teeth grinding, and gulping activities. The noise floor (or baseline) of the X and Y axes of the accelerometer module is ± 15 mV. Whereas the noise floor for the Z axis is slightly higher, approximately ±30 mV. However, the X, Y, and Z axes are relative to the subject's body postures. Therefore, the resultant noise floor (R) is computed for the

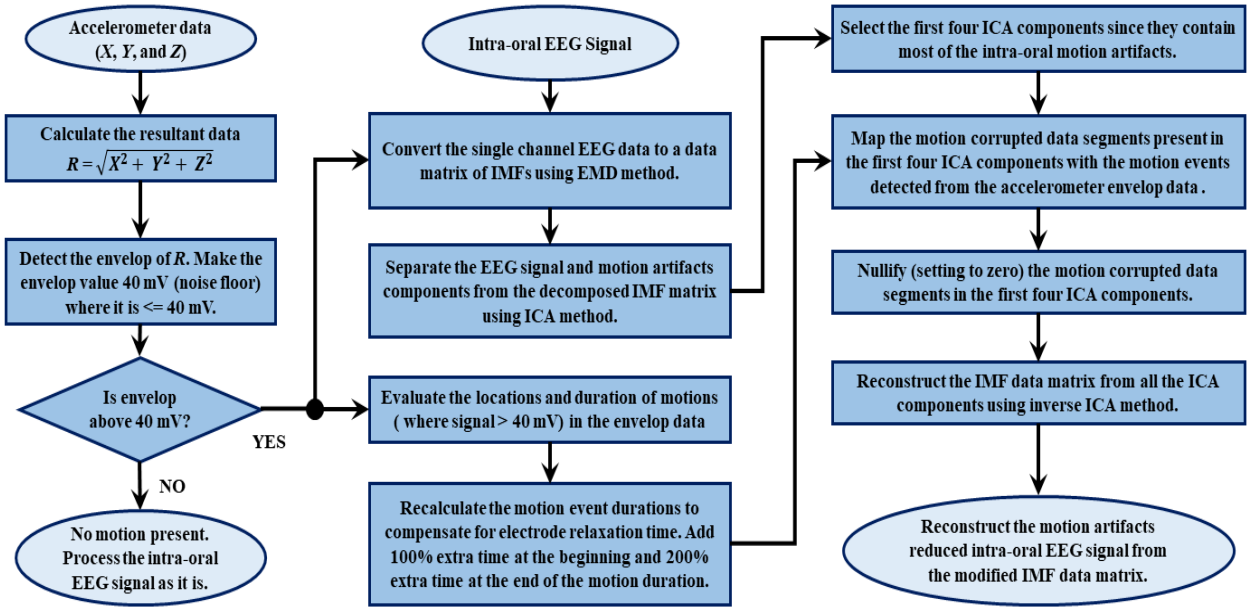

Fig. 4.5. The proposed algorithm using accelerometer data and EMD-ICA method for reducing motion artifacts from intra-oral EEG signals.

X, Y, and Z axes and found out to be around ± 40 mV. The noise floor ranges for X, Y, Z and the resultant (R) are already indicated with dashed lines in Fig. 4.4. Any responses captured by the accelerometer above this noise floor are considered motion events. A detailed flowchart of the proposed algorithm is presented in Fig. 4.5. The algorithm first acquires the intra-oral EEG and accelerometer X, Y, and Z data for a time window of 30 seconds. Then the algorithm calculates the resultant accelerometer data (R). Then envelop of the resultant data is acquired with a minimum threshold noise floor of 40 mV. Any value less than the noise floor (<= 40 mV) along the envelope is modified by making the value 40 mV during the envelope detection process. If the entire resultant envelope data remain at the noise floor (i.e. 40 mV), no intra-oral motion events are present and the algorithm processes the EEG data as it is for spectrum analyzing. If any events are detected on the resultant envelope data above the noise floor (i.e. 40 mV), we assume that a motion event has occurred. Then the resultant envelope data are analyzed to extract the start time, end time, and total duration of motion events. When the skin-electrode contact impedances change due to motion artifacts, the response time of the EEG (or any biopotential) electrodes change as well.

Therefore, the EEG baseline signal may take some extra time to settle down even after the end of a motion event. To compensate for the EEG baseline settling time, the start time, end time, and total motion durations of the detected motion events are recalculated. The algorithm adds an extra 100% time of the total motion duration at the beginning of the motion event and an extra 200% time of the total motion duration at the end of the motion event.

Intra-oral EEG data and the accelerometer data are acquired simultaneously. Therefore, the intra-oral EEG data should also experience motion artifacts on the exact time locations extracted and calculated from the accelerometer resultant envelope data. The intra-oral EEG signal is first decomposed using EMD method and then the decomposed IMF matrix (except the last residual signal) is used as inputs in fastICA to separate the components related to EEG signal and the noise. The first four independent components contained most of the most artifacts signatures in all study. Therefore, these components are mapped with the accelerometer resultant data to identify and then remove (i.e. set to zero) the motion impacted data segments. The modified independent components are then multiplied with their mixing matrix (inverse fastICA method) to reconstruct the motion artifacts reduced EMD IMFs. Finally, the regenerated IMFs are added together along with the residual signal to reconstruct a motion artifacts reduced intra-oral EEG signal. The algorithm is then repeated for the next time window.

4.5.3 EEG Processing using the Proposed Algorithm

Fig. 4.6 presents three sets of intra-oral EEG data and accelerometer data recorded with the three different kinds of intra-oral motions: (i) intra-oral EEG data with tongue movements, (ii) intra-oral EEG data with teeth grinding, and (iii) intra-oral EEG data with gulping, respectively. For all three sets of data presented in Fig. 4.6: graphs (a) shows the intra-oral EEG data with intra-oral motion artifacts; graphs (b) shows the resultant accelerometer data calculated from the X, Y, and Z axes outputs along with the 40 mV noise floor indicated by the dashed black lines; graphs (c) presents the corresponding resultant envelope data with minimum noise floor of 40 mV; graphs (d) shows the processed intra-oral EEG data after motion artifacts reduction using the proposed EMD-ICA based algorithm; and graphs (e) presents the original motion contaminated intra-oral EEG data and

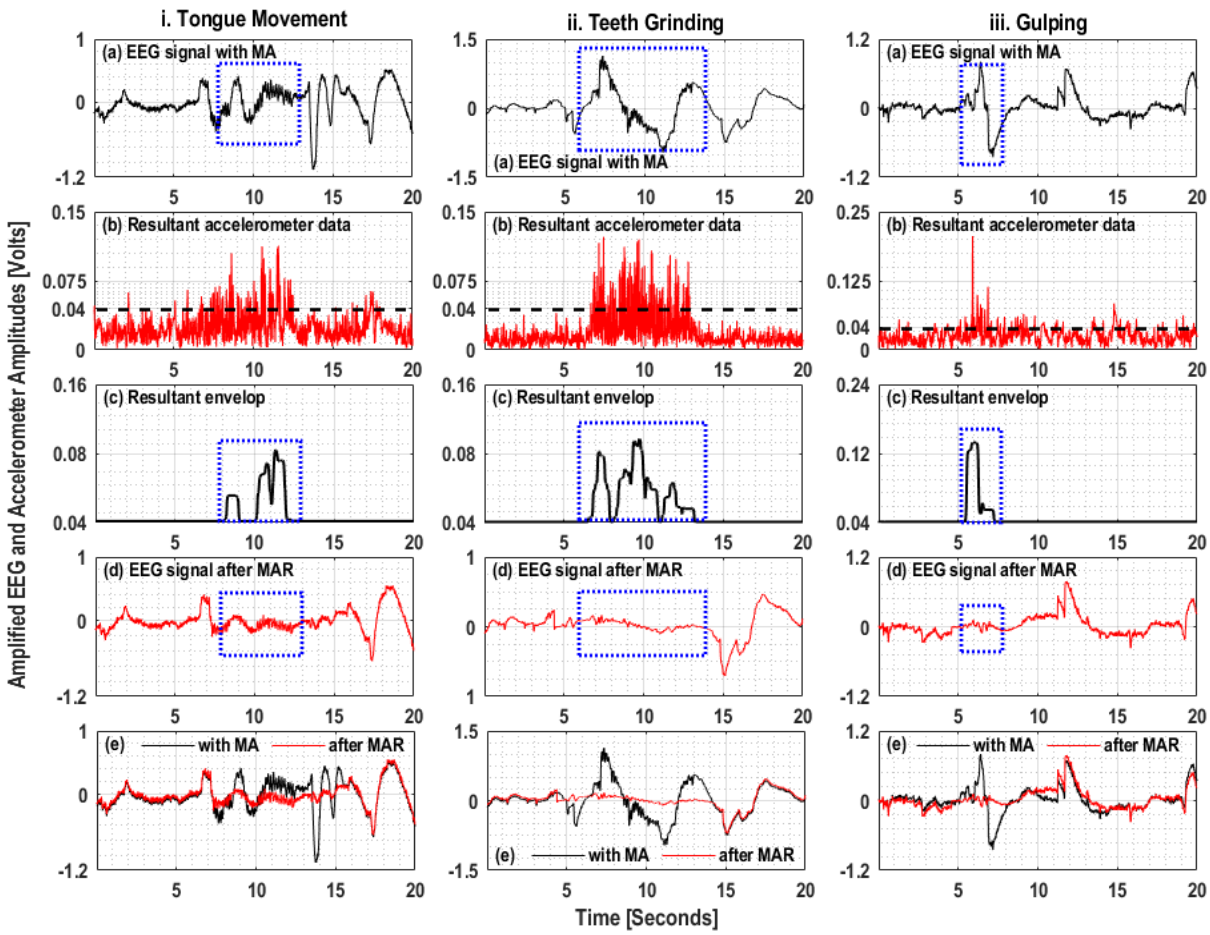

Fig. 4.6. Intra-oral EEG data processing using the proposed EMD-ICA based algorithm for motion artifacts reduction in motion contaminated EEG segments for three different type of intra-oral motion activities: (i) tongue movements with graphs (a – e), (ii) teeth grinding with graphs (a – e), and (iii) gulping with graphs (a – e). Here the term MA stands for 'motion artifacts' and the term MAR stands for 'motion artifacts reduction'.

the processed motion artifacts reduced intra-oral EEG data overlapped over each other. The dotted blue boxes presented in graphs (a), (c), and (d) show the total duration of motion events and their positions on the motion corrupted intra-oral EEG data, the resultant accelerometer envelope data, and the motion artifacts reduced intra-oral EEG data, respectively. It can be clearly seen from graphs (e) that the EMD-ICA based algorithm do minimize motion artifacts effectively from the motion contaminated EEG data segments while almost preserving the features in the other EEG

segments where motion artifacts are not present. One limitation of the algorithm is that sometimes it generates some small glitches (nearly insignificant) at the start and end timestamps of motion events after denoising, as we can see in graphs (d) for teeth grinding and gulping scenario in Fig. 4.6. However, these glitches can be attributed to the selected removal of motion contaminated segments from the ICA components.

4.5.4 The Proposed Algorithm Performance Validation

To quantify the effectiveness of the proposed algorithm, signal-to-noise (SNR) and correlation can be calculated from the EEG signals before and after noise (motion artifacts) removal. However, calculating SNR and correlation metrics require the knowledge of the "clean EEG signal" [32]. Since, it is not possible to extract the actual "clean EEG signal", we have to compute an EEG signal after all artifacts removed and consider that as our "clean EEG signal". The goal of the algorithm is to reconstruct an EEG signal after motion artifacts reduction which resembles the "clean EEG signal". Since, it was already mentioned in section 4.5.2 that the first four components of the ICA contain most of the motion artifact features. The "clean EEG signal" is computed by removing the first four ICA components completely and then employing inverse ICA-EMD method.

In this study, the first performance metric is measured by calculating the difference SNR (*ΔSNR*) of the EEG signal, with respect to the "clean EEG signal", before and after motion artifacts reduction [32]. The *ΔSNR* can be calculated using the following formula:

$$\Delta SNR = 10log_{10}\left(\frac{\sigma_x^2}{\sigma_{e_{after}}^2}\right) - 10log_{10}\left(\frac{\sigma_x^2}{\sigma_{e_{before}}^2}\right) \quad (1)$$

where σ_x^2 is the variance of the "clean EEG signal", $\sigma_{e_{after}}^2$ is the variance of the error signal after motion artifacts reduction, and $\sigma_{e_{before}}^2$ is the variance of the error signal before motion artifacts reduction. The error signals can be computed by subtracting the EEG signal from the "clean EEG signal" before and after noise reduction.

The second performance metric can be calculated by measuring the difference correlations between the EEG signal and the "clean EEG signal" before and after motion artifacts reduction [30]. This metric is known as percentage reduction is artifacts (λ) and can be calculated as follows:

$$\lambda = 100\left(\frac{R_{after}-R_{before}}{1-R_{before}}\right)\ \% \qquad (2)$$

where R_{before} and R_{after} are the correlation between the "clean EEG signal" and the EEG signal before and after motion artifacts reduction, respectively. As it can be seen from equation (2) that λ is directly proportional to R_{after}, which means that higher λ value indicates better artifact reduction.

Intra-oral EEG data are recorded in the presence of intra-oral motions (tongue movements, teeth grinding, and gulping) from three subjects and then processed through the proposed algorithm for motion artifacts reduction. Three datasets, with a duration of 15 seconds each, from each subject containing three different kinds of intra-oral motions (total nine datasets). The datasets are deliberately recorded with longer motion activity to quantify the usefulness of the proposed algorithm. The values of *ΔSNR* and λ are calculated from the 9 datasets mentioned above and presented in Table 4.3. The *ΔSNR* values gives us a measure of SNR improvement before and after motion artifacts reduction. Whereas, λ provides us a relative measure of motion artifacts reduction which also depends upon the amount of motion artifacts present in the signal. As it was mentioned in section 4.3.2 and can be seen in Fig. 4.6(i), tongue movements are relatively weak motion artifacts. Therefore, their impact on intra-oral EEG signals will be less which will yield low λ values after motion artifacts reduction. On the other hand, teeth grinding and gulping activities are relatively strong, again as mentioned in section 4.3.2 and can be seen in Fig. 4.6(ii) and 4.6(iii), respectively. Therefore, their impact on intra-oral EEG signal will be relatively large which will yield higher λ values after motion artifacts reduction.

Fig. 4.7 presents the alpha band responses of three datasets of intra-oral EEG data with 'eye open' and 'eye close' activities recorded during the three kind of intra-oral motion artifacts: (a) tongue movements, (b) teeth grinding, and (c) gulping, respectively. The three sets of intra-oral

TABLE 4.3

THE PROPOSED ALGORITHM PERFORMANCE QUANTIFICATION: THE ***ΔSNR*** AND THE PERCENTAGE REDUCTION IN ARTIFACTS (***λ***) CALCULATED FOR INTRA-ORAL EEG DATA RECORDED IN THE PRESENCE OF INTRA-ORAL MOTION ARTIFACTS

Subjects	Tongue Movements (3 Datasets)		Teeth Grinding (3 Datasets)		Gulping (3 Datasets)	
	ΔSNR (in dB)	***λ*** (in %)	***ΔSNR*** (in dB)	***λ*** (in %)	***ΔSNR*** (in dB)	***λ*** (in %)
1	20.79	7.14	31.02	40.10	7.57	23.01
2	19.86	5.73	19.22	39.61	27.42	40.05
3	5.96	4.65	19.16	31.61	11.87	32.36

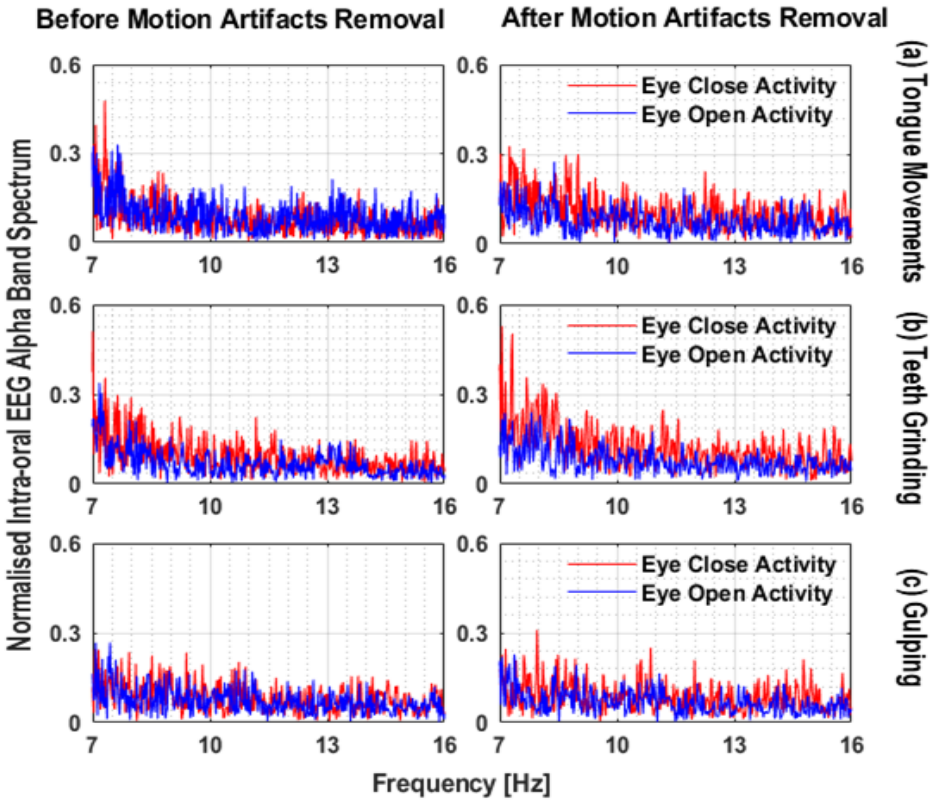

Fig. 4.7. The alpha (α) band spectrum of three intra-oral EEG datasets with 'eye open' and 'eye close' activities, before and after intra-oral motion artifacts removal using the proposed EMD-ICA based algorithm, recorded in the presence of: (a) tongue movements, (b) teeth grinding, and (c) gulping.

EEG spectrum are presented before and after the motion artifacts reduction using the proposed EMD-ICA based algorithm, as shown in Fig. 4.7. For tongue movement scenario in Fig. 4.7(a),

the alpha band responses are not clear enough to distinguish between ‘eye open’ and ‘eye close’ activities before the motion artifacts removal. But, the alpha band responses improve and become distinguishable for ‘eye open’ and ‘eye close’ activities after the motion artifacts reduction from the EEG signals. Similar alpha band responses are observed for gulping activity present in Fig. 4.7(c). Whereas, for teeth grinding scenario in Fig. 4.7(b), the alpha band responses are distinguishable for ‘eye open’ and ‘eye close’ activities even before motion artifacts reduction. However, after motion artifacts reduction, the alpha band spectrums further improve for ‘eye close’ in comparison to ‘eye open’ activity. This distinguishable change in alpha band responses for intra-oral EEG also matches with the scalp/forehead EEG alpha band responses as presented in Fig. 4.1(d) earlier and reported in [7], [36]. Thus, it can be concluded that the proposed algorithm indeed reduces motion artifacts from the intra-oral EEG signals while preserving and improving its important features.

4.5.5 Comparison of the Proposed Sensor-Fusion Method Performance with Other Existing Methods

To compare the performance of the proposed sensor fusion method with recent methods proposed for removing motion artifacts from intraoral EEG signal, the intra-oral EEG signals reported in Table 4.3 are also processed with three existing EEG denoising methods. The first method considered is DWT-ICA, which decomposes single channel EEG data into a data matrix using DWT and then uses ICA to separate the EEG and artifacts components [28]. The ICA components containing artifacts are removed and a clean EEG signal is reconstructed from the remaining components using inverse ICA and DWT. The second method employs EMD to decompose a single channel EEG data and then the decomposed IMFs are cross-correlated with the original signal [31]. The IMFs with cross-correlation less than 0.5 are marked as artifacts free and used for a clean EEG signal reconstruction. The third method uses EEMD to decompose the EEG signal into IMFs and then CCA is used to separate out artifacts components from the EEG signals [32]. Then, the CCA components containing artifacts are removed and a clean EEG signal is reconstructed from the remaining components. Fig. 4.8 presents one set of intra-oral EEG data

processed with the proposed sensor-fusion technique and the EEG denoising algorithms: DWT-ICA, EMD-CrossCorr and EEMD-CCA. As shown in Fig. 4.8(a), our proposed method uses sensor fusion to selectively identify the motion contaminated EEG segments and denoise that portion only whereas, the existing methods in presented here are employed on the entire EEG data. This may result in some unwanted loss in EEG signal features where motion artifacts are not present, as shown in Fig. 4.8(b), (c), and (d), respectively.

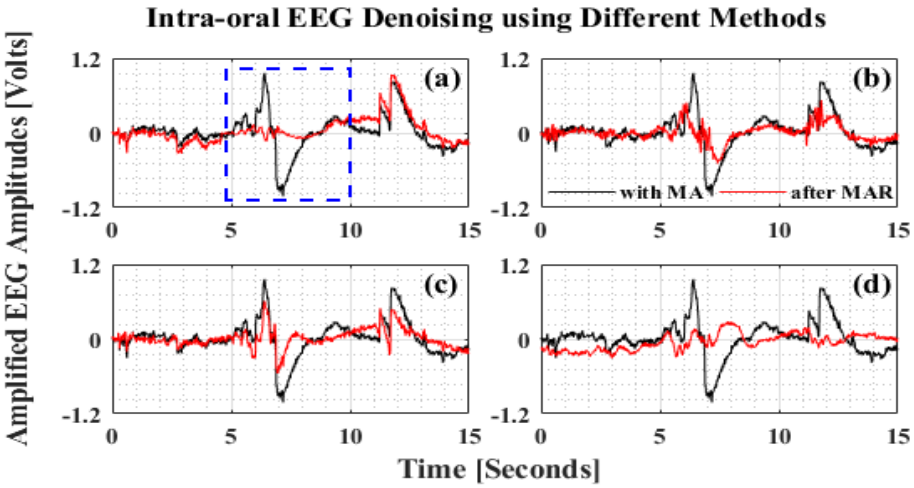

Fig. 4.8. One set of Intra-oral EEG data processed using different methods: (a) the proposed sensor-fusion method, (b) DWT-ICA method, (c) EMD with Cross-Correlation method, and (d) EEMD-CCA method. Here MA and MAR stand for 'motion artifacts' and 'motion artifacts reduction', respectively. The blue box shows the motion corrupted segment.

Table 4.4 presents the overall average values of the root mean square error (RMSE) and the change in power spectral density (ΔPSD) in all EEG bands calculated from the nine sets of intra-oral EEG data, after motion artifacts removal. The RMSE of a signal can be calculated using the following formula [31]:

$$RMSE = \sqrt{\frac{1}{N}\sum_{n=1}^{N}\{EEG_{before}(n) - EEG_{after}(n)\}^2} \quad (3)$$

where N is the EEG data length, EEG_{before} and EEG_{after} are the EEG signal before and after denoising, respectively. The RMSE is calculated only for the artifact free EEG segments whereas

the *ΔPSD* is evaluated for the entire signal. These metrics give a quantitative measure of distortion introduced in the EEG signals during signal processing and are expected to yield lower values for better performance [31]. The proposed sensor-fusion method achieves the lowest average RMSE value, which means our method introduces less distortion during EEG signal denoising. The *ΔPSD* value in delta region is also the lowest value, which may be attributed to the fact that our method processes only the motion contaminated EEG segments, thereby retaining more EEG information on the motion artifacts free EEG segments. Among the four bands the high values of *ΔPSD* in delta and theta region also indicates that motion artifacts mostly impact the EEG baseline during signal measurements.

TABLE 4.4

COMPARISON OF THE PROPOSED ALGORITHM WITH SOME STATE-OF-THE-ART EXISTING METHODS FOR INTRA-ORAL EEG DENOISING

Algorithms	***RMSE*** **(μ*V*)** (mean ± std)	***ΔPSD*** **(μ$V^2/\sqrt{Hz}$)**			
		Delta **(*δ*)** (mean ± std)	***Theta*** **(*θ*)** (mean ± std)	***Alpha*** **(*α*)** (mean ± std)	***Beta*** **(*β*)** (mean ± std)
DWT-ICA [28]	133.61 ± 99.42	3249.34 ± 2788.76	15.87 ± 14.83	2.87 ± 2.60	1.38 ± 1.27
EMD-CrossCorr [31]	119.35 ± 106.56	2705.16 ± 2587.22	2.36 ± 2.19	0.47 ± 0.43	0.06 ± 0.04
EEMD-CCA [32]	158.18 ± 106.73	3461.91 ± 2900.03	29.27 ± 27.33	7.58 ± 6.07	1.04 ± 0.71
The Proposed Algorithm	**22.43 ± 21.57**	**2398.35 ± 2141.10**	**25.80 ± 23.51**	1.90 ± 1.32	0.79 ± 0.66

4.6 Conclusion & Future Work

This paper presents a smart, wearable MAD with a sensor-fusion of EEG electrodes and accelerometer for the measurements of intra-oral EEG signals and intra-oral motions such as tongue movements, teeth grinding, and gulping simultaneously. The smart MAD also houses the sensor read-out circuitry implemented on a flexible polyimide substrate. The placement of accelerometer is optimized for proper intra-oral motion detection. The system metrics such as gain, CMRR, and EEG bandwidth of the single channel EEG AFE are also evaluated and found out to be greater than 57 dB, greater than 74 dB, and 0.16–40 Hz, respectively. Intra-oral EEG and

accelerometer data are acquired from three subjects and processed through the proposed EMD-ICA based algorithm for motion artifacts reduction. The efficacy of the proposed algorithm is validated by quantifying the difference between the SNR of the EEG signals before and after motion artifacts reduction and by calculating the correlation analysis based percentage artifacts reduction. The intra-oral EEG signals are also analyzed in the presence of motion artifacts to detect the basic 'eye open' and 'eye close' activities. The proposed sensor fusion method's performance is then compared with some other state-of-the-art EEG denoising algorithms. The comparison demonstrates that our method preserves more EEG features in comparison to the other existing methods after motion artifacts removal.

In future, the device design will be further improved by printing the measurement electrodes and their connecting wires on the smart MAD itself. The measurement system will be optimized by using lower power off-the-shelf components, thereby improving the battery life. The effectiveness of the proposed sensor fusion method to reduce artifacts from other sources of intra-oral and non-intra-oral motions such as yawning, head movements, change of body postures will also be investigated in future. Other signal decomposition techniques will also be explored for the algorithm part to further optimize the performance. The smart prototype will be used to acquire intra-oral EEG data from more participants and understand underlying EEG features for various brain activities. This smart MAD along with the EEG electrodes, accelerometer, and the algorithm have potential for MAD-based intra-oral EEG applications.

4.7 Bridging Text

This is the first reported complete smart MAD prototype capable of acquiring intra-oral EEG signals in the presence of intra-oral motion artifacts such as tongue movements, teeth grinding, and gulping. The sensor-fusion of EEG electrodes and accelerometer along with the proposed algorithm do a very efficient job in reducing the motion artifacts in the motion corrupted segments of the intra-oral EEG data. In future, the form factor of the smart MAD can be minimized by using smaller commercial off-the-shelf components and ICs. The EEG signal conditioning blocks can

be entirely replaced by a single biopotential measurement chip, further minimizing the sensor board size and power consumption. The smart MAD system will be used for acquiring intra-oral EEG signals for different brain activities and sleep for sleep stage classifications.

References

[1] A. Safayari and H. Bolhasani, "Depression diagnosis by deep learning using EEG signals: A systematic review," *Med. Novel Technol. Devices*, vol. 12, Dec. 2021, Art. no. 100102.

[2] M. K. Islam, A. Rastegarnia, and Z. Yang, "A wavelet-based artifact reduction from scalp EEG for epileptic seizure detection," *IEEE J. Biomed. & Health Inform.*, vol. 20, no. 5, pp. 1321–1332, Sept. 2016.

[3] B. Yang and H. Liu, "Automatic identification of insomnia based on single-channel EEG labelled with sleep stage annotations," *IEEE Access*, vol. 8, pp. 104281–104291, 2020.

[4] Z. Li *et. al.*, "Human cooperative wheelchair with brain–machine interaction based on shared control strategy," *IEEE/ASME Trans. Mechatronics*, vol. 22, no. 1, pp. 185–195, Feb. 2017.

[5] A. F. Jackson and D. J. Bolger, "The neurophysiological bases of EEG and EEG measurement: A review for the rest of us," *Psychophysiology*, vol. 51, no. 11, pp. 1061–1071, Nov. 2014.

[6] M. R. Mercier *et. al.*, "Advances in human intracranial electroencephalography research, guidelines and good practices," *NeuroImage*, vol. 260, p. 119438, 2022.

[7] J. W. C. Medithe and U. R. Nelakuditi, "Study of normal and abnormal EEG," *2016 3rd Int. Conf. Adv. Comput. & Commun. Syst. (ICACCS)*, Coimbatore, India, 2016, pp. 1–4.

[8] M. S. Cohen, "EEG data collection intrabuccal method and apparatus," WO Patent 107446A1, 2014, Jul. 10, 2014.

[9] R. Radmand, "Intra-oral electroencephalography device and method," U.S. Patent 0 060 611 A1, 2020, Feb. 27, 2020.

[10] S. Debbarma and S. Bhadra, "A smart mandibular device for intra-oral electroencephalogram monitoring," *2021 IEEE Sensors Conf.*, 2021, pp. 1–4.

[11] A. D. Boes *et. al.*, "Connectivity of sleep- and wake-promoting regions of the human hypothalamus observed during resting," *Sleep*, vol. 41, no. 9, pp. 1–12, May 2018, doi: 10.1093/sleep/zsy108.

[12] V. K. Kapur *et al.*, ''Clinical practice guideline for diagnostic testing for adult obstructive sleep apnea: An American academy of sleep medicine clinical practice guideline,'' *J. Clin. Sleep Med.*, vol. 13, no. 3, pp. 479–504, 2017.

[13] "Sleeping with a night guard: Is it safe? Soundview Family Dental™," (accessed: Apr. 24, 2023). [Online]. Available: https://soundviewfamilydental.com/blog/sleeping-witha-night-guard-is-it-safe/

[14] "Mouthguard: For grinding, snoring, apnea, sports, braces," (accessed: Apr. 24, 2023). [Online]. Available: https://www.healthline.com/health/mouth-guard

[15] "5 reasons to wear a night guard - Klement Family Dental," (accessed: Apr. 24, 2023). [Online]. Available: https://www.stpetedentist.com/blog/5-reasons-wear-night-guard/

[16] H. C. Nguyen, S. Debbarma, and S. Bhadra, "Flexible fabric electrodes integrated with mouthguard for Electroocoulogram measurement," *2023 IEEE Int. Conf. Flexible Printable Sensors Syst. (FLEPS), Boston, USA*, 2023. [Presented]

[17] R. Akhter and F. R. Beyette, "Machine learning algorithms for detection of noisy/artifact-corrupted epochs of visual oddball paradigm ERP data," *2022 7th Int. Conf. Data Sci. Mach. Learning Appl. (CDMA)*, Riyadh, Saudi Arabia, 2022, pp. 169–174.

[18] A. Dabbaghian *et. al.*, "A 9.2-g fully-flexible wireless ambulatory EEG monitoring and diagnostics headband with analog motion artifact detection and compensation," *IEEE Trans. Biomed. Circuits Syst.*, vol. 13, no. 6, pp. 1141–1151, Dec. 2019.

[19] A. Prochazka, O. Vysata, and V. Marik, "Integrating the role of computational intelligence and digital signal processing in education: Emerging technologies and mathematical tools," *IEEE Signal Process. Mag.*, vol. 38, no. 3, pp. 154–162, May 2021.

[20] C. Beach *et. al.*, "Motion artefact removal in electroencephalography and electrocardiography by using multichannel inertial measurement units and adaptive filtering," *Healthcare Technol. Lett.*, pp. 1–11, 2021, doi: 10.1049/htl2.12016.

[21] A. Islam *et. al.*, "Study and analysis of motion artifacts for ambulatory electroencephalography," *Int. J. Electr. Comput. Eng. (IJECE)*, vol. 12, no. 2, pp. 1520–1529, Apr. 2022.

[22] J. A. Uriguen and B. Garcia-Zapirain, "EEG artifact removal—state-of-the-art and guidelines," *J. Neural Eng.*, vol. 12, no. 3, pp. 1–23, 2015.

[23] K. L. Snyder *et. al.*, "Independent component analysis of gait-related movement artifact recorded using EEG electrodes during treadmill walking," *Frontiers Hum. Neurosci.*, vol. 9, pp. 1–13, 2015, Art. no. 639.

[24] X. Jiang, G. B. Bian, and Z. Tian, "Removal of artifacts from EEG signals: A review," *Sensors (Basel)*, vol. 19, no. 5, pp. 987, Feb. 2019, doi: 10.3390/s19050987.

[25] V. Roy *et. al.*, "Gaussian elimination-based novel canonical correlation analysis method for EEG motion artifact removal," *J. Healthc. Eng.*, vol. 2017, 2017, doi: 10.1155/2017/9674712.

[26] N. A. Chadwick, D. A. McMeekin, and T. Tan, "Classifying eye and head movement artifacts in EEG signals," *5th IEEE Int. Conf. Digit. Ecosyst. Technol. (IEEE DEST 2011)*, Daejeon, South Korea, 2011, pp. 285–291.

[27] H. Zhang *et. al.*, "Eegdenoisenet: A benchmark dataset for deep learning solutions of EEG denoising," *J. Neural Eng.*, vol. 18, no. 5, p. 056057, 2021.

[28] M. Grobbelaar *et al.*, "A survey on denoising techniques of electroencephalogram signals using wavelet transform," *Signals*, vol. 3, no. 3, pp. 577–586, Aug. 2022, doi: 10.3390/signals3030035.

[29] A. K. Maddirala and R. A. Shaik, "Motion artifact removal from single channel electroencephalogram signals using singular spectrum analysis," *Biomed. Signal Process. Control*, vol. 30, pp. 79–85, 2016.

[30] R. Ranjan, B. C. Sahana. and A. K. Bhandari, "Motion artifacts suppression from EEG signals using an adaptive signal denoising method," *IEEE Trans. Instrum. Meas.*, vol. 71, pp. 1–10, 2022.

[31] R. Patel *et. al.*, "Suppression of eye-blink associated artifact using single channel EEG data by combining cross-correlation with empirical mode decomposition," *IEEE Sensors J.*, vol. 16, no. 18, pp. 6947–6954, Sep. 2016.

[32] K. T. Sweeney, S. F. McLoone, and T. E. Ward, "The use of ensemble empirical mode decomposition with canonical correlation analysis as a novel artifact removal technique," *IEEE Trans. Biomed. Eng.*, vol. 60, no. 1, pp.97–105, 2013.

[33] R. Patel, K. Gireesan, and S. Sengottuvel, "Decoding non-linearity for effective extraction of the eye-blink artifact pattern from EEG recordings," *Pattern Recognit. Lett.*, vol. 139, pp. 42–49, 2020.

[34] S. Debbarma, S. Nabavi, and S. Bhadra, "A wireless flexible electrooculogram monitoring system with printed electrodes," *IEEE Int. Instrum. Meas.Technol. Conf. (I2MTC)*, Glasgow, United Kingdom, 2021, pp. 1–6.

[35] N. S. Manam *et. al.*, "Study of corrosion in biocompatible metals for implants: A review," *J. Alloys Compd.*, vol. 701, pp 698–715, 2017.

[36] D. -H. Jeong and J. Jeong, "In-ear EEG based attention state classification using echo state network," *Brain sciences*, vol. 10, no. 6, pp. 321, Mar. 2020.

[37] P. C. Petrantonakis and L. J. Hadjileontiadis, "A novel emotion elicitation index using frontal brain asymmetry for enhanced EEG-based emotion recognition," *IEEE Trans. Inf. Technol. Biomed.*, vol. 15, no. 5, pp. 737–746, Sep. 2011.

[38] W. Heide *et al.*, “Electrooculography: Technical standards and applications. The international federation of clinical neurophysiology,” *Electroencephalogr. Clin. Neurophysiol. Suppl.*, vol. 52, pp. 223–240, 1999.

[39] S. Debbarma and S. Bhadra, "A flexible wearable electrooculogram system with motion artifacts sensing and reduction," *IEEE Trans. Biomed. Circuits Syst.*, vol. 16, no. 2, pp. 324–335, April 2022.

[40] S. Debbarma and S. Bhadra, "A lightweight flexible wireless electrooculogram monitoring system with printed gold electrodes," *IEEE Sensors J.*, vol. 21, no. 18, pp. 20931–20942, 15 Sept.15, 2021.

[41] M. Guermandi, E. F. Scarselli, and R. Guerrieri, “A driving right leg circuit (DgRL) for improved common mode rejection in bio-potential acquisition systems,” *IEEE Trans. Biomed. Circuits Syst.*, vol. 10, no. 2, pp. 507–517, Apr. 2016.

[42] M. R. Nuwer *et al.*, “IFCN standards for digital recording of clinical EEG,” *Electroencephalogr. Clin. Neurophysiol.*, vol. 106, no. 3, pp. 259–261, Mar. 1998.

[43] A. Dermoune and T. Wei, “FastICA algorithm: Five criteria for the optimal choice of the nonlinearity function,” *IEEE Trans. Signal Process.*, vol. 61, no. 8, pp. 2078-2087, April15, 2013.

Chapter 5

Discussion

In the context of the present state-of-the-art commercial and non-commercial biopotential wearables reviewed in this thesis, it is evident that they have several design and usage related issues which can be broadly classified into the following categories: -

- Biopotential acquiring electrode design issues
- Biopotential measurement system design issues
- Motion artifacts in biopotential measurements
- Possible limitations of the biopotential wearable usages

This chapter presents a detailed discussion on the expectations and accomplishments of this research project which aims to address all the above issues and proposes smart wearable biopotential measurement systems which have potential applications for sleep study.

5.1 Biopotential Acquiring Electrode Design Issues

Most of the commercial biopotential wearables use rigid contact electrodes which are uncomfortable to wear for long term study [1]–[7]. Some works have explored flexible fabric-based electrodes. Although they are comfortable to wear, they also suffer from less sensitivity, require larger size for increased sensitivity, and are not suitable for compact biopotential wearable design [8]–[13].

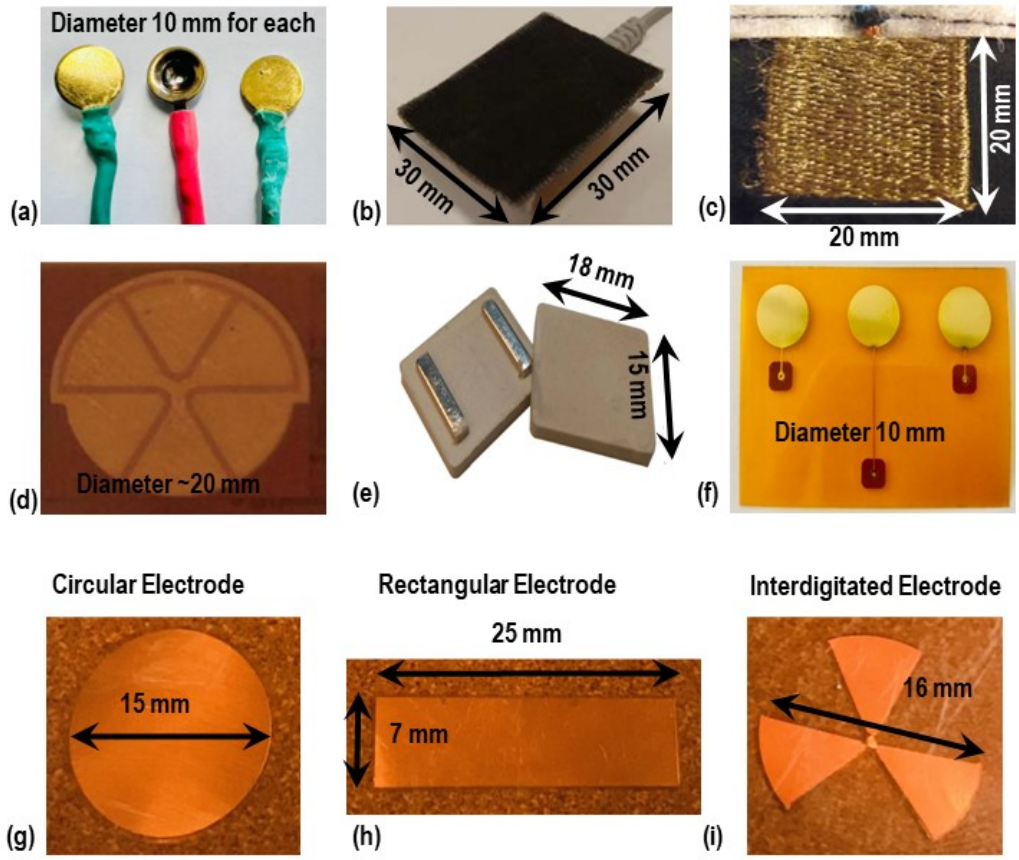

Fig. 5.1. Different rigid/flexible electrodes for EEG/EOG measurements: (a) commercial rigid flat and cup gold electrodes, (b) fabric-based flexible electrode reconstructed with permission from [12] © 2018 IEEE, (c) fabric-based flexible electrode reconstructed with permission from [13] © 2005 IEEE, (d) noncontact electrode reconstructed with permission from [14] © 2019 IEEE, (e) semi-rigid silicon based electrodes reconstructed with permission from [15] © 2017 IEEE, (f) flexible Polyimide based contact gold electrode printed for our applications reconstructed with permission from [16] © 2021 IEEE, (g) – (i) flexible Polyimide based non-contact gold electrodes with different shapes printed for our applications reconstructed with permission from [17] © 2022 IEEE.

To address this design constraint, we proposed an idea to use printed gold layer as the measurement electrodes. The electrodes were designed in Altium (CAD software for PCB design) and were printed on flexible Polyimide substrate. The flexible Polyimide substrate provides the printed gold electrodes sufficient degree of freedom and skin conformability to have them placed comfortably on the skin. The concept of using printed electrodes was reported in [14], but they did

not provide any performance characterization of the flexible electrodes. Here, in two of our biopotential measurement prototypes presented in chapters 2 and 4, the flexible printed electrodes are configured as contact electrodes [18]. Their skin-electrode contact impedance properties have been validated on the forehead with/without gel and in moist intra-oral environments. The sensitivities of the flexible contact electrodes are found out to be similar like the commercial gold flat electrodes with gel, as reported in chapter 2. In another biopotential measurement prototype proposed by us in chapter 3, the printed gold electrodes are covered with kapton film and configured as non-contact electrodes. The skin-electrode contact capacitances for the non-contact electrodes are measured and reported in chapter 3. The sensitivities of the non-contact electrodes are also computed and compared with the commercial rigid contact gold electrodes with gel. The non-contact electrodes show sensitivities 50 times (or more) higher than the conventional contact electrodes, as reported in chapter 3. Some of the rigid/flexible electrodes and our designed flexible gold electrodes (both contact and non-contact) are presented in Fig. 5.1.

5.2 Biopotential Measurement System Design Issues

As discussed in chapter 1, there are several system design standards and aspects that need to be addressed for a wearable system design. In the following subsections, we discussed about reasonable solutions to some of these design problems which we have implemented in our proposed biopotential measurement prototypes.

5.2.1 Measurement System PCB

Most of the commercial and non-commercial wearables use rigid PCBs for measurement system implementation which are not at all comfortable to use for wearable applications [1]–[13], [15], [18]–[22]. Therefore, we implemented our EOG/EEG measurement systems on flexible Polyimide substrates, just like the printed electrodes. Flexible substrates are lightweight, bendable, and skin-conformable [14]. Therefore, the use of flexible substrates is getting very popular in recent technologies, especially for wearable applications [14], [23], [24]. All our three proposed prototypes (presented in chapters 2, 3, and 4) for EOG/EEG measurements are implemented on

flexible Polyimide substrates. The weight of all three systems, along with their soldered components and batteries, were less than 12 grams which is very light to wear.

5.2.2 Electrode and Measurement System Integration

In most of the biopotential measurement wearable design, the measurement electrodes are bought or manufactured separately and interfaced with the measurement unit using either connecting wires or metallic snap buttons [8]–[13]. As mentioned before, only one work shows EEG measurement electrodes printed for their flexible instrument [14]. Here also, we followed similar design approach and printed the flexible gold electrodes on the bottom layer of our two EOG prototypes, as presented in chapters 2 and 3. Our reported works are the only reported flexible prototypes used for EOG applications. The top layer of the board is used to implement the circuit for EOG data acquisition. In case of our smart MAD for intra-oral EEG measurements, presented in chapter 4, the flexible printed electrodes are interfaced with flexible board using small wires. This is done to optimize and utilise the space available in the oral cavity. The intra-oral EEG electrodes are supposed to touch the palate, so they are placed inside the oral cavity. The measurement instrument along with the battery cannot be accommodated inside the oral cavity because of their size, dimension, and user comfort. Therefore, the EEG instrument is integrated along the outer curvature of the MAD, outside the oral cavity.

5.2.3 Biopotential Measurement Standards

All biopotential instruments should meet some standard system metrics to be qualified as good quality measurement systems set by international research groups for medical technologies such as IFCN [25]. The IFCN encourages the system design engineers to evaluate their system's gain, common mode rejection ratio (or CMRR), and input-referred noise levels to check if they meet the standard IFCN metrics or not. This ensures the signal amplifying and processing capability of the biopotential measurement system as we are trying to measure signals which are in the range of a few µVs to a few mVs. Our three proposed prototypes for EOG/EEG measurements have been tested for their gain, CMRR, and noise metrics and reported in chapters 2, 3, and 4, respectively.

All our proposed prototypes meet the IFCN standard metrics required for biopotential measurement.

The IFCN standard also recommends the use of driven right leg (or DRL) circuits for systems involving contact electrodes [25]. The DRL circuit is an arrangement for feeding the ground electrode back to the subject's body to minimize the common-mode signals during biopotential measurements. However, feeding an electrical voltage into a subject's body are always subject to potential risks of electrocution due to system failure and current discharge [25]. The DRL circuit can limit the amount of current injecting into the subject's body during such accidents and save the person from potential health risks. Two of our proposed system, presented in chapters 2 and 4, are also based on contact electrode applications and the DRL circuit is implemented in both systems to meet the IFCN standards.

5.2.4 Power Consumptions and Long-Term Monitoring

One major system requirement for long term monitoring is having a long battery life. This depends on the number of sensors and electronic components used in the circuit and their total power consumption. For long term monitoring like sleep study, the system needs to run for at least 7 to 8 hours. The commercial sleep monitoring devices reviewed here are optimized to run for 10 hours or more, which is reasonable [1]–[7]. However, this also requires bigger batteries with better energy storage, which explains the size of the rigid cases used for the system and battery integration in the commercial wearable reviewed in chapter 1. Therefore, it is important to identify the power-hungry components of the system and optimize the overall system design.

Our designed EOG prototypes in chapter 2 and 3, are powered with 120 mAh and 125 mAh rechargeable Li-ion batteries, respectively. Both of them have a battery life of approximately 7 hours which is good enough for sleep study. Our smart MAD based intra-oral EEG measurement prototype also uses accelerometer for intra-oral motion tracking and requires additional power for a longer battery life, as presented in chapter 4. Therefore, our smart MAD was powered with a 200 mAh rechargeable Li-ion battery and has a battery life of approximately 8 hours. The main power

TABLE 5.1

A DETAILED INFORMATION ON VOLTAGE, CURRENT, AND POWER CONSUMPTION OF OUR PROPOSED BIOPOTENTIAL MEASUREMENT PROTOTYPES

Circuit Components	EOG Prototype 1 [Chapter 1]		EOG Prototype 2 [Chapter 2]		Smart MAD Prototype for Intra-oral EEG [Chapter 3]	
Battery Capacity	120 mAh		125 mAh		200 mAh	
Voltage Regulator (TPS7333 LDR)	3.3 Volts		3.3 Volts		3.3 Volts	
Battery Life	7 hrs. 40 min. (appox.)		7 hrs. 15 min. (appox.)		8 hrs. 20 min. (approx.)	
CURRENT AND POWER CONSUMPTIONS						
	I in (mA)	*P* in (mW)	*I* in (mA)	*P* in (mW)	*I* in (mA)	*P* in (mW)
Instrumentation Amplifier (INA116/118)	1	3.3	2	6.6	1	3.3
Other OpAmps (LMC6482/6484)	3	9.9	3	9.9	4	13.2
Accelerometer (MXR9500MZ)	—	—	—	—	4	13.2
Microcontroller (Atmega328p)	2	6.6	2	6.6	2	6.6
Bluetooth (RN4871)	**10**	**33**	**10**	**33**	**10**	**33**
Total	16	52.8	17	56.0	21	69.3

consuming components in our design is Bluetooth 5.0 transceiver which consumes the maximum amount of power. Table 5.1 presents the power consumptions of our circuit prototypes presented in chapter 2, 3, and 4, respectively. There are commercial low power Bluetooth modules with integrated analog-to-digital converter (or ADC) modules available in the market which can be used to replace the entire microcontroller and Bluetooth module in our design. However, most of our research work have been done during the COVID-19 pandemic and shortly afterwards and many electronic components (including low power Bluetooth modules) were out of stock to buy during that time. Therefore, the wearable prototypes were designed with the available low power electronic components in the market. The selection of the low power electronic components and overall power optimization for our prototypes can be done in future work.

5.2.5 Integration of Measurement Setup with Wearable Platform

As mentioned before, all our EOG/EEG wearable prototypes are implemented on flexible boards. Given the flexibility of the proposed systems, two of them (presented in chapter 2 and 3) are skin conformable and can be easily integrated with headbands or eye-masks for EOG measurements. The two EOG systems don't need any rigid and bulky wearable platforms for integration, which is a major advantage in comparison to all commercial EOG/EEG wearables reviewed in the thesis. The smart MAD prototype is designed especially for intra-oral EEG measurements. The flexible measurement system is also surface conformable and can be integrated easily along the curvature of our custom-made MAD, as presented in chapter 4.

5.3 Motion Artifacts in Biopotential Wearables

The most challenging problem in biopotential measurements is the issue of motion artifacts and none of the non-commercial wearables (reviewed in this thesis from scholarly article), reported any smart hardware or software-based arrangements to tackle this problem. Only one research work report hardware arrangement based motion-artifacts removal technique for wearable EEG prototype, but they do not report any real-time EEG recording in the presence of motion artifacts [14]. One of our EOG prototypes, presented in chapter 3, uses parallel non-contact electrodes for motion artifacts sensing and reduction at the very first input stage. The system is validated thoroughly for eye blink activities already in the presence/absence of motions.

There are several other scholarly articles on sensor-fusion based methods [26]–[29], statistical methods [30]–[37], and even machine learning methods [38]–[40] related to motion artifacts reductions in EEG signals already reviewed in this thesis. In our MAD based intra-oral EEG prototype presented in chapter 4, we also used a sensor-fusion of EEG electrodes and an accelerometer to acquire EEG signal and intra-oral motions simultaneously. Then the acquired EEG and motion signals are processed in a MATLAB based algorithm through a time window of 30 seconds. The accelerometer data is used in a MATLAB based algorithm to identify intra-oral motion events. If motion events are detected, the MATLAB based algorithm then decomposes the

intra-oral EEG signal using empirical decomposition (EMD) and independent component analysis (ICA) technique to independent ICA components. In this study, the first four decomposed ICA components contained most of the motion artifacts present in the intra-oral EEG data, which are then mapped with the accelerometer data. The identified motion corrupted segments in the first four ICA components are then nullified. After that, a motion artifacts reduced EEG signal is reconstructed from all the ICA components using inverse ICA-EMD method. The efficacy of the proposed algorithm is also validated qualitatively and quantitatively. Then, the smart MAD along with the algorithm is then used to extract basic 'eye open' and 'eye close' features from intra-oral EEG spectrums in the presence/absence of intra-oral motions. It should be noted that this smart sensor-fusion along with the algorithm can remove corrupted EEG data even for body related movements during sleep. When a person changes their postures during sleep, it may disturb the intra-oral EEG recordings as well, which will still be picked up by the accelerometer sensor and the corrupted data will be removed by the algorithm, thus making this device more suitable for wearable applications. This sensor-fusion technique along with the algorithm can also be employed to our first EOG prototype in future designs and maybe used for scalp EEG recordings as well.

5.4 Possible Limitations of The Biopotential Wearable Usages

The limitations of our wearable EOG prototypes (presented in chapters 2 and 3) are that they are placed on forehead for measurements. Forehead may not be a good place to wear biopotential wearables intended for sleep study. Due to body/head movements during sleep the wearable platform (headbands or eye-masks) may get displaced and compromise the positions of the measurement electrodes, which will eventually corrupt the entire EOG recordings. Moreover, wearing headbands and eye-masks are still not that comfortable to wear during sleep.

The smart MAD based intra-oral EEG system, presented in chapter 4, overcomes this issue. Oral appliances (here MAD) are comfortable to wear and stays in the same position during body/head movements thus holding the measurement electrodes on the same locations, which is an advantage. The smart MAD for intra-oral EEG is a more suitable biopotential wearable

prototype in comparison to the EOG headband prototypes. But there are always some scopes in future to further improve the smart MAD design, use more compact circuit components and ICs, optimize algorithm, reduce power consumption, reduce battery size, and reduce the form factor of the overall system.

5.5 Summary

This research proposes three different wearable prototypes for biopotential (EOG and EEG) measurements. The wearable design constraints such as flexible electrode design, flexible EOG/EEG instrument design, skin conformability, ease of use, and performance limitations are carefully reviewed and implemented accordingly during the three wearable prototypes reported here. The biopotential wearable prototypes are also tested extensively for their performance evaluation and presented in detail in chapters 2, 3, and 4. All three proposed EOG/EEG prototypes are comfortable to use on their respective placement locations (forehead or oral cavity) and have potential to be used in sleep study and treat patients suffering from sleep disorders such as OSA.

References

[1] "MUSE: The Brain Sensing Headset," choosemuse.com. https://choosemuse.com/ (accessed Mar. 18, 2023).

[2] "DREEM: Sleep Pioneers," dreem.com. https://dreem.com/ (accessed Mar. 18, 2023).

[3] "Sleep Shepherd: Sleep Optimizer and Tracker," sleepshepherd.com. https://sleepshepherd.com/ (accessed Mar. 18, 2023).

[4] "SmartSleep: Deep Sleep Headband," The Brain Sensing Headset" usa, Philips.com. https://www.usa.philips.com/c-e/smartsleep/deep-sleep-headband.html (accessed Mar. 18, 2023).

[5] "EMOTIVE EPOC+: 14-Channel Wireless EEG Headset," emotive.com. https://www.emotiv.com/product/emotiv-epoc-x-14-channel-mobile-brainwear/ (accessed Mar. 18, 2023).

[6] "JiNS MEME," jinsmeme.com. https://jinsmeme.com/en/ (accessed Mar. 18, 2023).

[7] Y. S. Pai *et al.*, "NapWell: An EOG-based Sleep Assistant Exploring the Effects of Virtual Reality on Sleep Onset," *Virtual Reality*, vol. 26, pp. 437–451 Sept. 2021, doi: /10.1007/s10055-021-00571-w.

[8] J. Arnin *et al.*, "Wireless-based portable EEG-EOG monitoring for real time drowsiness detection," *2013 IEEE 35th Annu. Int. Conf. Engg. Medicine and Biol.*, 2013, pp. 4977-4980.

[9] S. -F. Liang et al., "Development of an EOG-based automatic sleep-monitoring eye mask," *IEEE Trans. Instrum. Meas.*, vol. 64, no. 11, pp. 2977–2985, 2015.

[10] X. Guo, W. Pei, Y. Wang, Y. Chen, H. Zhang, X. Wu, X. Yang, H. Chen, Y. Liu, and R. Liu, "A human-machine interface based on single channel EOG and patchable sensor," *Biomed. Signal Process. and Control*, vol. 30, pp. 98–105, 2016.

[11] A. A. Chlaihawi, B. B. Narakathu, S. Emamian, B. J. Bazuin, and M. Z. Atashbar, "Development of printed and flexible dry ECG electrodes," *Sens. Bio-Sens. Res.*, vol. 20, pp. 9–15, Sep. 2018.

[12] A. J. Golparvar and M. K. Yapici, "Electrooculography by wearable graphene textiles," *IEEE Sens. J.*, vol. 18, no. 21, pp. 8971–8978, 2018.

[13] A. T. Vehkaoja, J. A. Verho, M. M. Puurtinen, N. M. Nojd, J. O. Lekkala, and J. A. Hyttinen, "Wireless head cap for EOG and facial EMG measurements," *2005 IEEE 27th Annu. Conf. Engg. Medicine and Biol.*, 2006, pp. 5865–5868.

[14] A. Dabbaghian et al., “A 9.2-g fully-flexible wireless ambulatory EEG monitoring and diagnostics headband with analog motion artifact detection and compensation,” *IEEE Trans. Biomed. Circuits Syst.*, vol. 13, no. 6, pp. 1141–1151, Dec. 2019.

[15] C. -T. Lin *et al.*, “Forehead EEG in Support of Future Feasible Personal Healthcare Solutions: Sleep Management, Headache Prevention, and Depression Treatment,” *IEEE Access*, vol. 5, pp. 10612-10621, 2017.

[16] S. Debbarma and S. Bhadra. “A Sensor-Fusion Method for Motion Artifacts Reduction in Intra-oral EEG Signals.” *IEEE Sens. J.*, May 2023. [Submitted]

[17] S. Debbarma and S. Bhadra, “A Flexible Wearable Electrooculogram System with Motion Artifacts Sensing and Reduction,” *IEEE Trans. Biomed. Circuits Syst*., vol. 16, no. 2, pp. 324-335, April 2022.

[18] Y. M. Chi, T. Jung, and G. Cauwenberghs, “Dry-contact and noncontact biopotential electrodes: methodological review,” *IEEE Rev. Biomed. Eng.*, vol. 3, pp. 106–119, 2010.

[19] J. Xu *et al*., "A wearable 8-channel active-electrode EEG/ETI acquisition system for body area networks," *IEEE J. Solid-State Circuits*, vol. 49, no. 9, pp. 2005–2016, Sept. 2014.

[20] C. Beach, N. Karim and A. J. Casson, “A Graphene-Based Sleep Mask for Comfortable Wearable Eye Tracking,” 2019 IEEE 41st Annu. Int. Conf. Eng. Med. Biol. Soc. (EMBC), Berlin, Germany, 2019, pp. 6693-6696.

[21] S. -W. Kim, K. Lee, J. Yeom, T. -H. Lee, D. -H. Kim and J. J. Kim, “Wearable Multi-Biosignal Analysis Integrated Interface With Direct Sleep-Stage Classification,” IEEE Access, vol. 8, pp. 46131-46140, 2020.

[22] S. Rostaminia et al., “PhyMask: Robust Sensing of Brain Activity and Physiological Signals During Sleep with an All-textile Eye Mask,” ACM Trans. Comput. Healthcare, vol. 3, no. 3, pp. 1–35, Jul. 2022.

[23] W. Dang, V. Vinciguerra, L. Lorenzelli, and R. Dahiya, "Printable stretchable interconnects,” *Flexible and Printed Electronics*, vol. 2, no. 1, (2017), 013003, 2017.

[24] A. Pullanchiyodan, L. Manjakkal and R. Dahiya, "Metal Coated Fabric Based Asymmetric Supercapacitor for Wearable Applications," *IEEE Sens. J.*, vol. 21, no. 23, pp. 26208-26214, Dec. 2021.

[25] M. R. Nuwer et al., “IFCN standards for digital recording of clinical EEG,” *Electr. Clin. Neuroph.*, vol. 106, no. 3, pp. 259–261, Mar. 1998.

[26] J. Ottenbacher *et al.*, "Reliable motion artifact detection for ECG monitoring systems with dry electrodes," *2008 30th Annu. Int. Conf. IEEE Eng. Medicine & Biol. Soc.*, 2008, pp. 1695–1698.

[27] N. Van Helleputte *et al.*, "A 160 µA biopotential acquisition IC with fully integrated IA and motion artifact suppression," *IEEE Trans. Biomed. Circuits & Syst.*, vol. 6, no. 6, pp. 552–561, Dec. 2012.

[28] J. Xu *et al*., "A wearable 8-channel active-electrode EEG/ETI acquisition system for body area networks," *IEEE J. Solid-State Circuits*, vol. 49, no. 9, pp. 2005–2016, Sept. 2014.

[29] I. Daly, M. Billinger, R. Scherer and G. Müller-Putz, "On the Automated Removal of Artifacts Related to Head Movement From the EEG," *IEEE Trans. Neural Syst. Rehabil. Eng.*, vol. 21, no. 3, pp. 427–434, May 2013.

[30] K. L. Snyder, J. E. Kline, H. J. Huang, and D. P. Ferris, "Independent component analysis of gait-related movement artifact recorded using EEG electrodes during treadmill walking," *Frontiers Hum. Neurosci.*, vol. 9, pp. 1–13, 2015, Art. no. 639.

[31] S. Sadiya, T. Alhanai, and M. M. Ghassemi, "Artifact Detection and Correction in EEG data: A Review," *2021 10th Int. IEEE/EMBS Conf. Neural Eng. (NER)*, Italy, 2021, pp. 495–498.

[32] V. Roy *et. al.*, "Gaussian Elimination-Based Novel Canonical Correlation Analysis Method for EEG Motion Artifact Removal," *J. Healthc. Eng.*, vol. 2017, 2017, doi: 10.1155/2017/9674712.

[33] X. Jiang, G. B. Bian, and Z. Tian, "Removal of Artifacts from EEG Signals: A Review," *Sensors (Basel)*, vol. 19, no. 5, pp. 987, Feb. 2019, doi: 10.3390/s19050987.

[34] S. Shukla, V. Roy, and A. Prakash, "Wavelet based empirical approach to mitigate the effect of motion artifacts from EEG signal," *Proc. - 2020 IEEE 9th Int. Conf. Commun. Syst. Netw. Technol.(CSNT 2020)*, pp. 323–326, 2020.

[35] A. K. Maddirala and R. A. Shaik, "Motion artifact removal from single channel electroencephalogram signals using singular spectrum analysis," *Biomed. Signal Process. Control*, vol. 30, pp. 79–85, 2016.

[36] R. Ranjan, B. C. Sahana. and A. K. Bhandari, "Motion Artifacts Suppression From EEG Signals Using an Adaptive Signal Denoising Method," *IEEE Trans. Instrum. Meas.*, vol. 71, pp. 1-10, 2022.

[37] K. T. Sweeney, S. F. McLoone, and T. E. Ward, "The use of ensemble empirical mode decomposition with canonical correlation analysis as a novel artifact removal technique," IEEE Trans. Biomed. Eng., vol. 60, no. 1, pp.97–105, 2013.

[38] R. Akhter and F. R. Beyette, "Machine Learning Algorithms for Detection of Noisy/Artifact-Corrupted Epochs of Visual Oddball Paradigm ERP Data," 2022 7th Int. Conf. Data Sci. Mach. Learning Appl. (CDMA), Riyadh, Saudi Arabia, 2022, pp. 169–174.

[39] N. A. Chadwick, D. A. McMeekin, and T. Tan, “Classifying eye and head movement artifacts in EEG signals,” *5th IEEE Int. Conf. Digit. Ecosyst. Technol. (IEEE DEST 2011)*, Daejeon, South Korea, 2011, pp. 285–291.

[40] H. Zhang *et. al.*, “Eegdenoisenet: A benchmark dataset for deep learning solutions of EEG denoising,” *J. Neural Eng.*, vol. 18, no. 5, p. 056057, 2021.

Chapter 6

Conclusion and Future Work

6.1 Conclusion

This research work proposes three wearable biopotential (EOG and EEG) measurement prototypes with possible application for sleep study. The design plans of these prototypes were laid out after detailed review of the state-of-the-art commercial and non-commercial biopotential wearables. The key design considerations for biopotential wearable designs are as follows: the sensor placement locations for acquiring biopotential signals, use and development of commercially viable flexible measurement electrodes, possibility of implementing the measurement system on a skin-conformable flexible substrate, integration of the measurement system on a comfortable wearable platform which can be worn easily without seeking help from others, and addressing any sensor or system related parameters that can limit the wearable performance.

In our first prototype a wearable, flexible EOG measurement prototype is developed. In this prototype, the contact flexible gold EOG electrodes are printed as pads on the bottom layer and the sensor read-out circuitry is implemented on the top layer for a flexible Polyimide board, thus integrating them in a smart way and eliminating the challenges of interfacing electrodes with the system. The flexible system along with the battery weighs just 7.7 g, making it suitable for integrating with any soft fabric-based headband or eye-mask. The system is battery operated and has a battery life of approximately 7 hours and 40 minutes, thus making it suitable for long term

monitoring during (e.g. sleep study). The EOG device is already validated for sleep monitoring and sleep stage classification using a machine-learning based algorithm [1]. The limitations of this wearable are as follows: (a) the electrode sizes are small and requires electrode gel for a good quality EOG sensing, and (b) the EOG system is sensitive to motion artifacts. To address the issues of the first prototype, another flexible EOG wearable is designed with flexible parallel electrode pair for motion artifacts sensing and reduction during EOG measurement. The new system prototype is lightweight (only 8.75 g), has a long battery life (approximately 7 hours and 15 minutes), uses non-contact EOG electrodes which do not require electrode gel, and capable of measuring EOG signals in the presence of motion artifacts. However, headbands and eye-masks can be uncomfortable to wear during sleep for some people.

Given successful recording of EEG signals intra-orally and the popularity of using oral appliances (e.g. dental retainer, mouthguard, MAD etc.) in various treatments, we proposed a first custom-made MAD based prototype for intra-oral EEG monitoring. The smart MAD uses a sensor-fusion of EEG electrodes and accelerometer to monitor intra-oral EEG signal in the presence of intra-oral motions such as tongue movements, teeth grinding, and gulping. We also propose a MATLAB based algorithm which identifies the presence of intra-oral motions using the accelerometer sensor data. Then it uses empirical method decomposition (EMD) and independent component analysis (ICA) method to decompose the intra-oral EEG signal into ICA components. The first four ICA components are found to be containing most of the motion artifacts features in all of the studies. Therefore, the first four ICA components containing the intra-oral motion artifacts are mapped with the accelerometer data to identify the motion corrupted segments in the ICA components and nullify them accordingly. An inverse ICA-EMD method is applied on all the ICA components after modification to reconstruct a motion artifacts reduced intra-oral EEG signal. The smart MAD uses flexible printed Polyimide substrate-based gold electrodes as they are comfortable to wear intra-orally in comparison the commercial rigid electrodes. The measurement system is implemented on flexible PCB and integrated with the MAD itself. This smart MAD prototype has potential for intra-oral EEG based applications. One such possible application is

using the smart MAD to monitor EEG vitals intra-orally during sleep for sleep quality assessments. The smart MAD is more comfortable to wear in comparison to the headband/eye-mask based bipotential measurement wearables.

6.2 Future Work

The main motivation of this research work is to develop working biopotential wearable system prototypes and take all the necessary design precautions during system development. However, some analytical approaches could have been taken to further investigate the performances of the proposed systems, which were overlooked in our research. Moreover, the proposed prototypes can still be modified further to enhance their usability in terms of wearable platform design, sensor design, circuit performance, circuit protection, signal processing etc. A rough roadmap is provided below to address all these wearable design related concerns and improvements that can be investigated in future studies.

- **Printed Electrode Characterization:** In this research, the flexible printed contact and non-contact electrodes are characterized for their skin-electrode impedances and signal sensitivities. However, the impact of temperature, humidity, and their impact on the sensors' sensitivity/impedance properties have not been studied. A detailed study can be done solely focusing on the sensor (i.e. electrodes) design/characterization in simulation and under controlled environments.
- **Parametric Analysis of the Proposed Measurement Systems:** Another study that was overlooked in our research is to include a parametric analysis of the biopotential measurement systems done in the simulation environment (using software like Spice Simulators, ADS etc.). Such study will provide us to analyse the discreet passive components (e.g. resistors, capacitors, inductors etc.) with their specified tolerances and quantify their impact on the system metrics like gain, noise, signal bandwidth, CMRR etc. This study will help us for overall optimization of the system performance.

- **Wearable MAD and Intra-Oral Electrode Placement/Interfacing:** The present smart MAD, on the other hand, uses separate flexible electrodes attached with the smart MAD using biocompatible adhesive and uses small wires to interface the electrodes with the EEG acquisition. This creates slight discomfort to the wearer while using the current smart MAD prototype. In future, a custom-made MAD can be developed with the flexible electrodes and their routing wires printed on it, which will be more comfortable to wear, thus making the smart MAD further suitable for commercialization. It should be noted that the EOG wearable prototypes can be commercialised with proper integration in wearable headbands and eye-masks.
- **Further Improvements on the Proposed Prototype Design:** For all three prototypes, the system can be further improved by using smaller low power commercially available off-the-shelf components and ICs, thus optimising the form factor and power consumption of the system. An application specific low power IC can also be designed for this design. The analog front-end of the measurement unit can be powered with a modified power management block to provide higher voltage headroom to set higher gains for biopotential measurements and avoid system saturation due to motion artifacts. A low-power BLE module with integrated microcontroller can also be used to replace the entire digital part of the system. Smaller components can be used to further reduce the circuit dimensions.

  A sophisticated battery management unit can also be implemented with wireless charging block and a protection circuit. A protection circuit is included in circuit design to handle faulty battery and system failure related scenarios and avoid any potential health hazard, which is an important requirement for commercial wearable design.
- **Sensor-Fusion and Algorithm for Motion Artifacts Reduction:** In this research, we have proposed only one sensor-fusion based EMD-ICA algorithm to reduce motion artifacts from single channel EEG signals. But, there are several other signal decomposition methods like DWT, EEMD, CCA, PCA etc. which can be combined along with the sensor-fusion for EEG denoising. A comparative study of all these signal decomposition method can be done for further optimising the algorithm performance with more data.

- **EEG and EOG Feature Extraction:** Given the limited number of participants, we could acquire a large set of intra-oral EEG data for further. Now that we have a complete intra-oral EEG prototype, the device can be used to acquire intra-oral EEG from more participants and investigate/analyse the underlying complex EEG features related to various brain activities such as anxiety, stress, hypertension, sleep etc. This study will give us a clearer understanding of intra-oral EEG and its possible applications.

  Both EOG and intra-oral EEG signals can be acquired using our prototypes from a large number of volunteers and the data can be processed for feature extractions using advanced neural networks and machine learning algorithms.

- **Integration of other Smart Sensors:** A smart MAD based prototype was also developed in our lab using PPG sensor, accelerometer, and temperature sensor for monitoring intra-oral cardiorespiratory parameters, sleep postures, and body temperature, respectively [2]. All these smart sensors can also be accommodated, in the EOG hardware as well as in the smart MAD device. These will further improve the applicability of the proposed biopotential measurement wearables and make them capable of monitoring all the necessary physiological vitals (heart-rate, SpO_2, breath, body, temperature, sleep postures, and sleep stages).

References

[1] M. Hamza, S. Bhadra, and Z. Zilic, "Sleep Stage Detection on a Wearable Headband Using Deep Neural Networks," *2022 Global Internet of Things Summit (GloTS)*, Dublin, Ireland, 2022, pp. 187–198.

[2] S. Nabavi and S. Bhadra, "Smart Mandibular Advancement Device for Intraoral Monitoring of Cardiorespiratory Parameters and Sleeping Postures," *IEEE Trans. Biomed. Circuits Syst.*, vol. 15, no. 2, pp. 248–258, April 2021.

References in Alphabetical Order

"5 Reasons to Wear a Night Guard." *Klement Family Dental*, 24 Apr. **2023**, https://www.stpetedentist.com/blog/5-reasons-wear-night-guard/.

Akhter, Rafia, and Fred R. Beyette. "Machine Learning Algorithms for Detection of Noisy/Artifact-Corrupted Epochs of Visual Oddball Paradigm ERP Data." *2022 7th International Conference on Data Science and Machine Learning Applications (CDMA)*, **2022**, pp. 169–174.

Arnin, J., et al. "Wireless-Based Portable EEG-EOG Monitoring for Real Time Drowsiness Detection." *2013 35th Annual International Conference of the IEEE Engineering in Medicine and Biology Society (EMBC)*, **2013**, pp. 4977–4980.

Beach, Christopher, et al. "A Graphene-Based Sleep Mask for Comfortable Wearable Eye Tracking." *2019 41st Annual International Conference of the IEEE Engineering in Medicine and Biology Society (EMBC)*, **2019**, pp. 6693–6696.

"BeneVision N1." *Mindray.com*, 15 Mar. **2023**, https://www.mindray.com/en/media-center/press/mindray-launches-benevision-n1-for-uninterrupted-monitoring-during-intra-and-out-of-hospital-patient-transport.

"Bittium NeuroOne." *Bittium.com*, 17 Mar. **2023**, https://www.bittium.com/medical/bittium-neurone.

Boes, A. D., et al. "Connectivity of sleep- and wake-promoting regions of the human hypothalamus observed during resting wakefulness." *Sleep*, *41*(9), **2018**, pp. 1–12.

Brain, A. I. J. *Combined Laryngeal Mask and Reflectance Oximeter*. 1 Feb. **1994**.

Bratton, Daniel J., et al. "CPAP vs Mandibular Advancement Devices and Blood Pressure in Patients with Obstructive Sleep Apnea." *JAMA*, *314*(21), **2015**, p. 2280.

Bulling, Andreas, et al. "Eye Movement Analysis for Activity Recognition Using Electrooculography." *IEEE Transactions on Pattern Analysis and Machine Intelligence*, *33*(4), **2011**, pp. 741–753.

"Cardiocap 5." *Dremed.com*, 15 Mar. **2023**, https://www.dremed.com/datex-ohmeda-cardiocap-5/id/1691.

"CARESCAPE ONE Monitor." *Gehealthcare.ca*, 15 Mar. **2023**, https://www.gehealthcare.ca/en-ca/products/carescape-one.

Chadwick, Neisha A., David A. McMeekin, and Tele Tan. "Classifying eye and head movement artifacts in EEG signals." *5th IEEE International Conference on Digital Ecosystems and Technologies (IEEE DEST 2011)*, **2011**, pp. 285–291.

Chaudhuri, Aritra, et al. "A Low-Cost, Wearable, Portable EOG Recording System." *2016 International Conference on Systems in Medicine and Biology (ICSMB)*, **2016**, pp. 102–105.

Chen, Chen, et al. "Novel Flexible Material-Based Unobtrusive and Wearable Body Sensor Networks for Vital Sign Monitoring." *IEEE Sensors Journal*, *19*(19), **2019**, pp. 8502–8513.

Chi, Yu Mike, et al. "Dry-Contact and Noncontact Biopotential Electrodes: Methodological Review." *IEEE Reviews in Biomedical Engineering*, *3*, **2010**, pp. 106–119.

Chiang, Harmeet K., et al. "Dental Sleep Appliance Therapy for the Treatment of Obstructive Sleep Apnea." *Dental Sleep Medicine*, **2022**, pp. 233–266.

Chlaihawi, Amer Abdulmahdi, et al. "Development of Printed and Flexible Dry ECG Electrodes." *Sensing and Bio-Sensing Research*, *20*, **2018**, pp. 9–15.

COHEN, Mark Steven. *EEG Data Collection Intrabuccal Method and Apparatus*. 10 July **2014**.

Constantin, Catalin P., et al. "Biocompatibility of Polyimides: A Mini-Review." *Materials*, *12*(19), **2019**, p. 3166.

Dabbaghian, Alireza, et al. "A 9.2-G Fully-Flexible Wireless Ambulatory EEG Monitoring and Diagnostics Headband with Analog Motion Artifact Detection and Compensation." *IEEE Transactions on Biomedical Circuits and Systems*, *13*(6), **2019**, pp. 1141–1151.

Daly, Ian, et al. "On the Automated Removal of Artifacts Related to Head Movement from the EEG." *IEEE Transactions on Neural Systems and Rehabilitation Engineering*, *21*(3), **2013**, pp. 427–434.

Dang, Wenting, et al. "Printable Stretchable Interconnects." *Flexible and Printed Electronics*, *2*(1), **2017**, p. 013003.

Debbarma, Shibam, and Sharmistha Bhadra. "A Flexible Wearable Electrooculogram System with Motion Artifacts Sensing and Reduction." *IEEE Transactions on Biomedical Circuits and Systems*, *16*(2), **2022**, pp. 324–335.

Debbarma, Shibam, and Sharmistha Bhadra. "A Lightweight Flexible Wireless Electrooculogram Monitoring System with Printed Gold Electrodes." *IEEE Sensors Journal*, *21*(18), **2021**, pp. 20931–20942.

Debbarma, Shibam, and Sharmistha Bhadra. “A Smart Mandibular Device for Intra-Oral Electroencephalogram Monitoring.” *2021 IEEE Sensors*, **2021**, pp. 1–4.

Debbarma, Shibam, and Sharmistha Bhadra. “Intraoral Monitoring of Photoplethysmogram Signal to Estimate Cardiorespiratory Parameters.” *2nd International EAI Healthwear Conference*, **2021**, pp. 23–33.

Debbarma, Shibam, et al. “A Wireless Flexible Electrooculogram Monitoring System with Printed Electrodes.” *2021 IEEE International Instrumentation and Measurement Technology Conference (I2MTC)*, **2021**, pp. 1–6.

Debener, Stefan, et al. “Is Resting Anterior EEG Alpha Asymmetry a Trait Marker for Depression?” *Neuropsychobiology*, *41*(1), **2000**, pp. 31–37.

Deli, Gabriella, et al. “Comparison of the Efficacy of Unipolar and Bipolar Electrode Configuration during Subthalamic Deep Brain Stimulation.” *Parkinsonism & Related Disorders*, *17*(1), **2011**, pp. 50–54.

Dermoune, A., & Wei, T. “FASTICA algorithm: Five criteria for the optimal choice of the nonlinearity function.” *IEEE Transactions on Signal Processing*, *61*(8), **2013**, pp. 2078–2087.

Diniz, P. S. R. *Adaptive Filtering*. Springer, **1997**.

Diykh, Mohammed, et al. “EEG Sleep Stages Classification Based on Time Domain Features and Structural Graph Similarity.” *IEEE Transactions on Neural Systems and Rehabilitation Engineering*, *24*(11), **2016**, pp. 1159–1168.

“DREEM: Sleep Pioneers.” *Dreem.com*, 18 Mar. **2023**, https://dreem.com/.

“EEGO™ Mylab.” *Ant-Neuro.com*, 17 Mar. **2023**, https://www.ant-neuro.com/products/eego-mylab.

“EMOTIVE EPOC+: 14-Channel Wireless EEG Headset.” *Emotive.com*, 18 Mar. **2023**, https://www.emotiv.com/product/emotiv-epoc-x-14-channel-mobile-brainwear/.

“EOG Amplifier.” *Biopac.com*, 17 Mar. **2023**, https://www.biopac.com/product/electrooculogram-amplifier/.

“EOG Pod.” *Adinstruments.com*, 17 Mar. **2023**, https://www.adinstruments.com/products/eog-pod.

Ernsting, Clemens, et al. “Using Smartphones and Health Apps to Change and Manage Health Behaviors: A Population-Based Survey.” *Journal of Medical Internet Research*, *19*(4), **2017**, p. e101.

Flemons, W. Ward, et al. “Access to Diagnosis and Treatment of Patients with Suspected Sleep Apnea.” *American Journal of Respiratory and Critical Care Medicine*, *169*(6), **2004**, pp. 668–672.

Golparvar, Ata Jedari, and Murat Kaya Yapici. “Electrooculography by Wearable Graphene Textiles.” *IEEE Sensors Journal*, *18*(21), **2018**, pp. 8971–8978.

Guermandi, Marco, et al. “A Driving Right Leg Circuit (DGRL) for Improved Common Mode Rejection in Bio-Potential Acquisition Systems.” *IEEE Transactions on Biomedical Circuits and Systems*, *10*(2), **2016**, pp. 507–517.

Guerrero, Federico Nicolas, and Enrique Mario Spinelli. “A Two-Wired Ultra-High Input Impedance Active Electrode.” *IEEE Transactions on Biomedical Circuits and Systems*, *12*(2), **2018**, pp. 437–445.

Guo, Xuhong, et al. “A Human-Machine Interface Based on Single Channel EOG and Patchable Sensor.” *Biomedical Signal Processing and Control*, *30*, **2016**, pp. 98–105.

Hamza, Mian, et al. “Sleep Stage Detection on a Wearable Headband Using Deep Neural Networks.” *Internet of Things*, **2022**, pp. 187–198.

Heide, W., et al. “Electrooculography: technical standards and applications.” *The International Federation of Clinical Neurophysiology. Electroencephalography and clinical neurophysiology. Supplement*, *52*, **1999**, 223–240.

Helleputte, N. Van, et al. “A 160 $\Mu{\Rm a}$ Biopotential Acquisition IC with Fully Integrated IA and Motion Artifact Suppression.” *IEEE Transactions on Biomedical Circuits and Systems*, *6*(6), **2012**, pp. 552–561.

Hoffstein, Victor. “Review of Oral Appliances for Treatment of Sleep-Disordered Breathing.” *Sleep and Breathing*, *11*(1), **2006**, pp. 1–22.

“Intellivue X2.” *Philips.ca*, 15 Mar. **2023**, https://www.philips.ca/healthcare/product/HC865039/intellivue-mms-x2-measurement-module-monitor.

Iqbal, Sheikh M., et al. “Advances in Healthcare Wearable Devices.” *Npj Flexible Electronics*, *5*(1), **2021**, pp. 1–14.

Islam, Asma, et al. “Study and analysis of motion artifacts for ambulatory electroencephalography.” *International Journal of Electrical & Computer Engineering, 12*(*2*), **2022**, pp. 1520–1529.

Islam, Md Kafiul, et al. “A Wavelet-Based Artifact Reduction from Scalp EEG for Epileptic Seizure Detection.” *IEEE Journal of Biomedical and Health Informatics*, *20*(5), **2016**, pp. 1321–1332.

Jackson, A. F., & Bolger, D. J. “The neurophysiological bases of EEG and EEG Measurement: A review for the rest of Us.” *Psychophysiology*, *51*(11), **2014**, pp. 1061–1071.

Jeong, Dong-Hwa, and Jaeseung Jeong. “In-Ear EEG Based Attention State Classification Using Echo State Network.” *Brain Sciences*, *10*(6), **2020**, p. 321.

Jia, Wenyan, et al. “Characteristics of Skin-Electrode Impedance for a Novel Screw Electrode.” *2014 40th Annual Northeast Bioengineering Conference (NEBEC)*, **2014**, pp. 1–2.

Jiang, Xiao, et al. “Removal of Artifacts from EEG Signals: A Review.” *Sensors*, *19*(5), **2019**, p. 987.

"JiNS MEME." *Jinsmeme.com*, 18 Mar. **2023**, https://jinsmeme.com/en/.

Kalevo, Laura, et al. "Effect of Sweating on Electrode-Skin Contact Impedances and Artifacts in EEG Recordings with Various Screen-Printed AG/Agcl Electrodes." *IEEE Access*, *8*, **2020**, pp. 50934–50943.

Kim, Sung-Woo, et al. "Wearable Multi-Biosignal Analysis Integrated Interface with Direct Sleep-Stage Classification." *IEEE Access*, *8*, **2020**, pp. 46131–46140.

Kosmyna, Nataliya, et al. "Attentivu: A Wearable Pair of EEG and EOG Glasses for Real-Time Physiological Processing." *2019 IEEE 16th International Conference on Wearable and Implantable Body Sensor Networks (BSN)*, **2019**, pp. 1–4.

Kapur, V. K., et al. "Clinical practice guideline for diagnostic testing for adult obstructive sleep apnea: An American Academy of Sleep Medicine Clinical Practice guideline." *Journal of Clinical Sleep Medicine*, *13*(03), **2017**, pp. 479–504.

Larson, Alex, et al. "Electrooculography Based Electronic Communication Device for Individuals with ALS." *2017 IEEE Sensors Applications Symposium (SAS)*, **2017**, pp. 1–5.

Li, Zhijun, et al. "Human Cooperative Wheelchair with Brain–Machine Interaction Based on Shared Control Strategy." *IEEE/ASME Transactions on Mechatronics*, *22*(1), **2017**, pp. 185–195.

Liang, Sheng-Fu, et al. "Development of an EOG-Based Automatic Sleep-Monitoring Eye Mask." *IEEE Transactions on Instrumentation and Measurement*, *64*(11), **2015**, pp. 2977–2985.

Lin, Chin-Teng, et al. "Forehead EEG in Support of Future Feasible Personal Healthcare Solutions: Sleep Management, Headache Prevention, and Depression Treatment." *IEEE Access*, *5*, **2017**, pp. 10612–10621.

Lin, Min, and Bin Li. "A Wireless EOG-Based Human Computer Interface." *2010 3rd International Conference on Biomedical Engineering and Informatics*, *5*, **2010**, pp. 1794–1796.

Lontis, Eugen R., et al. "Wheelchair Control with Inductive Intra-Oral Tongue Interface for Individuals with Tetraplegia." *IEEE Sensors Journal*, *21*(20), **2021**, pp. 22878–22890.

Lu, Tsung-Chien, et al. "Healthcare Applications of Smart Watches." *Applied Clinical Informatics*, *7*(3), **2016**, pp. 850–869.

Lupu, Robert Gabriel, et al. "Eye Tracking User Interface for Internet Access Used in Assistive Technology." *2017 E-Health and Bioengineering Conference (EHB)*, **2017**, pp. 659–662.

Maddirala, Ajay Kumar, and Rafi Ahamed Shaik. "Motion artifact removal from single channel electroencephalogram signals using singular spectrum analysis." *Biomedical Signal Processing and Control*, *30*, **2016**, pp. 79–85.

Manabe, Hiroyuki, et al. “Direct Gaze Estimation Based on Nonlinearity of EOG.” *IEEE Transactions on Biomedical Engineering*, *62*(6), **2015**, pp. 1553–1562.

Medithe, John William, and Usha Rani Nelakuditi. “Study of Normal and Abnormal EEG.” *2016 3rd International Conference on Advanced Computing and Communication Systems (ICACCS)*, **2016**, pp. 1–4.

Mercier, Manuel R., et al. "Advances in human intracranial electroencephalography research, guidelines and good practices." *NeuroImage, 260*, **2022**, p. 119438.

Mignot, Emmanuel, et al. “Sleeping with the Hypothalamus: Emerging Therapeutic Targets for Sleep Disorders.” *Nature Neuroscience*, *5*(S11), **2002**, pp. 1071–1075.

“Mouthguard: For Grinding, Snoring, Apnea, Sports, Braces,” *Healthline.com*, 24 Apr. **2023**, https://www.healthline.com/health/mouth-guard.

“MUSE: The Brain Sensing Headset.” *Choosemuse.com*, 18 Mar. **2023**, https://choosemuse.com/.

Nabavi, Seyedfakhreddin, and Sharmistha Bhadra. “Oral Cavity Pressure Measurement-Based Respiratory Monitoring System with Reduced Susceptibility to Motion Artifacts.” *2020 42nd Annual International Conference of the IEEE Engineering in Medicine & Biology Society (EMBC)*, **2020**, pp. 5901–5904.

Nabavi, Seyedfakhreddin, and Sharmistha Bhadra. “Smart Mandibular Advancement Device for Intraoral Monitoring of Cardiorespiratory Parameters and Sleeping Postures.” *IEEE Transactions on Biomedical Circuits and Systems*, *15*(2), **2021**, pp. 248–258.

“NeuroCap™.” *Brainscientific.com*, 17 Mar. **2023**, https://brainscientific.com/products/ .

Nguyen, H. C., et al. “Flexible fabric electrodes integrated with mouthguard for electroocoulogram measurement.” *2023 IEEE International Conference on Flexible and Printable Sensors and Systems (FLEPS)*, **2023**, pp. 1–4.

Nuwer, Marc R., et al. “IFCN Standards for Digital Recording of Clinical Eeg.” *Electroencephalography and Clinical Neurophysiology*, *106*(3), **1998**, pp. 259–261.

Ottenbacher, Jorg, et al. “Reliable Motion Artifact Detection for ECG Monitoring Systems with Dry Electrodes.” *2008 30th Annual International Conference of the IEEE Engineering in Medicine and Biology Society*, **2008**, pp. 1695–1698.

Ouyang, Rui, et al. “Design and Implementation of a Reading Auxiliary Apparatus Based on Electrooculography.” *IEEE Access*, *5*, **2017**, pp. 3841–3847.

Pai, Yun Suen, et al. “Napwell: An EOG-Based Sleep Assistant Exploring the Effects of Virtual Reality on Sleep Onset.” *Virtual Reality*, *26*(2), **2021**, pp. 437–451.

Palumbo, Arrigo, et al. “Biopotential Signal Monitoring Systems in Rehabilitation: A Review.” *Sensors*, *21*(21), **2021**, p. 7172.

Park, Hangue, et al. “A Wireless Magnetoresistive Sensing System for an Intra-Oral Tongue-Computer Interface.” *2012 IEEE International Solid-State Circuits Conference*, **2012**, pp. 1241–1246.

Patel, R., et al. “Decoding non-linearity for effective extraction of the eye-blink artifact pattern from EEG Recordings.” *Pattern Recognition Letters*, *139*, **2020**. pp. 42–49.

Patel, R., et al. “Suppression of eye-blink associated artifact using single channel EEG data by combining cross-correlation with empirical mode decomposition.” *IEEE Sensors Journal*, *16*(18), **2016**, pp. 6947–6954.

Petrantonakis, P. C., and L. J. Hadjileontiadis. “A Novel Emotion Elicitation Index Using Frontal Brain Asymmetry for Enhanced EEG-Based Emotion Recognition.” *IEEE Transactions on Information Technology in Biomedicine*, *15*(5), **2011**, pp. 737–746.

Popa, Livia, et al. “Reading beyond the Glance: Eye Tracking in Neurosciences.” *Neurological Sciences*, *36*(5), **2015**, pp. 683–688.

“Prevent Biometrics: The Prevent Solution.” *Preventbiometrics.com*, 20 Mar. **2023**, https://preventbiometrics.com/our-story/.

Prochazka, Ales, Oldrich Vysata, and Vladimir Marik. “Integrating the role of computational intelligence and digital signal processing in education: Emerging technologies and mathematical tools.” *IEEE Signal Processing Magazine 38*(*3*), **2021**, pp. 154–162.

Pullanchiyodan, Abhilash, et al. “Metal Coated Fabric Based Asymmetric Supercapacitor for Wearable Applications.” *IEEE Sensors Journal*, *21*(23), **2021**, pp. 26208–26214.

Punjabi, N. M. “The Epidemiology of Adult Obstructive Sleep Apnea.” *Proceedings of the American Thoracic Society*, *5*(2), **2008**, pp. 136–143.

Radmand, Reza. *Intra-Oral Electroencephalography Device and Method*. 27 Feb. **2020**.

Ranjan, Rakesh, Bikash Chandra Sahana, and Ashish Kumar Bhandari. “Motion artifacts suppression from EEG signals using an adaptive signal denoising method.” *IEEE Transactions on Instrumentation and Measurement*, *71*, **2022**, pp. 1–10.

Rommelse, Nanda N.J., et al. “A Review on Eye Movement Studies in Childhood and Adolescent Psychiatry.” *Brain and Cognition*, *68*(3), **2008**, pp. 391–414.

Rostaminia, Soha, et al. “Phymask: Robust Sensing of Brain Activity and Physiological Signals during Sleep with an All-Textile Eye Mask.” *ACM Transactions on Computing for Healthcare*, *3*(3), **2022**, pp. 1–35.

Roy, Vandana, et al. “Gaussian elimination-based novel canonical correlation analysis method for EEG motion artifact removal.” *Journal of Healthcare Engineering*, *2017*, **2017**.

Sadiya, Sari, et al. “Artifact Detection and Correction in EEG Data: A Review.” *2021 10th International IEEE/EMBS Conference on Neural Engineering (NER)*, **2021**, pp. 495–498.

Safayari, A., & Bolhasani, H. “Depression diagnosis by deep learning using EEG Signals: A systematic review.” *Medicine in Novel Technology and Devices*, *12*, **2021**, Art. no. 100102.

Saganowski, S., et al. “Review of Consumer Wearables in Emotion, Stress, Meditation, Sleep, and Activity Detection and Analysis.” *ArXiv, abs/2005.00093*, **2020**, pp. 1–6.

Sedra, A. S., and K. C. Smith. *Microelectronic Circuits*, 7th ed., Oxford University Press Inc, **2015**, pp. 627–636.

Sharma, Ram A., et al. “Obstructive Sleep Apnea Severity Affects Amyloid Burden in Cognitively Normal Elderly. A Longitudinal Study.” *American Journal of Respiratory and Critical Care Medicine*, *197*(7), **2018**, pp. 933–943.

Shukla, Shailja, Vandana Roy, and Anand Prakash. “Wavelet based empirical approach to mitigate the effect of motion artifacts from EEG signal.” *2020 IEEE 9th International Conference on Communication Systems and Network Technologies (CSNT)*, **2020**, pp. 323–326.

“Sisu Sense: Because Every Hit Matters.” *Sisuguard.com*, 20 Mar. **2023**, https://www.sisuguard.com/sisusense/.

“Sleep Shepherd: Sleep Optimizer and Tracker.” *Sleepshepherd.com*, 18 Mar. **2023**, https://sleepshepherd.com/.

“Sleeping With a Night Guard: Is It Safe?” *Soundview Family Dental™*, 24 Apr. **2023**, https://soundviewfamilydental.com/blog/sleeping-witha-night-guard-is-it-safe/.

“SmartSleep: Deep Sleep Headband, The Brain Sensing Headset.” *Usa.philips.com*, 18 Mar. **2023**, https://www.usa.philips.com/c-e/smartsleep/deep-sleep-headband.html.

Snyder, Kristine L., et al. “Independent Component Analysis of Gait-Related Movement Artifact Recorded Using EEG Electrodes during Treadmill Walking.” *Frontiers in Human Neuroscience*, *9*, **2015**, pp. 1–13.

“SomnoMed Patient: The Comfortable Alternative to CPAP.” *Somnomed.com*, 20 Mar. **2023**, https://somnomed.com/en/.

“SOMNOmedics.” *Somnomedics.ce*, 15 Mar. **2023**, https://somnomedics.de/en/the-home-of-innovative-and-mobile-diagnostics/.

Sucres, Marlene Alejandra, et al. “EOG-Based Interface and Speech Recognition for Wheelchair Control.” *2019 IEEE International Conference on Engineering Veracruz (ICEV)*, **2019**, pp. 1–4.

Sullivan, Thomas J., et al. “A Low-Noise, Non-Contact EEG/ECG Sensor.” *2007 IEEE Biomedical Circuits and Systems Conference (BioCAS)*, **2007**, pp. 154–157.

Sun, Ye, and Xiong Bill Yu. “Capacitive Biopotential Measurement for Electrophysiological Signal Acquisition: A Review.” *IEEE Sensors Journal*, *16*(9), **2016**, pp. 2832–2853.

Sutherland, K., et al. “Oral appliance treatment for obstructive sleep apnea: an update.” *Journal of clinical sleep medicine : JCSM : official publication of the American Academy of Sleep Medicine, 10*(2), **2014**, pp. 215–227.

Svard, Daniel, et al. “Design and Evaluation of a Capacitively Coupled Sensor Readout Circuit, toward Contact-Less ECG and EEG.” *2010 Biomedical Circuits and Systems Conference (BioCAS)*, **2010**, pp. 320–305.

Sweeney, Kevin T., Seán F. McLoone, and Tomas E. Ward. “The use of ensemble empirical mode decomposition with canonical correlation analysis as a novel artifact removal technique.” *IEEE Transactions on Biomedical Engineering*, *60*(*1*), **2012**, pp. 97–105.

Taji, Bahareh, et al. “Effect of Pressure on Skin-Electrode Impedance in Wearable Biomedical Measurement Devices.” *IEEE Transactions on Instrumentation and Measurement*, *67*(8), **2018**, pp. 1900–1912.

Tang, Tao, et al. “An Active Concentric Electrode for Concurrent EEG Recording and Body-Coupled Communication (BCC) Data Transmission.” *IEEE Transactions on Biomedical Circuits and Systems*, *14*(6), **2020**, pp. 1253–1262.

Teplan, M. “Fundamentals of EEG measurement. Measurement.” *Science review, 2*(2), **2002**, pp. 1–11.

Trull, Elene, et al. “Implementation and Use of the Electrooculogram in Sleep Monitoring.” *2015 IEEE Virtual Conference on Applications of Commercial Sensors (VCACS)*, **2015**, pp. 1–13.

Udovicic, Goran, et al. “Wearable Technologies for Smart Environments: A Review with Emphasis on BCI.” *2016 24th International Conference on Software, Telecommunications and Computer Networks (SoftCOM)*, **2016**, pp. 1–9.

“*Ultra low input bias current instrumentation amplifier*.” INA116, Texas Instruments. Austin, TX. May **1995** [Revised September 2000].

Urigüen, J. A., & Garcia-Zapirain, B. “EEG artifact removal—state-of-the-art and Guidelines.” *Journal of Neural Engineering*, *12*(3), **2015**, pp. 1–23.

Vehkaoja, A.T., et al. “Wireless Head Cap for EOG and Facial EMG Measurements.” *2005 IEEE Engineering in Medicine and Biology 27th Annual Conference*, **2005**, pp. 5865–5868.

Virkkala, Jussi, et al. “Automatic Sleep Stage Classification Using Two-Channel Electro-Oculography.” *Journal of Neuroscience Methods*, *166*(1), **2007**, pp. 109–115.

Webster, John G. *Design of Pulse Oximeters*. Institute of Physics Publishing, **2003**.

“WholeYou: Live Out Loud Live Whole.” *Wholeyou.com*, 20 Mar. **2023**, https://www.wholeyou.com/.

Xu, Jiawei, et al. “A Wearable 8-Channel Active-Electrode EEG/ETI Acquisition System for Body Area Networks.” *IEEE Journal of Solid-State Circuits*, *49*(9), **2014**, pp. 2005–2016.

Xu, Jiawei, et al. “Active Electrodes for Wearable EEG Acquisition: Review and Electronics Design Methodology.” *IEEE Reviews in Biomedical Engineering*, *10*, **2017**, pp. 187–198.

Yang, Bufang, and Hongxing Liu. “Automatic Identification of Insomnia Based on Single-Channel EEG Labelled with Sleep Stage Annotations.” *IEEE Access*, *8*, **2020**, pp. 104281–104291.

Zheng, Wei-Long, et al. “Vigilance Estimation Using a Wearable EOG Device in Real Driving Environment.” *IEEE Transactions on Intelligent Transportation Systems*, *21*(1), **2020**, pp. 170–184.

Appendices

A MATLAB Code for the EOG Feature Extraction Algorithm presented in Chapter 2

```
function [Right_HEM, Left_HEM, Eye_Blink, Right_Wink, Left_Wink] = EOG_feature_extraction(EOG_Data)
{
    Fs = 200; % Sampling Frequency of the acquired data
    Pos_baseline_floor = 0.15; % Positive EOG baseline range
    Peak_Distance = 100; % Minimum distance between 2 consecutive Positive peaks
    Neg_baseline_floor = 0.15; % Negative EOG baseline range
    Valley_Distance = 100; % Minimum distance between 2 consecutive Negative peaks
    max_corres_peak_dist = 85;
    % Maximum distance between 2 corresponding Positive & Negative peaks

    [EOGPks, EOGPksLocation] =
    findpeaks(EOG_Data,'MinPeakHeight',Pos_baseline_floor,'MinPeakDistance',Peak_Distance);
    % Positive Peaks and their Locations detection

    EOG_Data_neg = (-1)* EOG_Data; % Flipping EOG signal along vertical axis
    [EOGVlys, EOGVlysLocation] =
    findpeaks(EOG_Data_neg,'MinPeakHeight',Neg_baseline_floor,'MinPeakDistance',Valley_Distance);
    % Negative Peaks and their Locations detection
    EOGVlys_neg = (-1)*EOGVlys; % Flipping back the detected Negative Peaks

    % Mapping the peak and valley locations
    count = 1;
```

```
for i = 1:1:length(EOGPksLocation)
   for j = 1:1:length(EOGVlysLocation)
      if ((EOGVlysLocation(j) − EOGPksLocation(i)) < max_corres_peak_dist)
         Pairlocations(count) = EOGPksLocation(i);
         Pairlocations(count+1) = EOGVlysLocation(j);
      end
   end
   count = count+2;
end
% Sorting the Positive and Negative peak locations in ascending order in one variable
Pairlocations = Pairlocations(Pairlocations~=0);
Pairlocations_sorted_new = sort(Pairlocations,'ascend');

% Remove repeated peak locations (if any)
row_count = 0;
for i = 1:2:length(Pairlocations_sorted_new)
      row_count = row_count+1;
      Pairlocations_sorted(1,row_count) = Pairlocations_sorted_new(i);
      Pairlocations_sorted(2,row_count) = Pairlocations_sorted_new(i+1);
end
for i = 2:1:length(Pairlocations_sorted(1,1:end))
   if (Pairlocations_sorted(1,i) == Pairlocations_sorted(2,i-1))
      if (abs(DataTest(Pairlocations_sorted(1,i-1))) > abs(DataTest(Pairlocations_sorted(2,i))))
      Pairlocations_sorted(1,i) = 0;
      Pairlocations_sorted(2,i) = 0;
      else
      Pairlocations_sorted(1,i−1) = 0;
      Pairlocations_sorted(2,i−1) = 0;
      end
   end
end

% Storing the Positive and Negatiuve EOG Peak locations in two different variables in ascending order
```

```
Pair_row_1 = Pairlocations_sorted(1,1:end);
Pair_row_1 = Pair_row_1(Pair_row_1~=0);
Pair_row_2 = Pairlocations_sorted(2,1:end);
Pair_row_2 = Pair_row_2(Pair_row_2~=0);
Pairlocations_final(1,:) = Pair_row_1;
Pairlocations_final(2,:) = Pair_row_2;

  % EOG Feature extraction logic, detecting sharp peaks
  for i = 1:1:length(Pairlocations_final(1,1:end))
    [Sharp_chk(1,i),Sharp_chk(2,i),Sharp_chk(3,i),Sharp_chk(4,i)] =
    sharp_peaks(EOG_Data,Pairlocations_final(1,i),Pos_baseline_floor);
    [Sharp_chk(5,i),Sharp_chk(6,i),Sharp_chk(7,i),Sharp_chk(8,i)] =
    sharp_peaks(EOG_Data,Pairlocations_final(2,i),Pos_baseline_floor);
  end
% EOG Feature Count Initialization
Right_HEM = 0; % Right Horizontal Eye Movements
Left_HEM = 0; % Left Horizontal Eye Movements
Eye_Blink = 0; % Eye Blinks
Right_Wink = 0; % Right Eye Winks
Left_Wink = 0; % Left Eye Winks

Sharp_final = Sharp_chk;

for i = 1:1:length(Sharp_chk(1,1:end))
   % Logic for  Horizontal Eye Movement Detection
   if(Sharp_chk(4,i) > 15 && Sharp_chk(8,i) < 15 && Sharp_chk(4,i) >= 2*Sharp_chk(8,i))
         if (Sharp_chk(5,i) > 0.6)
            Right_HEM = Right_HEM + 1;
            Sharp_final(9,i) = 10;
         elseif (Sharp_chk(5,i) < -0.6)
            Left_HEM = Left_HEM + 1;
            Sharp_final(9,i) = 20;
         end
   elseif (Sharp_chk(4,i) < 15 && Sharp_chk(8,i) > 15 && Sharp_chk(8,i) >= 2*Sharp_chk(4,i))
         if (Sharp_chk(1,i) > 0.6)
```

```
            Right_HEM = Right_HEM + 1;
            Sharp_final(9,i) = 10;
        elseif (Sharp_chk(1,i) < -0.6)
            Left_HEM = Left_HEM + 1;
            Sharp_final(9,i) = 20;
        end
    elseif ((Sharp_chk(4,i) <= 15 && Sharp_chk(8,i) <= 15 ) || (Sharp_chk(8,i) <= 2*Sharp_chk(4,i)) ||
            (Sharp_chk(4,i) <= 1.5*Sharp_chk(8,i)))
        Peak_to_peak = abs(Sharp_chk(1,i)) + abs(Sharp_chk(5,i));
        % Logic for Eye Blinks Detection
        if (Peak_to_peak > 0.4 && Peak_to_peak < 1.8)
            Eye_Blink = Eye_Blink + 1;
            Sharp_final(9,i) = 30;
        % Logic for Eye Winks Detection
        elseif ((Peak_to_peak > 1.8) && (Sharp_chk(1,i) > 0.3) && (Sharp_chk(5,i) < -0.3))
            Right_Wink = Right_Wink + 1;
            Sharp_final(9,i) = 40;
        elseif ((Peak_to_peak > 1.8) && (Sharp_chk(5,i) > 0.3) && (Sharp_chk(1,i) < -0.3))
            Left_Wink = Left_Wink + 1;
            Sharp_final(9,i) = 50;
        end
    end
end

% Print Total Number of Extracted Eye Activities
clc;
fprintf('Right HEM:- %d \n',Right_HEM)
fprintf('Left HEM:- %d \n',Left_HEM)
fprintf('Eye Blink:- %d \n',Eye_Blink)
fprintf('Right Eye Wink:- %d \n',Right_Wink)
fprintf('Left Eye Wink:- %d \n',Left_Wink)
}
end
```

```
% Sharp Peak Detection Logic
function [PeakValue, dX1, dX2, XInterceptdiff] = sharp_peaks(DataInput,PeakLocation,find_threshold)
{
    if (PeakLocation > 10)
       PeakValue = DataInput(PeakLocation);
       if (abs(PeakValue) > 0.6)
          find_threshold = 0.3;
       end

       % Check for Edge Points of Flat Peaks at Saturation
       EdgePoint1 = PeakLocation;
       EdgePoint2 = 0;
       if(abs(DataInput(EdgePoint1)) > 1.646 )
         for i = PeakLocation−10:1:PeakLocation+70
            if(DataInput(i+1) > 1.646)
               EdgePoint2 = i+1;
            end
         end
       end

       % Check the Slope of the Peaks both in Rising and Falling Edges to determine if it is Sharp or not
       if (EdgePoint2 > 0)
          count1 = EdgePoint1;
          count2 = EdgePoint2;
          err = EdgePoint2−EdgePoint1;
          if (PeakValue > 0)
             while (DataInput(count1) > PeakValue-find_threshold && (count1 < length(DataInput)))
                count1 = count1−1;
             end
             dX1 = count1;
             while (DataInput(count2) > PeakValue-find_threshold  && (count2 < length(DataInput)))
                count2 = count2+1;
```

```
        end
        dX2 = count2−err;
    else
        while (DataInput(count1) < PeakValue+find_threshold  && (count1 < length(DataInput)))
            count1 = count1−1;
        end
        dX1 = count1;
        while (DataInput(count2) < PeakValue+find_threshold  && (count2 < length(DataInput)))
            count2 = count2+1;
        end
        dX2 = count2−err;
    end
else
    count1 = EdgePoint1;
    count2 = EdgePoint1;
    if (PeakValue > 0)
        while (DataInput(count1) > PeakValue-find_threshold  && (count1 < length(DataInput)))
            count1 = count1−1;
        end
        dX1 = count1;
        while (DataInput(count2) > PeakValue-find_threshold  && (count2 < length(DataInput)))
            count2 = count2+1;
        end
        dX2 = count2;
    else
        while (DataInput(count1) < PeakValue+find_threshold  && (count1 < length(DataInput)))
            count1 = count1−1;
        end
        dX1 = count1;
        while (DataInput(count2) < PeakValue+find_threshold && (count2 < length(DataInput)))
            count2 = count2+1;
        end
        dX2 = count2;
```

```
        end
    end
    XInterceptdiff = dX2−dX1;
}
end
```

B MATLAB Code for the Motion Artifacts Reduction in Intra-oral EEG Signal using Accelerometer Data and EMD-ICA Method presented in Chapter 4

```
function [Moition_Artifact_Reduced_IntraOral_EEG] = IntrOral_EEG_Motion_Removal(RawEEG, RawAccX, RawAccY, RawAccZ)
{
% Accelerometer data reading

X_data = RawAccX;
Y_data = RawAccY;
Z_data = RawAccZ;

% Intra-oral EEG data reading
EEG_data = RawEEG;

% Accelerometer data preprocessing
X_data = smooth((X_data - mean(X_data)),10);
Y_data = smooth((Y_data - mean(Y_data)),10);
Z_data = smooth((Z_data - mean(Z_data)),50);

X_data = smooth(sqrt((X_data).^2),1);
Y_data = smooth(sqrt((Y_data).^2),1);
Z_data = smooth(sqrt((Z_data).^2),1);
```

```
% Calculating resultant accelerometer data
Reslt_data = smooth(sqrt((X_data).^2 + (Y_data).^2 + (Z_data).^2),1);

% Extracting resultant accelerometer envelop data after baseline (40 mVs) removal
Reslt_data_filt = max(Reslt_data,10);
Reslt_data_filt = Reslt_data_filt - 15;
[yuprslt0, ylowrslt0] = envelope(Reslt_data_filt,50,'analytic');
[yuprslt, ylowrslt] = envelope(yuprslt0,50,'analytic');
yuprslt = smooth(yuprslt,150);
yuprslt_mean = mean(yuprslt);

% Identifying the time segments where the intra-oral motion events occurred
segments = [];
count = 0;

for i=1:1:length(yuprslt)
   if (yuprslt(i)> yuprslt_mean)
      count = count + 1;
      segments(count) = i;
   end
end

% Identifying the start and end times of the motion events
endtimes = 0;
endpoints = [];

for i=2:1:length(segments)
   if ((segments(i)-1) ~= segments(i-1))
      endtimes = endtimes + 1;
      endpoints(endtimes) = segments(i-1);
   end
end
endpoints(endtimes+1) = segments(end);
```

```
starttimes = 1;
startpoints = [];
startpoints(starttimes) = segments(1);

for i=2:1:length(segments)
   if ((segments(i)-1) ~= segments(i-1))
      starttimes = starttimes + 1;
      startpoints(starttimes) = segments(i);
   end
end

% Extending motion duration for accommodating electrode relaxation time count
startpoints_updated = [];
endpoints_updated = [];

if (length(startpoints) == length(endpoints))
   for i=1:1:length(startpoints)
      extra_time1 = round((endpoints(i) - startpoints(i))*1);
      extra_time2 = round((endpoints(i) - startpoints(i))*2);
      startpoints_updated(i) = startpoints(i)- extra_time1;

      if (startpoints_updated(i) <= 0) % if the sgement is identified at the beginning of the dataset
        startpoints_updated(i) = 1;
      end
      endpoints_updated(i) = endpoints(i) + extra_time2;
      if (endpoints_updated(i) > length(yuprslt)) % if the sgement is identified at the end of the dataset
        endpoints_updated(i) = length(yuprslt);
      end
    end
end

% Decomposing EEG data using EMD
[imfs, res, info] = emd(EEG_data);
```

```
[rows,colms] = size(imfs);

% Separating ICA components using fastICA algorithm
[icas, A, W] = fastica(imfs');
icas_after_noise_removal = icas;

% Mapping the motion segments extracted from 'the resultant accelerometer envelope data' with the first four decomposed ICA components and nullifying them accordingly
if (length(startpoints_updated) == length(endpoints_updated))
   for i=1:1:length(startpoints_updated)
       for k=1:1:4
          icas_after_noise_removal(k,(startpoints_updated(i):endpoints_updated(i))) = 0;
       end
   end
end

% Reconstruction of the denoised EEG using inverse ICA – EMD method
inv_icas = A*icas_after_noise_removal;
inv_icas = inv_icas';

total_rescon_imfs = zeros(rows,1);
for i=1:1:colms
   total_rescon_imfs = total_rescon_imfs + inv_icas(:,i);
end
rescon_EEG = res + total_rescon_imfs;
}
Moition_Artifact_Reduced_IntraOral_EEG = rescon_EEG;
end
```